Dynamic Stability Analysis of a Multi-Stage Axial Compressor with Design Implications

by

Emmanuel Blanvillain

Submitted to the Department of Aeronautics and Astronautics
in partial fulfillment of the requirements for the degree of

MASTER OF ENGINEERING IN AERONAUTICS AND ASTRONAUTICS

at the

MASSACHUSETTS INSTITUTE OF TECHNOLOGY

February 2003

Author_____
Department of Aeronautics and Astronautics
December 20, 2002

Certified by_____
Charles Boppe
Senior Lecturer, Department of Aeronautics and Astronautics
Thesis Supervisor

Certified by_____
Professor Zoltán Spakovszky
C.R. Soderberg Assistant Professor of Aeronautics and Astronautics
Thesis Supervisor

Accepted by_____
Professor Edward M. Greitzer
H.N. Slater Professor of Aeronautics and Astronautics
Chair, Committee on Graduate Students

Dynamic Stability Analysis of a Multi-Stage Axial Compressor with Design Implications

by

Emmanuel Blanvillain

Submitted to the Department of Aeronautics and Astronautics
on December 20, 2002, in partial fulfillment of the
requirements for the degree of
Master of Engineering in Aeronautics and Astronautics

Abstract

This thesis is the first year effort of a joint engineering project initiated by Snecma Moteurs, ENSAE, ECL and MIT. The objective of this joint project is to conceive, design, implement and operate an advanced core compressor for an unmanned flight vehicle in the light of three design visions: a classical design vision using state-of-the-art tools, a design vision based on system integration and operability and a design vision robust to uncertainties in compressor stability. This thesis focuses on the dynamic stability analysis of a multi-stage candidate compressor and delineates the design implications for increased stability. The present study addresses three main issues:

System Aspects of Engine Stability A study of the system aspects of engine surge is conducted from operational, cost and regulatory perspectives. The cost of operating a single type of reduced-stability engine for a major US airline can reach up to $10 million a year, which corresponds to 8% of the annual revenue potentially generated by the fleet powered by these engines.

Analysis of Compressor Dynamic Stability in a Multi-Stage Environment An existing dynamic compressor system model is adapted and extended to a candidate multi-stage compressor. A detailed outline of requirements for the necessary input for this model is assessed. This dynamic compressor model is used to investigate the dynamic behavior of the CREATE compressor. The dynamic behavior of this machine is dissected and the dynamics of individual stages are analyzed in the context of the overall compression system pre-stall dynamics.

Design Guidelines for Enhanced Compressor Stability Three effects on the dynamic stability of a 4-repeating-stage compressor are considered: the effect of blade-row inertia, the effect of blade-row performance and the effect of axial coupling between blade-rows. Redistributing the inter-blade-row gap length along the compressor to modify the axial coupling extends the stable compressor operability range in terms of flow coefficient by 4.6%. A 20% reduction in total pressure loss sensitivity to blade-row inlet flow angle on all blade-rows extends the stable compressor operability range by 14.3%. These results highlight the potential improvement of compressor dynamic stability by appropriately redesigning the machine and delineate guidelines for the following years of the joint engineering project between Snecma and the three universities.

Thesis Supervisor: Charles Boppe
Title: Senior Lecturer, Department of Aeronautics and Astronautics

Thesis Supervisor: Professor Zoltán Spakovszky
Title: C.R. Soderberg Assistant Professor of Aeronautics and Astronautics

Acknowledgments

I first want to thank Professor Spakovszky for his support in my research, and for the numerous insights he provided. I also want to thank Professor Boppe for the guidance and encouragement he provided all along this project.

In am also grateful to Professors Hansman and Waitz for sharing with me their knowledge of Air Transportation.

Finally, I want to thank all the members of the joint project, including the engineers at Snecma for their support and insightful guidance, Professors Carrere from ENSAE and Trebinjac from ECL, as well as all the students who contributed to the project.

Contents

List of Figures

List of Tables

Nomenclature

Acronyms

AD Airworthiness Directive

CFD Computational Fluid Dynamics

CREATE Compresseur de Recherche pour l'Etude des effets Arodynamiques et TEchnologiques (Research Compressor for the study of Aerodynamical and Technological Effects)

ECL Ecole Centrale de Lyon

EGT Exhaust Gas Temperature

EPR Engine Pressure Ratio

FAA Federal Aviation Administration

FAR Federal Aviation Regulation

HPC High Pressure Compressor

HPT High Pressure Turbine

IGV Inlet Guide Vanes

IOD Internal Object Damage

MLW Maximum Landing Weight

MTOW Maximum Take Off Weight

ENSAE Ecole Nationale Supérieure de l'Aéronautique et de l'Espace

UAV Unmanned Aeronautical Vehicle

Greek

α absolute flow angle

β relative flow angle

δ deviation angle, perturbation

ϕ flow coefficient

γ ratio of specific heats

γ_s stagger angle

λ blade passage inertia

Ω rotational speed

ω loss coefficient

ω_n rotation rate

ψ_{ts} total-to-static pressure ratio

π Engine Pressure Ratio

ρ gas density

σ solidity

σ_n growth rate

τ unsteady-losses time-lag

Roman

c_p specific heat at constant pressure

c_{xR} axial chord of the rotor

c_{xS} axial chord of the stator

$\dot{m}$ mass flow

M Mach number

$N1$ rotation speed of the low spool

$N2$ rotation speed of the high spool

p static pressure

R mean radius

R perfect gas constant

r radius

S cross sectional area

T static temperature

U wheel speed

V velocity

W *or* V_x axial velocity

x axial location

Superscripts

$\tilde{}$ spatial Fourier coefficient

$\bar{}$ mean value

$'$ in relative frame

Subscripts

$_1$ at inlet

$_2$ at exit

$_{is}$ isentropic

$_r$ rotor

$_s$ stator

$_\theta$ in tangential direction

$_t$ stagnation quantity

$_x$ in axial direction

Chapter 1

Introduction

1.1 Technical Background

1.1.1 Rotating Stall and Surge

Axial compressors used in gas turbine engines can experience aerodynamic instabilities under certain operating conditions. These instabilities can either be rotating stall and/or surge.

Surge is a circumferentially uniform low-frequency instability (3-10 Hz) that affects the entire engine. When surging, the compressor experiences oscillations of alternatively positive and negative flow, which can cause severe engine damage.

On the other hand, rotating stall is characterized by one or several reduced velocity regions in the annulus, due to the stalling of one or several blades. These regions, called stall cells, travel circumferentially at a fraction of the compressor rotation rate, with much higher frequency than surge (usually 20-50% of rotor speed). A review of flow instabilities in compression systems is given by Greitzer [12].

The mechanisms that initiate these flow instabilities are named inception mechanisms. They are reviewed in the following section.

1.1.2 The Path to Instability: Inception Mechanisms of Rotating Stall and Surge

Camp and Day [4] have identified two main pathways for stall inception: "spike-like" disturbances and "modal oscillations." Both phenomena can occur in the same compressor, either independently or simultaneously, and strongly depend on stage matching.

Spike is characterized by the localized stalling of one blade-row which emerges into stall cells and causes the compressor to stall. This is a short wave-length and local phenomenon that can emerge

from a few blade-passages only.

As opposed to spike-like disturbances, modal oscillations are much longer length-scale circumferential perturbations. The term "modal" refers to circumferential modes, the first mode with a wavelength equal to the circumference, the second mode twice its circumference, etc. Unlike spike-like disturbances, modal oscillations usually extend over a wide circumferential sector of the annulus, and over the full length of the machine.

Camp and Day suggest a criterion, based on stage-matching, that determines which of these two phenomena is going to arise. If somewhere in the compressor a rotor incidence exceeds its "critical value," i.e. the incidence that causes separation and flow stagnation, spike is likely to trigger stall before the zero-slope point of the total-to-static pressure characteristic is reached (at negative slope). On the other hand, if the stage matching is such that no rotor incidence exceeds its critical value, modal oscillations are likely to occur near the top of the total-to-static pressure characteristic (at zero slope).

This thesis will focus on modal stall inception since this type of inception is known to be present in many high-speed axial compressors [18].

1.2 Previous Work

Extensive experimental and theoretical studies have been conducted on rotating stall and surge in axial flow compressors (see Cumpsty [5] for review).

Rotating stall and surge are the mature forms of small amplitude flow perturbations that are the natural resonances of oscillation in the compressor system. These small disturbances grow when background flow conditions are such that their damping becomes negative and the compression system drops into an unstable state, rotating stall or surge. Based on these observations, a modeling methodology has been developed by Moore and Greitzer [14]. A review of these different approaches to modeling the nonsteady fluid dynamics associated with two-dimensional compressor flow field can be found in Longley [13].

The fundamental Moore-Greitzer model was extended into a number of descriptions and was applied to a variety of applications (cf. Bonnaure [3], Feulner [10], Paduano [15], Spakovszky [17]). The present study will mainly focus on the compressor dynamic system model developed by Spakovszky [16]. Its modular structure renders modeling flexibility and enable to resolve the dynamics of individual blade-rows, inter-blade-row gaps and intermediate ducts. This model can thus deal with dynamic interaction effects between components. In addition, the low-order, analytical nature of the model allows to dissect the dynamic stall phenomena and facilitates the explanation of physical mechanisms.

1.3 Motivations

1.3.1 Consequences of a Surge Event

Several incidents and accidents, involving both hull losses and fatalities, have been attributed to catastrophic engine surge throughout aviation history. Even during less dramatic events, an in-flight surge can have serious consequences on the airline's operations, and affect the passengers' perception of the airline. To limit potential risks associated with surge events, industry design practice and certification authorities impose a substantial margin, called surge-margin, intended to keep the engine operating away from the surge boundary.

1.3.2 Current Practice: Sub-Optimal Design due to Surge Margin

Surge margin is a measure based on steady-state arguments, and is used as the main metric for compressor operational stability. However, many uncertainties affect this surge margin, such as inlet distortion, transient operation, icing, and engine deterioration. Increasing the level of surge-margin to account for these uncertainties in compressor design is usually accompanied by a reduction in blade loading and diffusion, typically moving away from points of high efficiency. Especially in multi-stage machines, stage matching and the loading distribution strongly affect the surge margin and it is clear that trade-offs between compressor performance and stability have to be made.

1.3.3 Potential Benefits of a Compressor Designed for Stability

With the physical understanding of compressor stability gained over the past fifteen years, many problems have been solved and existing designs have been improved. However, a next step in the understanding of the dynamic pre-stall behavior of axial compressors is to incorporate this knowledge early in the design phase. This thesis discusses the so-far unposed question of how an axial compression system would have to be designed if dynamic stability was a prime design variable, and what potential improvements such a decision could render.

In order to answer the above question and to educate the engineers of the future, a cooperative effort was initiated with the engine manufacturer Snecma Moteurs and two French engineering schools: ENSAE and ECL. More details about this joint project follow.

1.4 Context of the Project

1.4.1 Joint Project

In 2001, Snecma Moteurs, the Ecole Nationale Supérieure de l'Aéronautique et de l'Espace (ENSAE), the Ecole Centrale de Lyon (ECL) and the Massachusetts Institute of Technology (MIT) signed a cooperative academic agreement. The objectives of this cooperative academic agreement were:

- To conduct an educational program on "Complex Air And Propulsion Systems";
- To prepare students to cope with complex systems in complex environments and international teams and to recruit students for industry practice;
- To leverage complementary strengths of the US and French educational systems and to immerse students in an international environment (e.g. student exchange program);
- To offer students opportunities to acquire direct industry experience (e.g. engineering system projects, industry internships etc.).

The joint project's primary mission, following the MIT Aero/Astro Department educational framework, is to Conceive, Design, Implement and Operate (CDIO) an advanced core compressor for an unmanned flight vehicle. It was suggested that a potential candidate compressor for such a vehicle could be an advanced research compressor designed by Snecma Moteurs called CREATE (Compresseur de Recherche pour l'Etude des effets Aérodynamiques et TEchnologiques). This compressor has been used in previous academic projects and could therefore provide benchmarking information, from both a theoretical and an experimental point of view.

The collaboration between the three universities is based on the expertise that each of them has developed over the years in specific areas. Therefore, all teams are working concurrently on the same project using three different but complementary design visions as illustrated in Figure 1-1. Each of these will be further delineated in Section 1.4.2. The three visions are expected, after simultaneous research efforts, to blend into a unique final design, to be later implemented and tested.

1.4.2 Suggested Visions of Compressor Design

Classical Design Vision Using State-of-the-Art Tools

This part of the joint effort is performed by ECL because of the strong links that have been established during the previous years with Snecma Moteurs, in terms of computational and testing capabilities. The first objective for the team at ECL is to adapt existing CFD codes to the candidate compressor and to improve the turnaround time of these high-fidelity computations using parallel computing. This will set a basis for interactions with the other engineering schools and will

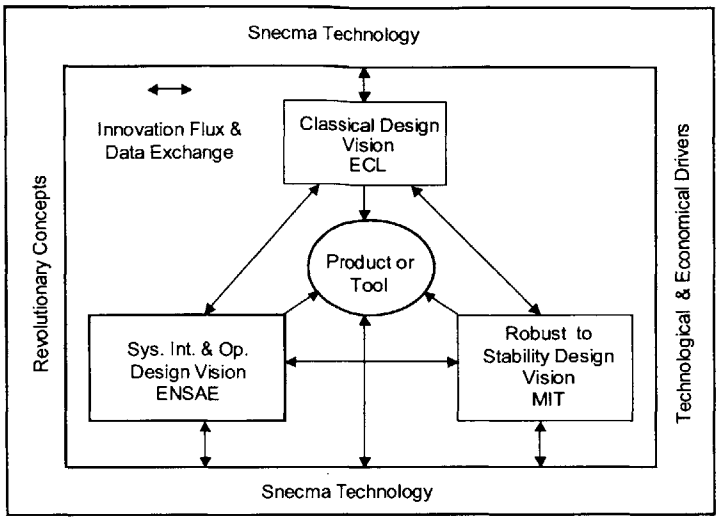

Figure 1-1: Joint Project Framework

also allow for an inverse design process to be progressively set up based on an iterative procedure. Moreover, taking advantage of the baseline design of the CREATE compressor that is implemented in a test rig at ECL, the team has also been assigned the mission to help in the validation of the computational tools developed by the other teams.

Design Vision Based on System Integration and Operability

This part of the joint effort is performed by ENSAE due to the expertise of the school in the field of aircraft integration, flight dynamics and propulsion. The first objective is to identify a candidate unmanned aeronautical vehicle (UAV). To enable benchmarking in terms of performance, operability and design, an existing UAV is chosen as the baseline. In a second step, cycle and aircraft integration studies of the engine to power the UAV are conducted, delineating the performance and operability requirements for the core compressor. The core compressor design will be based on an advanced CREATE compressor design that results from the three complementary design visions. Finally, the third step is a preliminary aero-mechanical study of certain engine components.

Design Vision Robust to Uncertainties in Compressor Stability

This part of the joint effort is performed by MIT. The Gas Turbine Laboratory has developed an expertise in the area of compressor stability from both theoretical and experimental studies during the last fifteen years. The first objective of the MIT team is to evaluate the current industry practice with regards to stability, especially in the light of surge margin and engine stability prediction. Then, an existing dynamic system model [16] is adapted to the CREATE compressor and the pre-stall

dynamic behavior of the baseline design is investigated. Then, a sensitivity analysis is conducted to determine which of the design parameters have the strongest impact on dynamic compressor stability. An assessment of how these results can be used in a design framework where stability is a prime design objective is then made.

1.4.3 Joint Project Timeline

On a preliminary basis, the project span is suggested to be three to four years as presented in Figure 1-2. It is intended to incorporate the CDIO approach on the project level over three years, as well as within each year of the program. The first year is dedicated to the conception and preliminary design of the technical approach to the core compressor, including tool development. The second year focuses on the final design and implementation of the core compressor. The third year is dedicated to hardware manufacturing, assembly and experimental testing of the compressor. As mentioned earlier, strong interaction between MIT, the French engineering schools and Snecma Moteurs is expected as the project moves forward.

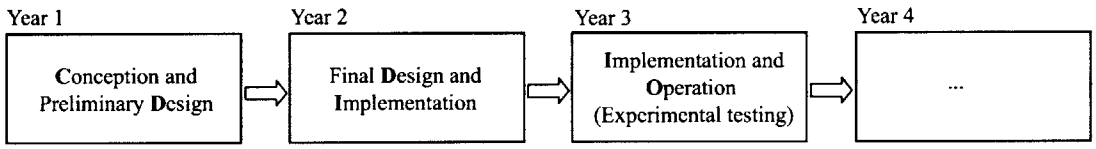

Figure 1-2: Project Timeline Highlighting C, D, I, O Elements

1.4.4 Present Thesis in the Light of the Overall Project

This thesis represents the first year effort of the MIT contribution to the joint project. The main purpose of this work is to conceive and develop the tools that will be further used in consecutive years of the project. Also, an analysis will be conducted using the developed tools, to define preliminary design guidelines for enhanced compressor stability. Even though only the "Conceive" and "Design" parts of CDIO are developed on a joint project level, the entire CDIO methodology is implemented in this thesis. The "Conceive" approach establishes stability as a prime design objective in the design process. In order to apply this concept, an existing multi-actuator disk dynamic system model [16] is adapted to the candidate compressor. The high number of cases studied as well as the increased complexity of the problem requires a new interface to be designed to bring flexibility and commonality as well as code-enhancements to render efficiency in the computations. This tool development work forms most of the "Design" component of the thesis. The tool hereby adapted is

then implemented ("Implement" phase). Testing and validation of these tools are performed before a sensitivity analysis can be conducted under the "Operate" phase.

1.5 Objectives

This thesis focuses on:

- Estimating the impact of a surge event and of reduced-stability margin engines on an airline's operations and costs;
- Establishing a detailed outline of requirements for the mean-flow calculation and the necessary form of input data for the compressor dynamic system model [16];
- Analyzing the blade-row interaction effects on stability in a multi-stage environment;
- Establishing design guidelines for a compressor with increased dynamic stability.

1.6 Contributions

The contributions of this thesis can be summarized as follows:

1. Analysis of the system aspects of a surge event: operational and cost impacts for an airline, certification authorities recommendations on engine stability, derived industry design practices;
2. Implementation of an existing dynamic compressor system model for a multi-stage environment;
3. Integration of this dynamic analysis compressor system model into a robust and efficient tool to analyze compressor stability;
4. Determination of detailed outline of requirements for the mean-flow calculation and for the input data necessary for the dynamic compressor system model;
5. Dissection of the system dynamics in the light of blade-row interaction in a multi-stage environment and preliminary investigation of the eigenvalue structure of the compression system dynamics;
6. Assessment of the effects of blade-row inertia, blade-row performance and axial coupling on multi-stage compressor dynamic stability;
7. Delineation of preliminary design guidelines for enhanced stability.

1.7 Thesis Organization

First, in Chapter 2, a very high-level analysis of surge is conducted to describe how surge is perceived from an operational, cost and regulatory point of view. Chapter 3 adapts and implements an existing two-dimensional linearized incompressible unsteady aerodynamic model [16] to a 3-stage high-pressure compressor to investigate the dynamic pre-stall behavior of the machine. Then, Chapter 4 presents a more thorough dynamic analysis conducted on a standard repeating-stage compressor and assesses the impact of design changes on dynamic stability. Finally, Chapter 5 summarizes the results and proposes future work to be done.

Chapter 2

System Aspects of Compressor Stability

This chapter presents the consequences of surge from an operational, a cost and a regulatory perspective. By highlighting the potential harm caused by a surge event, this chapter strongly assesses the need for a new design approach to compressor stability.

2.1 Surge and Stall from an Operability Point of View

This section describes the manifestation of surge events from a flight crew point of view [7]. The first manifestation of surge at high-power engine settings during take-off is an audible bang, far beyond any other engine noise level, accompanied by aircraft yaw and vibrations. In severe cases, reverse flow caused by surge can be accompanied by visible flames propagating out of the engine inlet and the core exhaust nozzle.
Engine surge can be classified into four categories:

- Single, self-recovering surge cycle;
- Multiple surge cycles prior to self-recovery;
- Multiple surge cycles requiring pilot action in order to recover;
- Non-recoverable surge.

If the engine does not recover from surge without crew intervention, the pilot needs to cut back the thrust lever until the engine recovers and then slowly advance it again. If surge is initiated again, engine power must be cut to idle or even shutdown. In most cases engine surge does not cause severe

engine damage. However, sustained surge might overheat the turbine and induce compressor blade vibrations that can lead to an internal object damage (IOD).

From a regulation authority point of view (cf.FAA [9]), surge events such as the ones discussed above are often classified as "Group 3 take-off surge"(Group 3 corresponding to the most severe type of surge, more likely to occur during take-off.) The FAA uses this term to refer to engines that experiences any of the following symptoms:

- Unusual engine noise, such as rumble and loud bangs;
- Unstable engine parameters (N1, N2, EPR, fuel flow);
- Increase in EGT;
- Flames out of the inlet, the exhaust or both.

Engine surge can be initiated by various internal events such as engine deterioration or enlarged tip clearance, as well as by external causes such as icing, foreign object ingestion or inlet distortion. These events can trigger aerodynamic instabilities that develop into rotating stall and surge.

Before the inception of rotating stall and surge is discussed more thoroughly in Chapters 3 and 4, a brief study of the consequences of an in-flight surge is conducted, both from an operational and a financial perspective, to assess how critical dynamic instability can be during the lifetime of an engine.

2.2 Consequences of Rotating Stall and Surge

2.2.1 Operational Consequences

The operational consequences are subdivided into two categories:

- The operational consequences immediately following the event, based on the decisions made by the pilots, the air traffic control, and the airline;
- The long term operational consequences, based on the decisions made by the regulation authorities to face the issue and avoid its recurrence.

Immediate Operational Consequences

A standard scenario is discussed here, based on actual occurrences of surge events. The assumption is made that surge occurs during take-off or at the early stages of a climb. In this case, after surge is detected by the flight crew, the decision is usually made to return to the airport. If the total weight of the aircraft after take-off exceeds the Maximum Landing Weight (MLW), a significant amount

of the onboard fuel has to be dumped before the landing can be conducted. Once the airplane is grounded, the passengers have to be reallocated to other flights, and, if needed, rebooked to flights of other airlines. In the case of insufficient seat availability, passengers may have to wait until the following day to take their flight. The flight crew also has to be reassigned to an aircraft in the new flight schedule after the original flight schedule is disrupted.

After the incident, the affected engine has to undergo inspection, and, if severe damage is detected, the engine has to be replaced. In certain cases of light damage, the maintenance can be performed on wing. The repair work is performed by the airline's mechanics, who have to be flown on site if the location of the incident does not have a maintenance base for the airline. Additional ground tests are performed on the new engine before the airplane can return to service. If the engine that experienced surge has been removed from wing, it is then shipped to one of the airline's maintenance facilities and has to undergo further inspections, repairs, and testing before it can go back to service. The consequences of surge events strongly depend on other factors, such as the location of the surge occurrence (i.e., with or without a maintenance facility, or an available spare aircraft/engine) as well as the load factor of the flights used to reallocate the passengers, that, if too high, can cause severe cascade effects in passenger reallocation (the passengers of the canceled flight taking the seats of booked passengers on another flight, the later also rebooked on an additional flight etc.)

Long-Term Operational Consequences

The consequences analyzed here are based on the decisions made by the certification authorities to avoid the recurrence of surge events, usually after a dramatic event has demonstrated the limitations of the pre-existing regulations. The present study extensively uses the Airworthiness Directive (AD) 2001-08-52 issued by the FAA [6] (updated in [9]), which deals with low-stability engines. In this AD, four requirements are stated for airlines operating engines subjected to this AD. The airlines have to:

- Limit the presence of the potentially reduced-stability engines to no more than one per aircraft;
- Remove specified engines from service before they reach their cycle limits;
- Refurbish all the potentially affected engines before they return to service;
- Make sure that the cycle mismatch between the HPC and the HPT of any of these engines does not exceed 1500 cycles.

In the following section, the cost associated with the events described in this section is estimated, to assess the financial impact of a surge event.

2.2.2 Cost Consequences

The costs associated with the events described above can be divided into three categories: costs related to the handling passengers, costs directly associated with the aircraft, and other costs related to the airline.

Passenger Related Costs

As mentioned above, passengers have to be reallocated to other flights. In the case where seats are available on the airline's other flights, no additional expenses incur. If the flights are full and passengers have to be rebooked on other airlines, an extra charge may apply. However, the reallocation of passengers between airlines is a standard practice so that airlines alternatively request and offer extra seats. The balancing effect over the year may therefore reduce the net cost for the airline.
In some special circumstances, however, due to high load factors, usually during peak periods, passengers may have to wait one day before they are reallocated, which implies hotel and meal compensations to be paid by the airline. In addition, they may be reallocated on overbooked flights, thus generating overbooking fees for some of the newly-affected passengers (cascade effect). Consequently, a very rough estimate of costs associated with handling passenger can be made based on a worst case scenario. If a standard hotel and meal fee of $200 is compared to the average ticket price on a wide-body aircraft, which is about $250, the worst case corresponds to the case when all passengers have to be refunded. Based on a 250-passenger aircraft with an average ticket price of $250, the passenger related costs would be $62,500.
The airline may also have to bear losses in the long run due to a reduction of the repurchase intent rate associated with a public image of low safety that may affect the airline in the period following the incident. However, this effect is very difficult to be estimated and will not be accounted for here.

Aircraft Related Costs

Aircraft costs in the event of surge are directly associated with the aircraft fuel, parts and maintenance.
The cost related to the fuel dumped can easily be estimated. For the present study, a fully-loaded twin-engine wide-body aircraft is selected. Assuming surge at take-off or in the early stages of the climb-out phase, the fuel burned between take-off and the occurrence of surge can be neglected and thus the amount of fuel to be dumped is equal to the difference between MTOW and MLW. Based on an average of $1/gallon of fuel, the net cost ranges between $10,000 and $20,000.

As for maintenance costs, having to fly the mechanics to the aircraft is a negligible source of expenses, as they generally travel on the airline's flights. Nevertheless, the farther the mechanics are located from the aircraft, the higher the cost associated with aircraft unavailability. Engine

inspection cost for a suspect engine is based on an industry standard of fifteen man-hours. Ground testing for a replacement engine is based on an industry standard of four man-hours, with a labor rate of $55/hr plus the fuel and oil needed to run the engine for four hours. The FAA [9] specifies that any engine that had a Group 3 surge event must undergo a High Pressure Compressor (HPC) overhaul with an estimated cost of $400,000. In the case of further engine damage, a complete engine overhaul may be required, with an approximate cost of $2,000,000. Table 2.1 summarizes aircraft-related costs.

Source	Lower estimate (in US $)	Higher estimate (in US $)
Fuel Dump	10,000	20,000
Engine Inspection	825	825
Engine Change	2,000	5,000
Ground Testing	4,000	4,000
HPC or Engine Overhaul	400,000	2,000,000
Subtotal	416,825	2,029,825

Table 2.1: Aircraft Costs Related to a Surge Event

Airline Related Costs

The term "airline costs" refers to general costs related to a surge event, which are usually absorbed into the overall cost structure of the airline.

Short-Term Costs In the present study, the location of the surge event occurrence is a determining driver for costs.

First, the cost of the shipment of an engine from and to the aircraft directly scales with the distance between the aircraft and its maintenance base. For emergency reasons, the cost of getting the engine to the aircraft is much higher than the cost to bring the damaged engine to the maintenance base. The standard cost of a shipment is about $10,000 for a domestic shipment, $30,000 for a transatlantic shipment and up to $200,000 for a very long range shipment.

Second, the cost of aircraft unavailability is directly proportional to its unavailable flight time, which is mainly driven by the time required to replace the engine, including the time necessary to ship the new engine. Based on an approximate daily revenue which ranges between $60,000 and $100,000 for a wide-body aircraft (1 to 1.7 flight/day on average with an average revenue of $62,500 per flight [2]) and the aircraft downtime ranging from one to four days, the total short-term costs can accrue up to $400,000.

Concerning the flight crew reallocation, the cost of flying them to their new aircraft is essentially negligible, for the same reasons as the ones mentioned for the mechanics.

The airline-related costs are summarized in Table 2.2.

Source	Lower estimate (in US $)	Higher estimate (in US $)
Cost of aircraft unavailability	60,000	400,000
Shipment of new engine to aircraft	0	200,000
Shipment of old engine to maintenance base	0	25,000
Subtotal	60,000	625,000

Table 2.2: Surge Event Related Airline Costs

Long-Term Recurring Costs Some indirect costs are more difficult to estimate since they are embedded into the overall cost structure of the airline. The costs related to the application of an AD are of this type. First, an AD implies direct costs in terms of extra inspection and maintenance. Estimates made by the FAA ([1] & [9]) show that 35% of the potentially affected engines would require annual on-wing testing at a cost of $2,000 per test. Another 17% of the engines would require annual off-wing testing, at a cost of $15,000 per test. Based on a failure rate of 12% for this off-wing test, 2% of the total number of engines would have to undergo high pressure compressor overhaul, at a unit cost of $400,000. Finally, unscheduled removal would affect 2% of the potentially affected engines, costing $5,000 each.

The results presented in Table 2.3 indicate an annual cost of about $11,350 per affected engine.

Maintenance Event Type	Probability	Event Cost (in US $)	Average Cost per Engine (in US $)
On-wing Testing	0.35	2,000	700
Off-wing Testing	0.17	15,000	2,550
HPC Overhaul	0.02	400,000	8000
Unscheduled Removal	0.02	5,000	100
TOTAL			11,350

Table 2.3: Long Term Recurring Costs Associated with Low-Stability Engines

More spare engines may also have to be purchased to operate the same fleet, due to early engine retirements and the restriction of one potentially reduced-stability engine per aircraft. However, based on the number of engines subject to this directive (about 50 out of 2115 existing engines of this affected engine type), the probability of having two potentially reduced-stability engines on the same twin-jet is very low (on the order of 0.05%) and consequently, the associated expenses can be considered minor. To a lesser extent, the inventory and supply chain issues related to the AD requirement may also generate additional costs.

Total Costs: Estimation of Engine Surge Related Costs for a Standard US Airline

For simplicity, and due to the data availability from the FAA, a simulated case study is conducted here for a standard US airline with 25% market share.

First, the total cost associated with one surge event is computed, based on the cost breakdown of the previous paragraphs. The results are shown in Table 2.4.

Source	Lower estimate (in US $)	Higher estimate (in US $)
Passenger related costs	0	62,500
Aircraft related costs	416,825	2,829,025
Airline related costs	60,000	625,000
Surge Event Total Cost	476,825	3,516,525

Table 2.4: Total Costs Associated with a Surge Event

Second, the total cost associated with low-stability engines are compiled for a one-year period, in the case of the simulated airline. Given the airline size, the FAA [9] estimates the total number of surge events to be two events per year. In addition, if the assumption is also made that the airline owns 25% of the engines with reduced stability, the airline's annual long term recurring costs are estimated to be $2,000,000. Table 2.5 summarizes the results.

Source	Lower estimate (in US $)	Higher estimate (in US $)
Direct costs associated with 2 surge events	953,650	7,033,050
Recurrent costs (Long-Term)	2,000,000	2,000,000
TOTAL ANNUAL COST	2,953,650	9,033,050

Table 2.5: Annual Airline Costs

The previous results show that the annual penalty the airline has to pay for these reduced-stability engines can reach almost $10 million. For the thrust class considered, this is the price of a new engine. Visualizing this result in terms of actual operating revenue is very insightful. Given the airline size, the number of aircraft powered by the low-stability engine type is estimated to be about 50. With the following assumptions of one flight per aircraft per day, $62,500 of revenue per flight and a 10% net margin, it takes the aircraft powered by low-stability engines about a month to generate a revenue of $10 million. Thus, the airline essentially operates these aircraft one month of the year (i.e. about 8% of the year) just to cover the costs for the low stability of their engine fleet. This situation is even more unacceptable in times when the US airline industry is struggling for survival.

These conclusions are delineated, of course, without even considering the catastrophic impact that a hull loss due to an engine surge may cause (aircraft loss, fatalities, lawsuits etc.)

One way to reduce the likelihood of a surge event and its dramatic consequences is to make early decisions in the design process to consider stability as a primary design objective. Another way to reduce the probability of such events is for certification authorities to impose safer design practices on the engine manufacturers. These two possibilities are briefly described below.

2.2.3 Consequences for Flight Regulation

In addition to the operational directives the certification authorities publish (e.g., the AD previously discussed), these authorities also provide general recommendations and requirements regarding engine certification. In the US, the Federal Aviation Regulation (FAR) Part 33 [8] specifies the conditions engines must meet in order to be certified. An excerpt from FAR Part 33 related to surge and stall states:

> 33.65 Surge and stall characteristics.
> When the engine is operated in accordance with operating instructions required by 33.5(b), starting, a change of power or thrust, power or thrust augmentation, limiting inlet air distortion, or inlet air temperature may not cause surge or stall to the extent that flameout, structural failure, overtemperature, or failure of the engine to recover power or thrust will occur at any point in the operating envelope.

As shown in the statement above, these recommendations are very general and do not impose strict design practices on the manufacturers. However, based on experience, standard design practices have been developed in industry and are further described next.

2.2.4 Surge Event Consequences for Design Practice

In order to address the requirements dictated by the certification authorities, engine manufacturers have adopted a *conservative* measure for surge and rotation stall called the "surge margin." A large enough surge margin is expected to guarantee stable operations throughout the flight envelope. One definition of surge margin, as generally done by industry, (cf. Figure 2-1) is

$$Surge\ margin = \left.\frac{\pi_{surge} - \pi_{operating}}{\pi_{operating}}\right|_{\dot{m}_{corr}=constant} \tag{2.1}$$

The surge margin also accounts for uncertainties related to inlet distortion, transient engine operations, engine deterioration and possible damages due to foreign object ingestion.

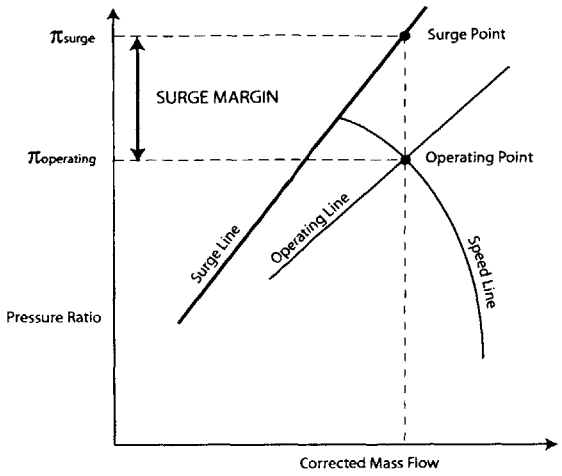

Figure 2-1: Compressor Map Illustrating Surge Margin

Current industry practice is to have a surge margin of the order of 20% to 25% for commercial engines. A surge margin breakdown for a high-pressure compressor at a fixed operating point can be found in Williams [19] and is summarized in Table 2.6.

Cause	Surge margin utilized
Inlet Distortion	7 %
Engine to engine scatter	3.5 %
Deterioration	5 %
Control tolerances	2 %
Reynolds number effects	1 %

Table 2.6: Surge Margin Breakdown for a HPC for a Fixed Operating Point

However, unlike the operating pressure ratio $\pi_{operating}$, the pressure ratio where surge is initiated π_{surge} is difficult to predict. In current design process, surge line prediction still heavily relies on empirical correlations as stated by Cumpsty [5]:

> "At present the most reliable method of estimating the stall or surge point is to use information obtained from tests of similar machines."

However, surge margin is a rather "static" metric, and is affected by many uncertainties such as inlet distortion, transient operation, icing, and engine deterioration. Therefore, based on the knowledge developed on compressor dynamic stability, a more adequate metric for stability should account for the dynamic behavior of the compressor. Recently, new tools such as a simple one-

dimensional unsteady model were developed and applied to predict the surge point on a compressor characteristic. However, these methods rely heavily on the performance curve and can only be a first step towards new stability analysis tools.

A more elaborate tool thus has to be used to predict the surge limit. In this thesis, an existing two-dimensional dynamic compressor modeling tool [16] is implemented on an existing compressor to assess its dynamic stability (Chapter 3). Design guidelines to enhance compressor stability in the light of dynamic system stability rather than based on surge margin are then delineated in Chapter 4.

Chapter 3

Tool Development and Derived Requirements

3.1 Structure of the Model

In order to capture the dynamic flow behavior near stall, the Dynamic System Model developed by Spakovszky [16] describes the flow as modal oscillations (cf 1.1.2) of the aerodynamic quantities (velocity and pressure) around a mean steady state. The equations of motion of the flow, as discussed in 3.3.1, thus involve the mean-flow velocities and pressure. As a consequence, this information, determined by a mean-flow calculation, has to be fed into the model in order to determine the behavior of the unsteady aerodynamic parameters. The structure of this tool that is expanded here (cf Figure 3-1) is therefore divided into two main parts: the Mean-Flow Model calculation and the Dynamic Model calculation. They are presented in more detail in Sections 3.2 and 3.3, respectively.

3.2 Mean-Flow Calculation

3.2.1 Background and Inputs

In order to provide the necessary inputs to the dynamic model, a mean-flow calculation has to be conducted. To generate these inputs, a compressible mean-flow analysis of the high-speed compressor is selected, even though the dynamic compressor model is incompressible. This compressible mean-flow calculation gives a better representation of the mean-flow parameters for the high-speed, variable duct area candidate compressor. Since the dynamic model requires as input one-dimensional mean-flow data, a one-dimensional compressible mean-line code is implemented, all thermodynamic quantities being computed at the Euler radius (the radius that divides the annulus into two equal

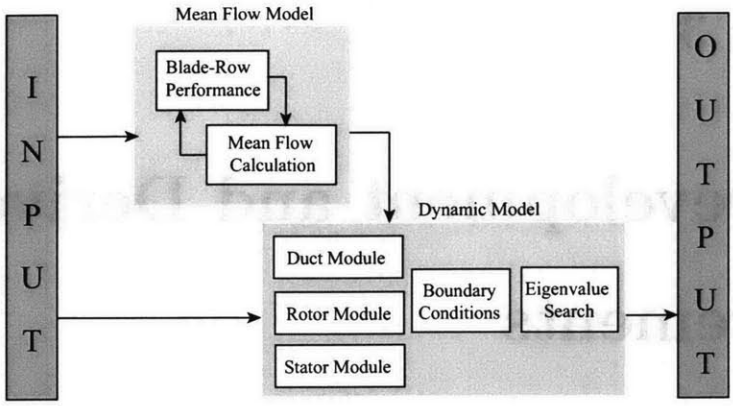

Figure 3-1: Overall Structure of the Model

areas) for the different stages.

The mean-flow calculation uses the data provided by Snecma Moteurs for the CREATE compressor. CREATE is a high-speed 3-stage compressor, with six blade-rows with different designs, a variable duct area and different inter blade-row gap lengths.
The data provided by Snecma Moteurs for this compressor are:

- The three-dimensional geometry;
- The total pressure loss coefficients as a function of inlet flow angle for each blade-row at design speed;
- The inlet conditions.

The compressible mean-flow calculation forms an implicit problem and thus an iterative blade-row by blade-row analysis is conducted. This procedure is described in more detail in Appendix A.

3.2.2 Blade-Row Correction Factors and Validation

The described procedure is implemented for the CREATE compressor and the results are compared to performance data provided by Snecma Moteurs. A higher pressure ratio is observed compared to the Snecma data based on CFD. Consequently, to represent the compressor performance closer to the CFD based data, two correction factors are implemented: a flow deviation correction and a blockage correction.

Effect of Flow Deviation

The flow at the exit of the blade-rows was assumed to follow the mean exit blade metal angle. However, because of boundary layer separation, in practice, the flow usually deviates by an angle δ.

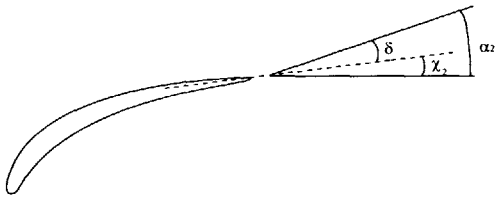

Figure 3-2: Deviation Angle at the Exit of a Blade-Row

Given the high solidity of the blading, a constant two-degree deviation is first assumed. However, with these settings, the pressure-ratios obtained are about 15% higher than the pressure-ratios from Snecma (cf. Figure 3-3). Therefore, a semi-empirical deviation model, based on Carter's rule, is implemented, assuming parabolic arc blade profiles. The deviation angle can be written as

$$\delta = \frac{m_c(\gamma_s)}{\sqrt{\sigma}} \cdot (\beta_1 - \beta_2) \ , \tag{3.1}$$

where $m_c(\gamma_s)$ is an empirical coefficient that depends on the stagger angle, $\beta_1 - \beta_2$ is the turning and σ is the solidity of the blade-row.

Effect of Flow Blockage

A correction factor that accounts for blockage is included in the mean-flow calculation. In the present model, the sensitivity of the total-to-total pressure ratio to blockage rate changes is small.

Consequently, in the following calculations, the effect of deviation will be included, and the blockage coefficients will be adjusted to match the data from Snecma: either the inlet flow angles for each blade-row or the axial velocity at the inlet of each blade-row (Note: This research studies the compressor pre-stall dynamics at mass flows close to the stability limit. Thus, the deviation and blockage factors are adjusted such that the blade-row inlet flow angles, or the axial velocity, provided by Snecma Moteurs are matched for the lowest mass flow points on the speed line.)

Comparison of Predictions to Snecma Performance Data

The first validation that can be performed is to compare the deviation angles from Carter's rule to the ones from the Snecma data[1]. The results, in Table 3.1, show very good agreement except for the first rotor, which operates at negative incidence and therefore has a very small deviation angle. Thus, the semi-empirical deviation model is applied to all blade-rows, except rotor 1, instead of the constant two-degree deviation previously used. For the rotor 1 case, however, the deviation is set to the constant Snecma data value corresponding to the lowest mass flow point on the speed line.

Blade-Row	Deviation angle from Carter's rule	Deviation angle from Snecma data	Error
R1	4.4 deg.	3.0 deg.	1.4 deg.
S1	4.9 deg.	4.8 deg.	0.1 deg.
R2	4.3 deg.	4.0 deg.	0.3 deg.
S2	5.3 deg.	4.8 deg.	0.5 deg.
R3	4.3 deg.	5.0 deg.	-0.7 deg.

Table 3.1: Comparison of Deviation Angles Between Carter's Rule Prediction and Snecma Data for the Available Mass Flow Rate Closest to Stall

The second validation is to compare the total-to-total pressure ratios obtained with the corrections to the Snecma performance curve. These results are plotted in Figure 3-3.

The results show a pressure ratio between two and five percent above the CFD-based Snecma data, which, given the simplicity of the model and the data available, can be considered acceptable. In addition, the blockage added is of the order of one or two percent and never exceed five percent, which seems reasonable.

For the following calculations, Carter's rule is selected to model exit flow deviation and blockage is adjusted to match the flow angles from Snecma.

3.2.3 Conclusion and Derived Requirements for the Mean-Flow Calculation

The previous results show that, with appropriate corrections to include effects of blockage and deviation, this simple one-dimensional mean-flow calculation can provide realistic information about the mean-flow parameters at the inlet and exit of each blade-row. One way to improve the accuracy of the performance prediction is to perform the calculations based on a more complete set of data. The blade-row performance, for instance, should be expressed as a function of both the inlet flow angle and the Mach number. However, data obtained CFD still inherently retains uncertainty, especially for the blade-row performance curve that highly depend on the turbulence model that

[1]The deviation angles were obtained by computing the differences between the blade metal angles and the flow angles provided

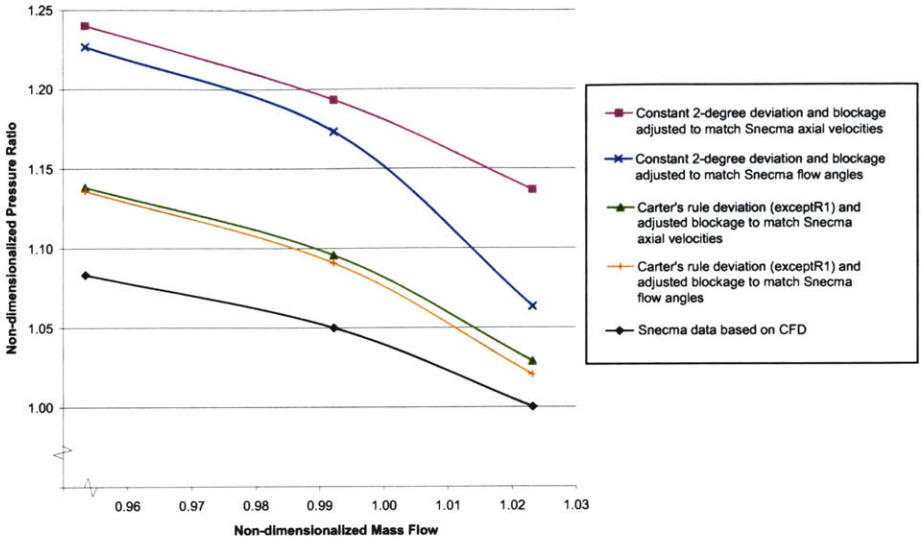

Figure 3-3: Compared Near Peak Total-to-Total Pressure Ratios for Adjustments of Blockage Rate and Deviation using Carter's Rule

is chosen. The best way to obtain the mean-flow parameters robustly and accurately would be to move away from three-dimensional CFD and to use a *mean line deck* tool, based on a combination of empirical correlations and experimental data for this compressor.

3.3 Dynamic Model

3.3.1 Model Description

The objective of the model developed by Spakovszky [16] is to determine the fundamental flow resonances (modes or eigenvalues of the flow field) that govern the compression system dynamics. The compression system can be broken up into several components: upstream duct, rotors, inter blade-row gaps, stators and downstream duct. For each of these components, the governing unsteady equations are linearized and solved analytically. The closed solutions for the flow perturbation are then cast in matrix form, to make the linking between each component easier. The modules generated are then connected together to form the overall compression system. To close the problem, boundary conditions are applied upstream and downstream of the compression system. This yields an eigenvalue problem that needs to be solved in order to find the natural resonances of the compression system (system modes or eigenvalues). Each complex eigenvalue $s = \sigma_n - j\omega_n$ corresponds to a pre-stall wave of sinusoidal shape. The subscript n denotes that the wave has n lobes on the

circumference and is thus called an n-th spatial harmonic pre-stall wave. Each wave rotates around the annulus at a rotation rate ω_n, the imaginary part of the eigenvalue. The real part of the eigenvalue σ_n is the growth rate and indicates whether the wave amplitude grows in time and the resonance is unstable (positive growth rate), or decays in time and the resonance is thus stable (negative growth rate). The least stable of all eigenvalues or natural flow resonances determines the stability of the compression system. The stall point that is used to compute the improvement in flow coefficient in Chapter 4 corresponds to the flow coefficient for which the least stable mode becomes unstable.

A brief overview of each of the modules, as well as the stacking process, is given below. For a detailed derivation of the equations and matrices, see Spakovszky [16]. In its stacked form, the eigenvalue problem can be written as:

$$\det(Y_{sys,n}) = 0 \qquad \text{with} \qquad Y_{sys,n} = \begin{bmatrix} EC \cdot X_{sys,n} \\ IC \end{bmatrix} \tag{3.2}$$

X_{sys} contains the stacked transmission matrices (or modules). In the case of a single-stage machine as depicted in Figure 3-4, the modules are: the inlet duct module, the rotor module, the inter-blade-row gap module, the stator module and the exit duct module. X_{sys} can be written, for each spatial harmonic n:

$$X_{sys,n} = T_{ax,n}(x_4, s)^{-1} \cdot B_{sta,n}(s) \cdot B_{gap,n}(s) \cdot B_{rot,n}(s) \cdot T_{ax,n}(x_1, s) \tag{3.3}$$

where $T_{ax,n}$ is the transmission matrix for a duct

$$T_{ax,n} = \begin{bmatrix} e^{nx} & e^{-nx} & e^{-\left(\frac{s}{\overline{V_x}}+jn\frac{\overline{V_\theta}}{\overline{V_x}}\right)x} \\ je^{nx} & -je^{-nx} & \left(-\frac{sj}{\overline{V_x}n}+\frac{\overline{V_\theta}}{\overline{V_x}}\right)e^{-\left(\frac{s}{\overline{V_x}}+jn\frac{\overline{V_\theta}}{\overline{V_x}}\right)x} \\ \left(-\frac{s}{n}-\overline{V_x}-j\overline{V_\theta}\right)e^{nx} & \left(\frac{s}{n}-\overline{V_x}+j\overline{V_\theta}\right)e^{-nx} & 0 \end{bmatrix} e^{jn\theta}, \tag{3.4}$$

$B_{rot,n}$ is the transmission matrix for a rotor

$$B_{rot,n} = \begin{bmatrix} 1 & 0 & 0 \\ \tan\beta_2 & 0 & 0 \\ \left[\tan\beta_2 - \tan\alpha_1 - \lambda_r(s+jn) \right. & -\frac{\partial L_R}{\partial \tan\beta_1}\frac{1}{\overline{V_x}(1+\tau_R\cdot(s+jn))} + \overline{V_{\theta 1}} & 1 \\ \left. + \frac{\partial L_R}{\partial \tan\beta_1}\frac{\tan\beta_1}{\overline{V_x}(1+\tau_R\cdot(s+jn))} - \overline{V_{\theta 2}}\ \tan\beta_2 \right] & & \end{bmatrix} e^{jn\theta}, \quad (3.5)$$

and $B_{sta,n}$ is the transmission matrix for a stator

$$B_{sta,n} = \begin{bmatrix} 1 & 0 & 0 \\ \tan\alpha_2 & 0 & 0 \\ -\lambda_s s + \frac{\partial L_S}{\partial \tan\alpha_1}\frac{\tan\alpha_1}{\overline{V_x}(1+\tau_s\cdot s)} - \overline{V_{\theta 2}}\ \tan\alpha_2 & -\frac{\partial L_S}{\partial \tan\alpha_1}\frac{1}{\overline{V_x}(1+\tau_S\cdot s)} + \overline{V_{\theta 1}} & 1 \end{bmatrix} e^{jn\theta}. \quad (3.6)$$

Note that B_{gap} is defined as

$$B_{gap,n} = T_{ax,n}(x_3, s).T_{ax,n}(x_2, s)^{-1} \quad (3.7)$$

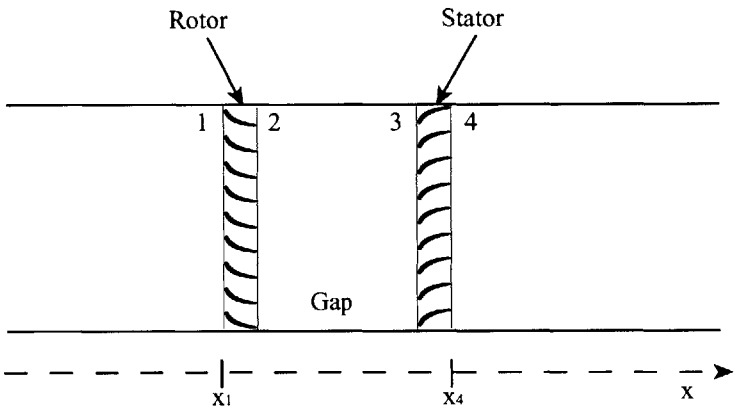

Figure 3-4: Single Stage Compressor Model

For multi-stage compressors, compared to Equation 3.3, additional transmission matrices corresponding to additional stages have to be stacked. For example, in the case of a two stage machine,

X_{sys} can be written as:

$$X_{sys,n} = T_{ax,n}(x_6, s)^{-1} \cdot B_{sta2,n}(s) \cdot B_{gap2,n}(s) \cdot B_{rot2,n}(s) \cdot B_{gapA,n}(s) \cdot B_{sta1,n}(s) \cdot B_{gap1,n}(s) \cdot B_{rot1,n}(s) \cdot T_{ax,n}(x_1, s) \quad (3.8)$$

The implementation of this dynamic compression model is discussed in the next section.

3.3.2 Adaptation and Extension of the Model

Inlet Swirl Sensitivity Addition

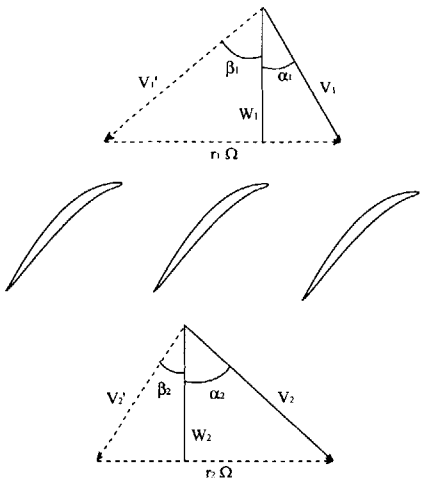

Figure 3-5: Velocity Triangles for the Rotor

In the original Moore-Greitzer formulation, two assumptions are made about blade-row flow angles:

- For high-solidity blading a constant relative exit flow angle β_2 can be assumed (cf. Figure 3-5);
- A constant absolute inlet flow angle α_1 (cf. Figure 3-5.) can be assumed in the case of perfect IGV upstream of the first rotor.

As such, the compressor characteristic is not sensitive to the inlet swirl angle.
In this study, information on swirl sensitivity is available and swirl sensitivity is considered.
In order to relax the high-solidity blading assumption, the effect of deviation (i.e. $\widetilde{V_{\theta 2}} = \mathrm{f}(\widetilde{V}_{x1}, \widetilde{V}_{\theta 1})$) needs to be introduced. Due to the lack of data, this effect is not considered in the present study.

Originally, with the above assumptions, the matching conditions across the rotor yield:

$$P_{t2} - P_{t1} = 1 + (\tan\beta_2 - \tan\alpha_1) \cdot V_{x1} - L_R - \lambda_r \cdot \left(\frac{\partial V_{x1}}{\partial \tau} + \frac{\partial V_{x1}}{\partial \theta} \right) \tag{3.9}$$

where

$$\psi_{is} = 1 + (\tan\beta_2 - \tan\alpha_1) \cdot V_{x1} = \psi_{is}(V_{x1}) \tag{3.10}$$

is the isentropic total pressure rise, function of the axial velocity V_{x1} only.

In general and in the case of inlet swirl sensitivity the isentropic total pressure rise characteristic also depends on $V_{\theta 1}$, such that:

$$\psi_{is} = \psi_{is}(V_{x1}, V_{\theta 1}) \tag{3.11}$$

Linearizing the matching conditions across the rotor then yields:

$$\begin{aligned} \delta P_2 + \overline{V_{\theta 2}} \cdot \delta V_{\theta 2} - \delta P_1 - \overline{V_{\theta 1}} \cdot \delta V_{\theta 1} = {} & \frac{\partial \psi_{is}}{\partial V_{x1}} \cdot \delta V_{x1} + \frac{\partial \psi_{is}}{\partial V_{\theta 1}} \cdot \delta V_{\theta 1} - \frac{\partial L_R}{\partial \tan\beta_1} \cdot \delta \tan\beta_1 \\ & - \lambda_R \left(\frac{\partial(\delta V_{x1})}{\partial \tau} + \frac{\partial(\delta V_{x1})}{\partial \theta} \right) \end{aligned} \tag{3.12}$$

Introducing the Laplace transform and assuming a periodic solution in θ (spatial Fourier series), the above can be written for the n-th spatial harmonic:

$$\begin{aligned} \widetilde{P}_{2,n} + \overline{V}_{\theta 2} \cdot \widetilde{V}_{\theta 2,n} - \widetilde{P}_{1,n} - \overline{V}_{\theta 1} \cdot \widetilde{V}_{\theta 1,n} = {} & \frac{\partial \psi_{is}}{\partial V_{x1}} \cdot \widetilde{V}_{x1,n} + \frac{\partial \psi_{is}}{\partial V_{\theta 1}} \cdot \widetilde{V}_{\theta 1,n} - \frac{\partial L_R}{\partial \tan\beta_1} \frac{\widetilde{V}_{\theta 1,n} - \tan\beta_1 \widetilde{V}_{x1,n}}{\overline{V}_x (1 + \tau_R \cdot (s + jn)} \\ & - \lambda_r (s + jn)) \cdot \widetilde{V}_{x1,n}. \end{aligned} \tag{3.13}$$

Under the assumption of high-solidity, Equation 3.11 yields

$$\psi_{is} = 1 + \tan\beta_2 \cdot V_{x1} - V_{\theta 1}, \tag{3.14}$$

and the sensitivities of the isentropic total pressure rise characteristic to V_{x1} and $V_{\theta 1}$ become

$$\frac{\partial \psi_{is}}{\partial V_{x1}} = \tan\beta_2 \quad \text{and} \quad \frac{\partial \psi_{is}}{\partial V_{\theta 1}} = -1 \, . \tag{3.15}$$

The rotor matching condition (Equation 3.13) for a high solidity blade-row with inlet swirl sensitivity

can then be written as

$$\widetilde{P}_{2,n} + \overline{V}_{\theta 2} \cdot \widetilde{V}_{\theta 2,n} - \widetilde{P}_{1,n} - \overline{V}_{\theta 1} \cdot \widetilde{V}_{\theta 1,n} = \tan\beta_2 \cdot \widetilde{V}_{x1,n} - \widetilde{V}_{\theta 1,n} - \frac{\partial L_R}{\partial \tan\beta_1} \frac{\widetilde{V}_{\theta 1,n} - \tan\beta_1 \widetilde{V}_{x1,n}}{\overline{V}_x(1 + \tau_R \cdot (s + jn) - \lambda_r(s + jn)) \cdot \widetilde{V}_{x1,n}}. \quad (3.16)$$

The transmission matrix for a rotor can then be written:

$$B_{rot,n} = \begin{bmatrix} 1 & 0 & 0 \\ \tan\beta_2 & 0 & 0 \\ \left[\tan\beta_2 - \lambda_r(s+jn) + \frac{\partial L_R}{\partial \tan\beta_1} \frac{\tan\beta_1}{\overline{V_x}(1+\tau_R\cdot(s+jn))} - \overline{V_{\theta 2}}\ \tan\beta_2\right] & -\frac{\partial L_R}{\partial \tan\beta_1} \frac{1}{\overline{V_x}(1+\tau_R\cdot(s+jn))} + \overline{V_{\theta 1}} - 1 & 1 \end{bmatrix} e^{jn\theta}. \quad (3.17)$$

This modification is used in the following study.

Inputs to the Dynamic Compressor Model

Due to the linearization, the mean flow-field parameters appear in the transmission matrices written in Equations 3.4, 3.6 and 3.17. As mentioned earlier, these parameters are provided by the mean-flow calculation and are the inputs to the dynamic model.

The required mean-flow parameters are $\overline{V_\theta}$, $\overline{V_x}$, α, β, the axial locations, the rotor and stator inertias λ_{rot}[2], λ_{sta}[3], and the sensitivity of total pressure loss to blade-row inlet flow angle $\frac{\partial L_S}{\partial tan(\alpha_1)}$.

All inputs are appropriate non-dimensionalized variables. Most of these parameters are either derived directly from the geometry or are output from the mean-flow calculation. The sensitivities of the total pressure loss to blade-row inlet angles are also computed in the mean-flow calculation. Some additional processing of these sensitivities is required and described in Appendix B.

Processing of Blade-Row Total Pressure Loss Characteristic

Appendix B describes in more detail the computational steps required to obtain the sensitivity of the total pressure loss to the blade-row inlet angles. Based on points computed from the Snecma data set, a least square fit is performed to represent the blade-row loss characteristic as a polynomial function of the blade-row inlet flow angle. With the proper settings, adequate fits for the pre-stall region are obtained (for high incidence angles). However, extrapolation outside the domain of the data provided by Snecma is much more uncertain. This is particularly striking in the case of the

[2]defined as $\lambda_{rot} = \frac{c_{xR}}{R \cdot cos^2\gamma_R}$
[3]defined as $\lambda_{sta} = \frac{c_{xS}}{R \cdot cos^2\gamma_S}$

first rotor, because only half of the loss bucket was provided in the original data.

However, using these blade-row total pressure loss characteristic and the results from the mean-flow calculation, the matrices described in Equations 3.4, 3.6 and 3.17 can be evaluated. In order to obtain the dynamics of the compression system, the eigenvalue problem (cf Section 3.2) must be solved. After all the input are processed as described above, the eigenvalue problem can be solved numerically.

Search Routines

Originally Implemented Search Routines Originally, Spakovszky [16] developed two numerical methods to determine the solution of Equation 3.2.

The first one, the "Contour Plot Method," is a graphical method which plots in the complex plane the zero-contours of the real and imaginary parts of the determinant of Y_{sys} (cf Equation 3.2). The eigenvalues are located at the intersection of these curves, i.e. where the complex determinant of Y_{sys} equals zero. This method provides helpful information about the location of the eigenvalues with moderate accuracy, but can be computationally expensive. The second one, the "Shot-Gun Method," is a highly efficient numerical procedure for determining the eigenvalues accurately. The main idea of the method is to fire a given number of random shots in the complex plane, centered around an initial target. The determinant is then evaluated only for these locations and a weight is attributed to each shot, based on the value of the determinant at this point. A center of gravity of all the points is then computed and selected as the target for the next round. The number of bullets is reduced by one and the new shots are fired. The convergence is reached in the last round when there is only one bullet remaining. The last target corresponds to the location of the eigenvalue. Due to its range limitation (fixed for each calculation), a good initial target for the first round is required. Consequently, the most efficient procedure is to combine adequately the two methods mentioned above, the "Contour Plot Method" providing an initial target for the "Shot-Gun Method."

These two methods were tailored for single stage compressors and provide very satisfying results for this case. However, for the present study that focuses on multi-stage machines, they have limitations:

- First, in their implementation, since each eigenvalue search has to be set individually.
- Second, the procedure of the "Shot-Gun Method" does not take advantage of the potential simplifications of this particular problem (reduction of the problem to $\mathbb{R}^+$), since it was developed as a general technique that can be applied to any multi-dimensional mapping function.

The challenge in the present case is to create a search framework that matches the needs for speed and robustness of the present problem. In order to address the need for robustness, the number of tuning parameters in the search algorithm must be reduced or suppressed, the dependency on the

initial guess has to be decreased and all the eigenvalues must be found in one single computation. To address the need for speed, a more efficient algorithm, tailored for this particular problem, must be chosen and implemented.

Improvement in the Search Algorithm: Addressing the Need for Computational Speed
Both original procedures were developed to study a function from $\mathbb{C} \rightarrow \mathbb{C}$, which creates inherent complexity as $\mathbb{C}$ is not an ordered space[4]. But as the only purpose in this search is to locate the roots of this function, the magnitude of the complex determinant can be chosen to be the objective function instead of the determinant itself. This causes no information loss since the magnitude of a complex number becomes zero under the same condition as the complex number itself. This way, the function of interest is defined from $\mathbb{C} \rightarrow \mathbb{R}^+$, a domain that can be identified with $\mathbb{R}^2 \rightarrow \mathbb{R}^+$. Consequently, the problem that needs to be solved is the following: finding the zeros of a two-variable real-value positive definite function, which are therefore its minima. This is typically an optimization problem for a single objective, two-variable function. Several existing optimization techniques are available and a selection of these techniques has been implemented for this particular problem, with source codes either from Matlab or from open software. Two types of techniques were tested: deterministic techniques and heuristic techniques.

Deterministic Techniques:

- Simplex Search Method [source: Matlab routine 'fminsearch'];
- Sequential Linear Programming [source: Matlab routine 'fmincon'];
- Steepest Gradient Technique [source: E.Blanvillain].

Heuristic techniques:

- Optimized Step Size Random Search [source: Sheela V. Belur routine 'ossrs'];
- Simulated Annealing [source: Lester Ingber routine 'asa'];
- Genetic Algorithm (GA) [source: Matlab routine 'ga'] ;
- Shotgun Method [5](which can be thought as a genetic algorithm with a drastic selection algorithm and no mating or mutation).

[4]the standard $\leq$ ordering rule does not apply to this space

[5]The original shotgun method was adapted here to be used as a standard optimization routine and applied to any problem. (source: Z.S.Spakovszky routine 'shotgun')

In order to really measure the effectiveness of each of these routines, tests must be performed in the worst conditions, i.e. when the number of roots to be searched for is relatively high (i.e. three sets of modes or more). Therefore, all routines are tested in the case of a multi-root problem (cf Section 3.3.2). The results show that most routines are unable to find all the roots of the problem and get trapped in local minima. Surprisingly, three of the four heuristic techniques get trapped in local minima. Only the Shotgun Method manages to find all the roots but requires a long computation time due to the high number of calculations required. Moreover, good guesses are mandatory to avoid the Shotgun Method being trapped. On the other hand, two deterministic techniques perform quite well: the Simplex Search Method and the Sequential Linear Programing. It turns out that the Simplex Search requires about two time less computational time than the Sequential Linear Programing. Therefore, this technique will be used for all eigenvalues searches.

Improvement in the Search Method: Addressing the Need for Robustness In the current problem, several roots per harmonic are found. Therefore, the search algorithm must be run several times with several initial guesses provided by the contour plots method. A set of harmonics (usually from 1 to 6) will be associated with each initial guess. However, it may happen that the search algorithm finds the same root twice, even with different initial guesses. Therefore, the program has to track the roots previously found so that they are not selected twice. So after each root is determined, it is stored in a database and every time a new root is found, it is compared to this database. In case the root is already in the database, the search method will be repeated, but with a different initial guess. Because there is high confidence in the initial guesses (from the contour plot method), the previous initial guess will be kept and only a small random offset in both σ and ω direction will be added to it to get the new initial guess. This method works but does not always guarantee that the roots are found quickly since it may take many different initial guesses before the correct root is found. This process relies heavily on a random number generator that generates the new initial guess. To make sure that no root can be found twice or more, Penalty Methods will be implemented.

Penalty Methods Penalty methods is a term often referred in optimization problems to implement constrained problems, i.e. to prevent the search algorithm to look in a certain region of the design space. In the present case, the constraint is that no eigenvalue should be found more than once. To better understand the requirements for these penalty methods, visualizing the determinant on a 3D-plot can be useful. It appears that there are sinks corresponding to the zeros of the function. The search algorithm basically "falls" into these sinks to find the zeros. An effective way to find the zeros no more than once is to fill the sink as soon as the zero associated with it has been found. However, a careful approach is required since:

- The creation of local minima where the search algorithm could be trapped must be avoided;
- The creation of obstacles that could prevent the search algorithm to access the entire domain must be avoided;
- The risk of accidentally filling a neighbor sink is potentially high.

Consequently,

- The penalty function must be compact (in the spatial sense) and have a "peaky" shape ;
- The penalty function must apply very locally.

The Gaussian function will be selected as the candidate penalty function. A detailed description of these penalty methods is described in Appendix C.

In order to assess the efficiency of the penalty methods, a test is performed for a 2-stage compressor, without unsteady loss time-lags. Six harmonics per set of modes are considered, so that twenty-four eigenvalues must be found. To be able to benchmark effectively the search algorithms, poor initial guesses are selected, i.e. (0,0) for each set of modes. The average number of iterations needed to find all the roots is computed and averaged over ten runs. The results of this test are given in Table 3.2.

Search Routine Implemented	Number of iterations required
Baseline	777
With Penalty Methods	126

Table 3.2: Performance of the Baseline Search Routine Compared to an Improved Routine with Penalty Methods

The improvement obtained from the penalty methods is significant. However, the number of iterations is still about five times what the optimal number would be. Other improvements are therefore required and are addressed below.

Initial Guess Even if the penalty methods help in this respect, the time associated with the root search still strongly depends on the quality of the initial guesses. And since the contour plot does not always explicitly shows all the roots (unless very detailed zoom is performed over the entire area, which is long an tedious), inappropriate guesses can lead to an unsuccessful search. So, the next step in improving the code is to find a way to reduce the dependence on the initial guesses. Because the observation is made that the harmonics are usually lined-up, the root obtained for the previous harmonic can be used as an initial guess for the current harmonic. This process is illustrated in Figure 3-6.

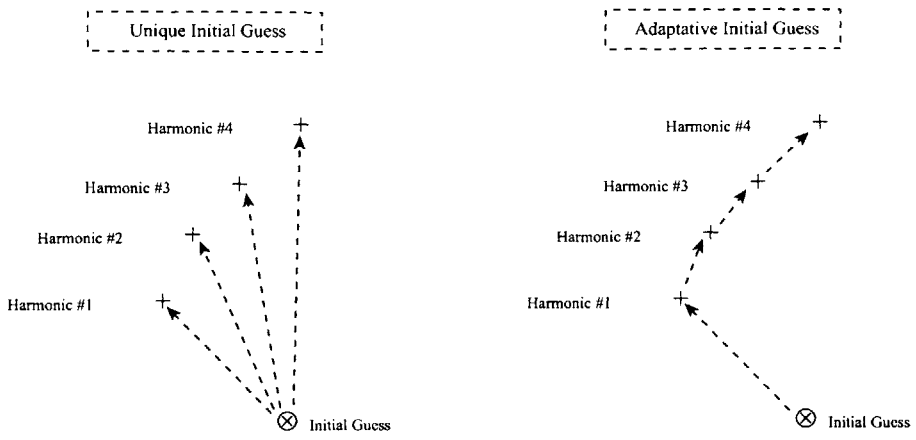

Figure 3-6: Improvement in Initial Guess

The advantage of this technique is that if the initial guess is poorly chosen, this affects the search process for the first harmonic only. For the others, the initial guess is always close and the root is usually found within two or three iterations at most. Therefore, the search is only time expensive for the first harmonic associated with each target. The same test as the one conducted for the penalty methods is performed. Results are given in Table 3.3. These results demonstrate the significant

Search Routine Implemented	Number of iterations required
Baseline	777
With Improved Initial Guess	30

Table 3.3: Compared Performances of the Baseline Search Routine and the Improved Routine with Improved Initial Guess

improvement obtained by using improved initial guesses. This is a great improvement since it allows the user to be less dependant on the contour plot method, which is time consuming and difficult to adjust.

Therefore, both improvement in the initial guess and penalty methods are implemented for all computations.

3.3.3 Application of the Dynamic Compression Model to the CREATE Compressor

In this section, the methods previously derived are applied to the candidate Snecma compressor, to provide insight about the pre-stall dynamics of this 3-stage machine. At first, several studies of the CREATE compressor are made, for both isolated stages and the full machine. Eigenvalue descriptions are provided in each case. A special focus is then put on the evolution of these modes

to the onset of instability.

Description of the Compressor System Eigenvalues

For a better understanding of the compressor dynamics, a progressive approach towards complexity is used here, starting with one isolated stage of the CREATE compressor.

Note: The reference points shown in Figure 3-7 are constructed using the mean line calculation for the data points provided by Snecma.

The results are depicted on Figures 3-7 and 3-8, and show the eigenvalues of CREATE's second stage, in an isolated case[6], with and without unsteady loss time-lags.
The results without unsteady loss time-lags display a pattern similar to what Spakovszky [16] described. In the present case, the gap length Δx, non-dimensionalized by the mean radius, is about 0.05 which has been referred in [16] to a regime of "Strong Interaction." The two modes per harmonic observed here are consistent with the behavior corresponding to this regime, one being close to the stability limit and one being highly damped.

When the unsteady loss time-lags are introduced, two more modes appear, one associated with each blade-row. These modes are not critical to the compressor stability but impact the two previous modes, affecting the least stable mode, and thus the overall stability of the compressor, as previously stated by Frechette [11]. The major impact of the unsteady loss time-lags on the compressor stability is a stabilizing effect. Consequently, using a simplified model without unsteady loss time-lags is simply a more conservative approach to stability estimation.

After the tools are compared to the results from Frechette [11] and Spakovszky [16] for the case of a single-stage compressor, and validated, the interaction effects are studied in a more complex environment: the full 3-stage compressor.

A simple guess would be to expect the eigenvalue map of the 3-stage compressor to be the compilation of the eigenvalue maps of the three isolated stages, with three highly-damped modes and three low-damped modes for the case without unsteady loss time-lags. However, Figures 3-9 and 3-10 shows that the blade-row interaction effects play a very significant role in a multi-stage environment and that therefore the result is different from the simple guess. For the case without unsteady loss time-lags, for each harmonic, only one mode is low-damped, whereas five are highly damped. It is too early at this point to determine the dynamic behavior of each mode. This topic is addressed in Chapter 4.

When time-lags are introduced to model unsteady losses, additional dynamics appear, with the presence of one more set of modes per blade-row. These six new modes are very close to each other,

[6] i.e. with infinite upstream and downstream ducts

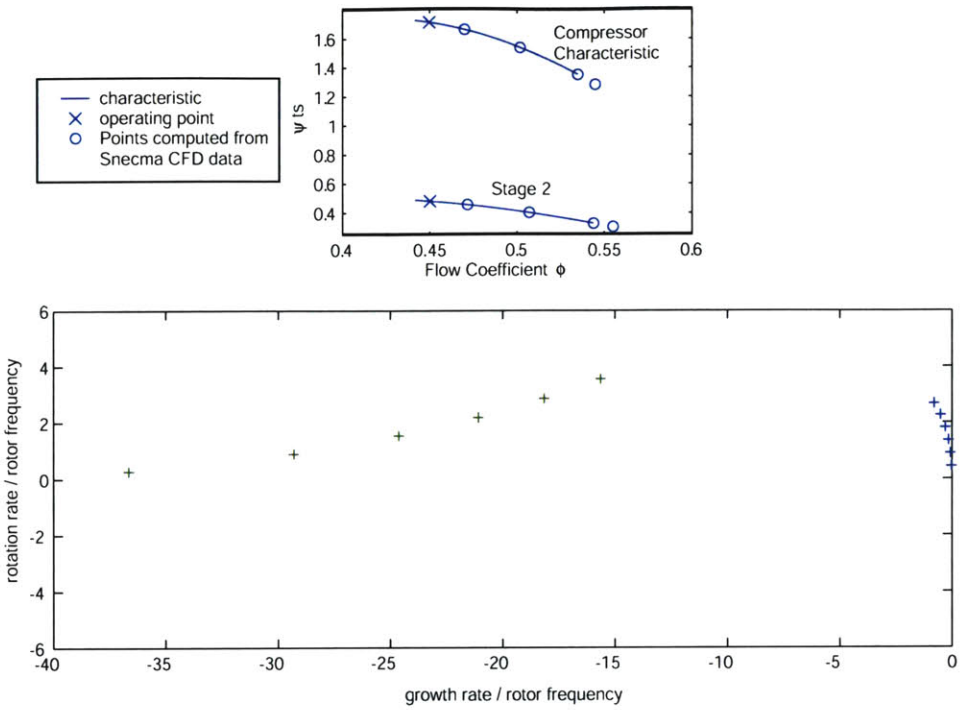

Figure 3-7: A: Eigenvalues of the Isolated Second Stage of the CREATE Compressor without Unsteady Losses Time-Lags

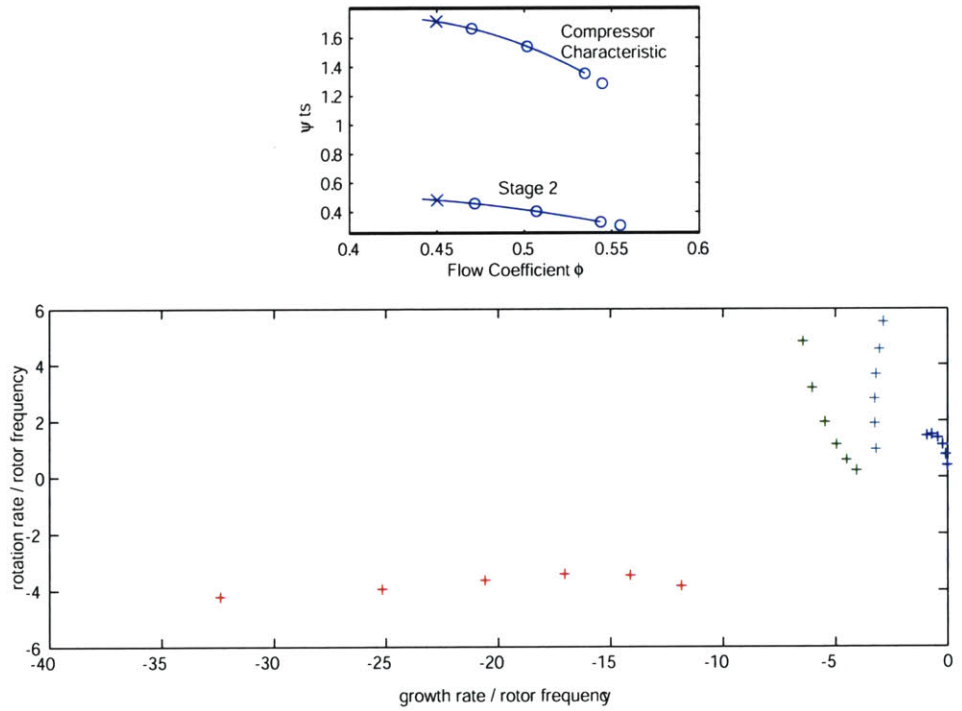

Figure 3-8: B:Eigenvalues of the Isolated Second Stage of the CREATE Compressor with Unsteady Losses Time-Lags

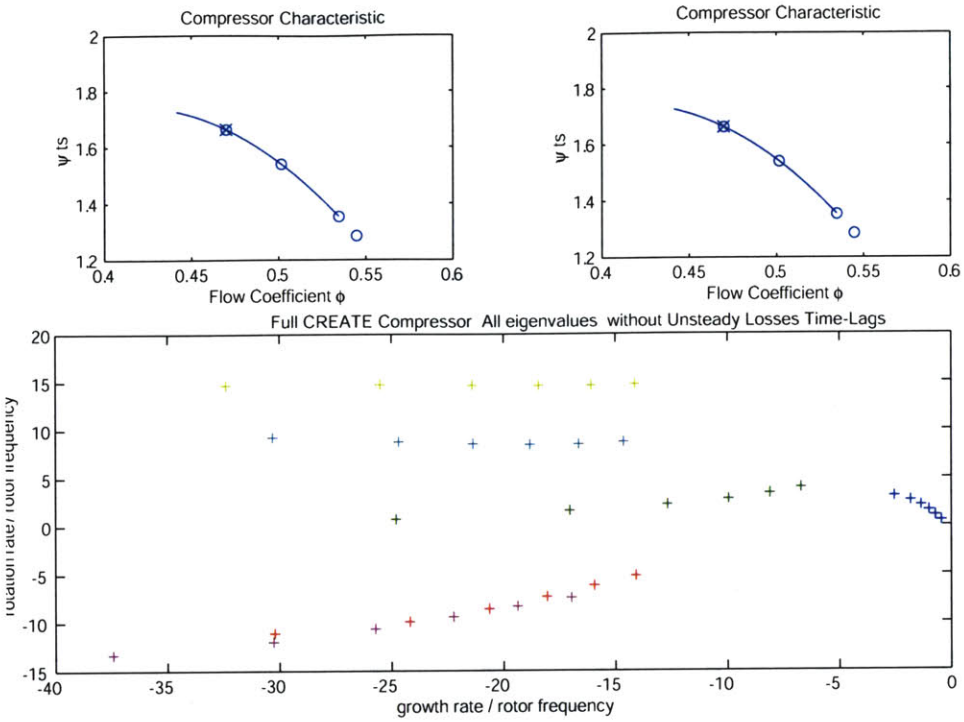

Figure 3-9: A: Eigenvalues of the Full CREATE Compressor without Unsteady Losses Time-Lags

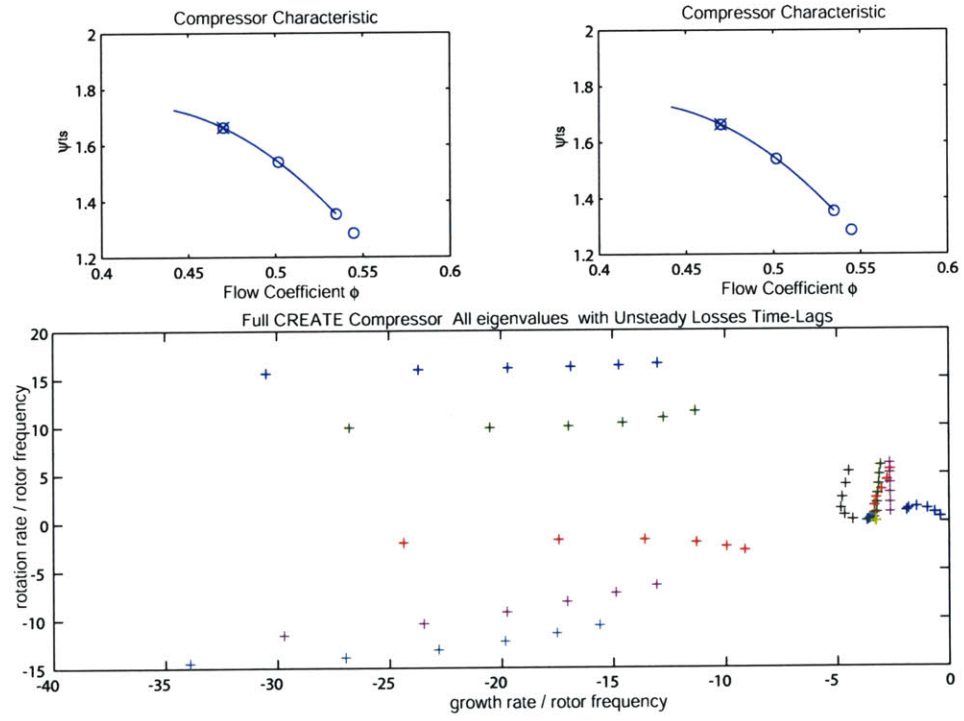

Figure 3-10: B: Eigenvalues of the Full CREATE Compressor with Unsteady Losses Time-Lags

potentially illustrating a similar behavior due to a similar physical origin. In this case, the presence of these new modes seems to have a repelling effect on the previous modes. This behavior is explained by an analogy with control theory where the poles tend to repel each other (as previously stated by Spakovszky [16]).

At this stage, providing explanations for the previous results is challenging, due to the complexity of the system modeled (variable flow path, different stage designs and matching, different inter blade-row gaps). In order to address these issues, there is a need for a simpler model of a standard 3-stage compressor, with constant duct area, repeating stages with 50% reaction, using an incompressible mean-flow calculation.

Path into Instability

Let's consider the case of the 3-stage CREATE compressor without unsteady loss time-lags. It has been noticed above that there is only one set of modes critical to compressor stability. This is confirmed by Figure 3-11, for the CREATE compressor without unsteady loss time-lags at instability point.

The focus is therefore on this set of modes. The eigenvalues are plotted for various flow coefficients in Figure 3-12.

As the flow coefficient decreases, incidence angles tend to increase on the blade-rows, thus increasing the risk of blade stalling and moving towards lower stability. Figure 3-12 illustrates this point since the growth rate σ of the low-damped modes gets closer to zero as the flow coefficient decreases. Note: The flow coefficients selected correspond, on the left, to the last data point provided by Snecma, and on the right, to the instability limit. For the CREATE compressor, the dynamic instability limit is therefore outside of the domain covered by the data from Snecma. This is discussed later in this section.

The instability point is reached for $\phi = 0.443$ here and the first harmonic becomes unstable first. A possible validation to this result would be to compare this value to the one from the actual CREATE compressor. However, the only information available in this respect is the last data point provided ($\phi = 0.47$), computed from CFD. This does not mean that this point is actually the stability limit but rather that for this point, the CFD model, and consequently the flow field, is still stable. So, having a flow coefficient for the instability point smaller than this value is expected. However, the value obtained ($\phi = 0.443$) is far from this last data point available (about 40 % off the range of data). This can be problematic in two ways: first it might indicate that the instability limit predicted here is far from the one obtained from CFD and second, the farther the flow coefficient is from the set of data available, the lower the confidence in the extrapolations performed on the

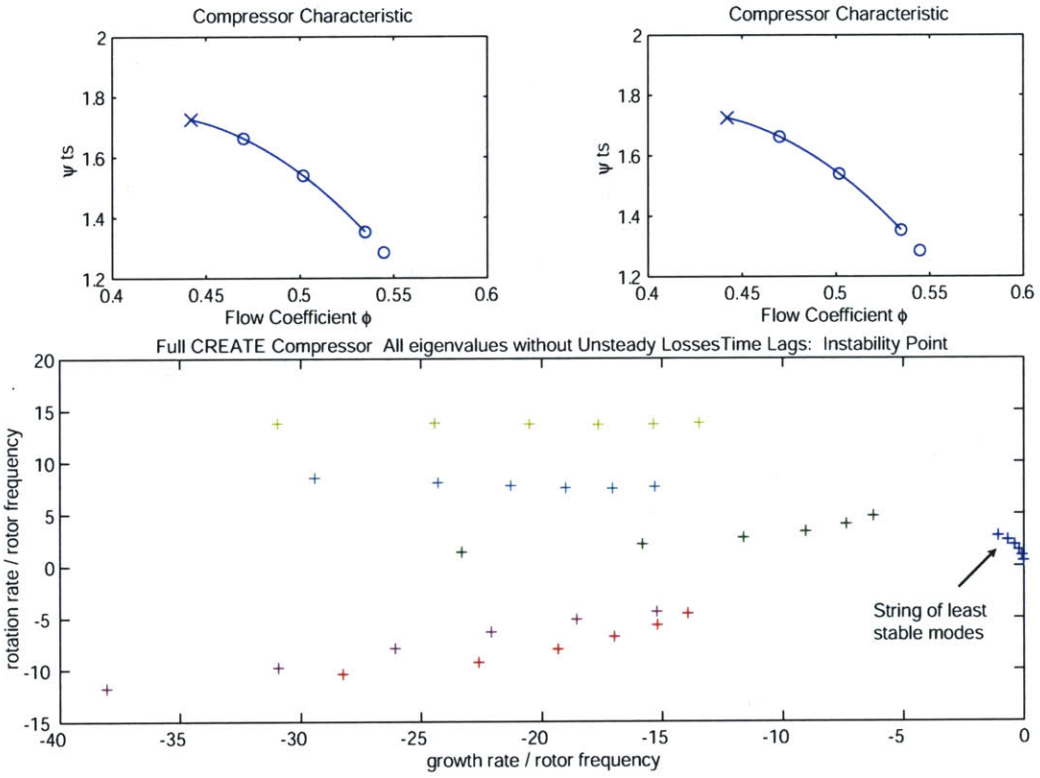

Figure 3-11: Eigenvalues of the Full CREATE compressor without Unsteady Losses Time-Lags - Instability Point

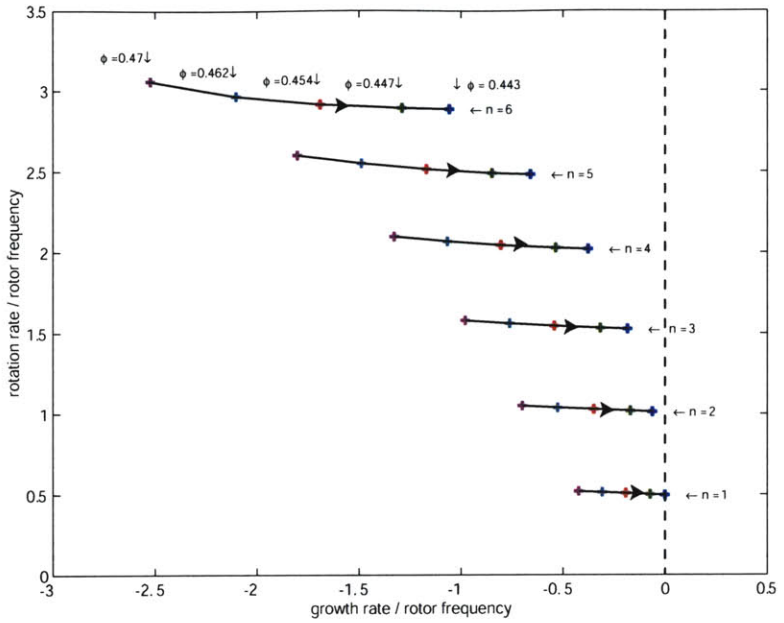

Figure 3-12: Locus of the Low-damped Eigenvalues of the Full CREATE Compressor as the Flow Coefficient Decreases

blade-row performance curves and thus the confidence in the results.

Independent study of the stages could bring an explanation to this behavior. The instability limits in terms of flow coefficient are summarized in Table 3.4. The variation of the compressor stable operating range is also computed in Table 3.4(this concept is more thoroughly discussed in Section 4.3.3). First, as mentioned in Longley [13], a full compressor is supposed to be less stable than its individual stages. In Figure 3-12, the instability point for the entire compressor is obtained for $\phi = 0.443$ whereas for the second stage alone presented in Figure 3-8, ϕ was 0.450 for instability. This conflicts with the argument from Longley, that was established for repeating-stages compressors. This unusual behavior might therefore relate to mismatched stages, as suggested by Cumpsty [5] [p369-370]. If stages 2 and 3 are now stacked together, instability is reached for $\phi = 0.458$ (above $\phi = 0.450$) (cf Figure 3-13), thus illustrating the effect mentioned by Longley [13].

CREATE Configuration	Flow Coefficient at Instability Limit	Stability Gain
Stage 1 only	0.405	+41%
Stage 2 only	0.450	-7.6%
Stage 3 only	0.451	-8.6%
Stages 2 and 3	0.458	-16.3%
3-stage CREATE compressor	0.443	0%

Table 3.4: Instability Limits for Different Configurations of the CREATE Compressor

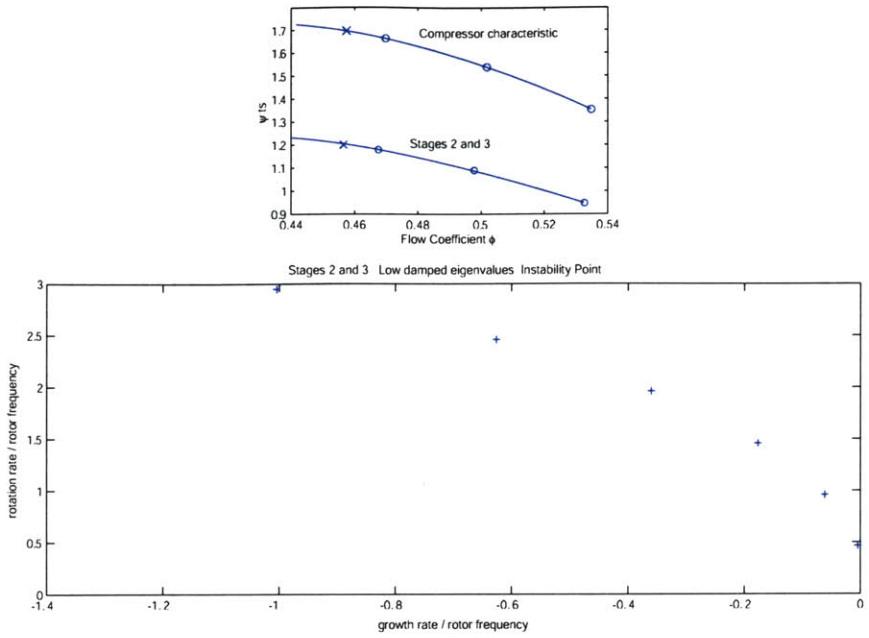

Figure 3-13: Eigenvalues of Stage 2 and 3 of the CREATE Compressor Stacked - Instability Point

Based on these observations, the reasons for the high stability of the compressor might lie in the first stage. If studied separately, stage 1 reaches instability for $\phi = 0.405$, which is far from the last data point available (about 90% off the range of the data). It is then suggested that stage 1 might be responsible for this unexpectedly-high level of stability. The first rotor operates at negative incidence at design point and at a very small incidence over the rest of its operating range, which suggests that it is only likely to stall at low flow coefficients, and therefore is very stable. The uneven stage-matching of the CREATE compressor generates an extra complexity that cannot be easily handled in the early stages of this analysis. Therefore, in Chapter 4, the analysis is conducted on a repeating stage compressor.

3.3.4 Conclusion and Derived Requirements for the Dynamic Model

The results from 3.3.3 provide very useful insights about the dynamics of the 3-stage CREATE compressor. It especially highlights the fact that in all situations, based on this existing design and in the domain studied, only one set of eigenvalues is critical to the compressor stability and therefore most of the attention must be focused on this set of modes for design improvements.

In order to be able to improve this design for stability, interactions between the design parameters and the compressor's stability have to be established. But, in order to understand the physical phenomena that initiate these interactions, a much simpler compressor is required. A constant duct area

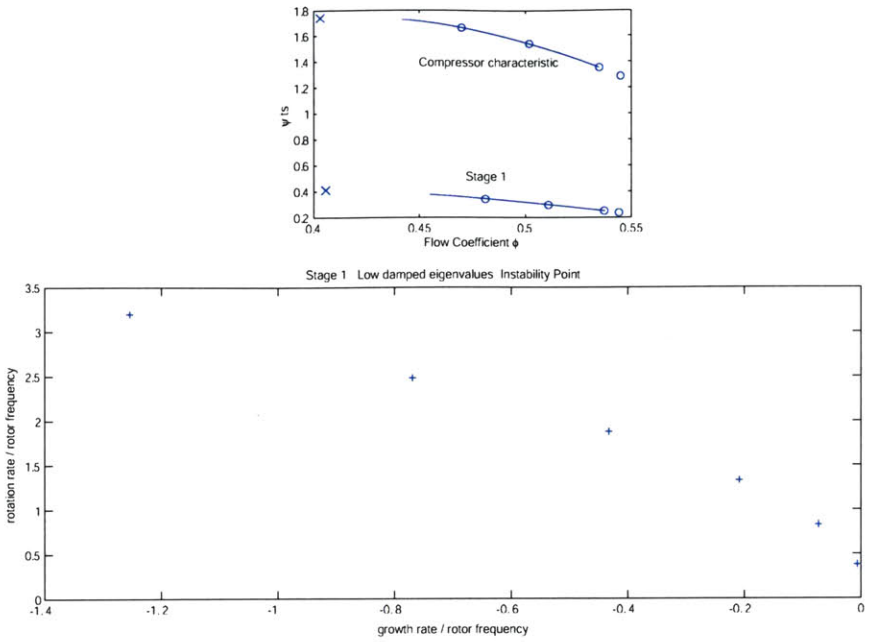

Figure 3-14: Eigenvalues of the Isolated First Stage of the CREATE Compressor without Time Lags

compressor is therefore chosen for the next step, with data provided by an incompressible mean-flow calculation, and repeating stages with 50% reaction. This model is used in the next chapter.

In spite of the interesting trends obtained from 3.3.3, the results have proved not to be completely satisfying. This can be attributed to the numerous transformations required to generate the appropriate data, that therefore introduce errors and bias in the process. In addition, it has been shown that CFD might not be the most appropriate tool to generate the required data. So an ideal solution would be to have a tool that could produce the blade-row performance for each blade-row as a function of the compressor mass flow. If such a tool was available, it would also enable numerous calculations to be performed in the region of interest and would consequently allow the total pressure loss sensitivity to blade-row inlet flow angle (i.e. the slope of the blade-row loss curves) to be computed using finite differences instead of derivative of polynomials. Moreover, such a tool could include the Mach number dependency on the blade-row performance curves, as well as a flow angle deviation model, which would both allow further developments of the present analysis. All these needs combined could be addressed by a mean line deck, which would be the most appropriate data generator for the next step of the project.

Chapter 4

Analysis of Blade-Row Interaction on Compressor Stability in a Multi-Stage Environment

4.1 Statement of Objectives

The objective of this chapter is to understand how the overall stability of the multi-stage compressor is influenced by the compressor geometry and individual blade-row performance. This will help to establish design guidelines for a compressor designed for increased dynamic stability. In this study three effects are considered:

1. The effect of blade-row inertia, defined as $\lambda = \frac{c_x}{R \cdot cos^2\gamma}$ and governed by the blade chord and stagger angle;
2. The effect of blade-row performance, expressed in terms of sensitivity of total pressure loss to blade-row inlet flow angle, $\frac{\partial L}{\partial tan(\beta)}$;
3. The effect of axial coupling, driven by the inter blade-row gap lengths, as stated by Spakovszky [16].

4.2 Impact of Design Parameters on Dynamic Stability

Based on the analysis conducted in Chapter 3, it can be conjectured that only one string of modes is critical to the compressor stability, and that this string of modes is driven by the dynamics of all blade-rows. The effects described above are therefore studied for all blade-rows. The stabilizing

effect on the critical mode are measured in terms of flow coefficient gain, scaled by the range of flow coefficient considered.

As previously stated in Chapter 3, the lower the flow coefficient associated with the stall point, the more stable the compressor studied is. Therefore, a way to measure the dynamic stability improvement associated with changes in the compressor design is to use the improvement obtained in flow coefficient. This improvement is non-dimensionalized by the "range" of flow coefficient, as shown in Figure 4-1. The metric obtained is named "Stability gain".

$$Stability\ gain\ =\ \frac{\delta\phi}{\Delta\phi} \tag{4.1}$$

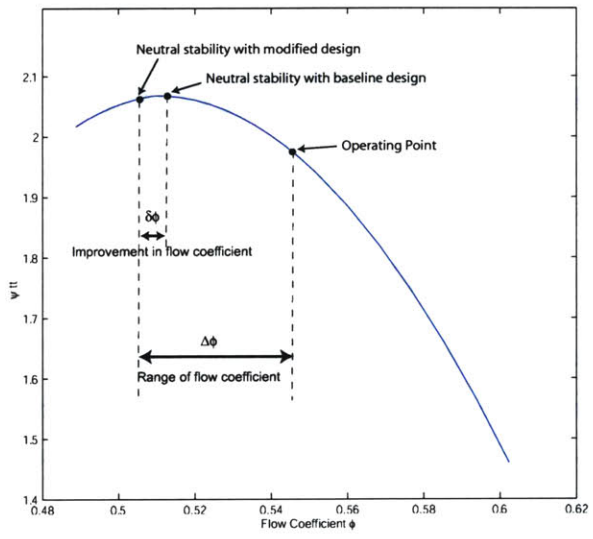

Figure 4-1: Measure of Improvement in Stability

Each of the effects listed in Section 4.1 is computed and improvements associated can be seen from the compressor characteristic depicted in Figure 4-2, (which is a close-up of the upper part of the characteristic shown in Figure 4-1.) Table 4.1 summarizes all the different improvements in stability gain generated by the design changes considered.

Effect Studied	Stability Gain
Blade-Row Inertia Redistribution	0.03%
Gap-Length Redistribution	4.60%
10% Reduction in Total Pressure Loss Sensitivity to Inlet Flow Angle	6.54%

Table 4.1: Effects of Design Changes on Stability Gain

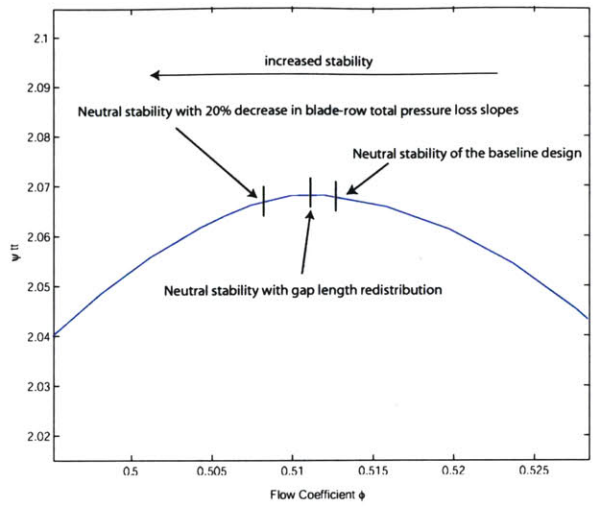

Figure 4-2: Comparison of Effects of Blade-Row Performance and Gap Length Redistribution on the Flow Coefficient at Neutral Stability

These results demonstrate that noticeable stability gain improvement can be obtained by applying the changes previously mentioned to the design of the compressor. An analysis of each of the three individual effects is conducted next, in order to obtain a better understanding of how these effects influence the compressor stability.

4.3 Detailed Analysis of Blade-Row Interaction

4.3.1 Description of the Standard Compressor

Following the recommendations made in Chapter 3, a compressor of simpler geometry and performance than the CREATE compressor is implemented here. The objective of this thought experiment is to capture to the first order all the dynamic effects in a multi-stage environment. The following design choices are therefore made:

- Incompressible mean-flow calculation with constant-area ducts;
- 50% reaction blading with constant axial velocity (cf. Figure 4-3);
- Four repeating stages;
- Uniform axial coupling between each pair of blade-rows;
- Generic loss bucket(cf. Figure 4-4);
- No deviation and no blockage modeled.

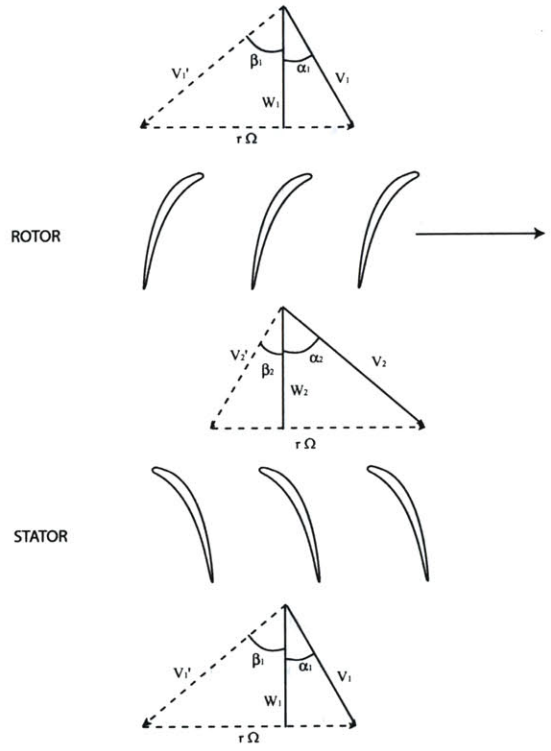

Figure 4-3: 50% Reaction Blading with Constant Axial Velocity

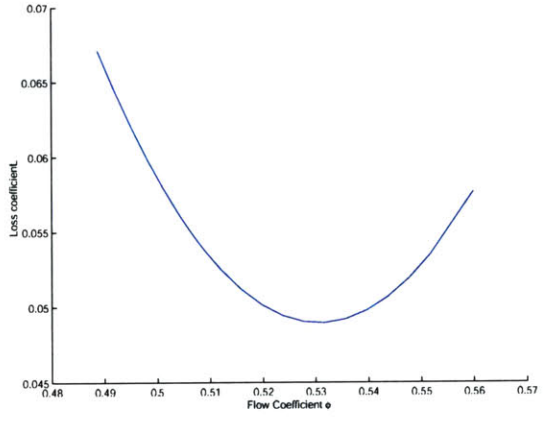

Figure 4-4: Standard Loss Bucket

This 4-repeating-stage compressor will be referred to as the "4-stage standard compressor."

To validate the tool adapted and extended in Chapter 3, the dynamics of the standard compressor are first modeled according to a classical Moore-Greitzer [14] formulation, i.e., the following assumptions are made:

- All blade-rows are lumped into a single semi-actuator disk (no gaps between blade-rows);
- No unsteady loss effects are modeled;
- The isentropic compressor characteristic is considered swirl-insensitive.

Under these assumptions, the linearized Moore-Greitzer solution [16] yields, for the growth rate σ_n and the rotation rate ω_n of the n-th spatial pre-stall harmonic mode:

$$\sigma_n = \frac{\frac{\partial \psi^{ts}}{\partial \phi}}{\mu + \frac{2}{n}} \quad \text{and} \quad \omega_n = \frac{\lambda\, n}{\mu + \frac{2}{n}} \,. \tag{4.2}$$

The solution shows that the compression system is neutrally stable when the slope of the total-to-static pressure rise characteristic becomes zero. For this flow coefficient, all spatial harmonic pre-stall modes are neutrally stable, since the numerator of σ does not depend of n. The results for spatial harmonic modes n=1 through n=6 are shown in Figure 4-5.

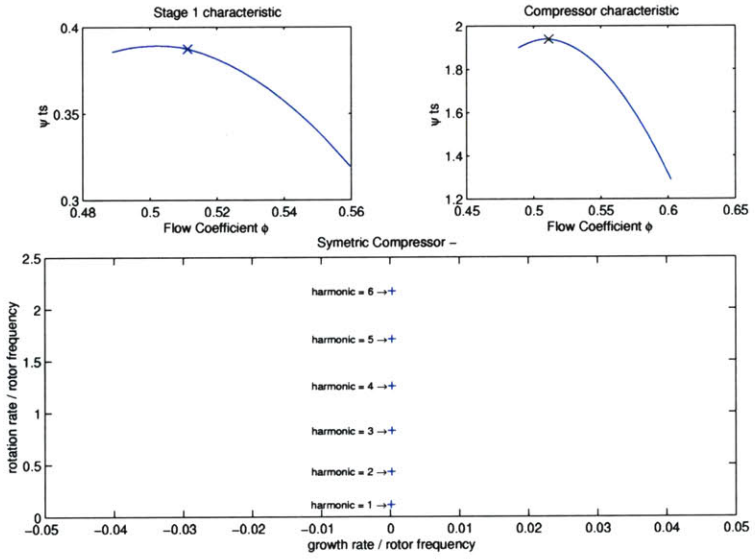

Figure 4-5: Results for the Moore-Greitzer Formulation of the Dynamics of the 4-Stage Standard Compressor

The results show that the modes are neutrally stable when the flow coefficient corresponds to the flow coefficient at the peak of the characteristic, i.e., when the slope of the characteristic becomes

zero. In addition, when the flow coefficient is decreased past this peak, the modes become unstable. The model implemented here for the multi-stage machine is therefore consistent with the Moore-Greitzer [14] formulation.

4.3.2 Description of the Compressor Modes

In Chapter 3, the dynamic analysis of the CREATE compressor has shown that only one string of modes was critical to the compressor stability. A similar finding for the 4-stage standard compressor presented in this chapter would allow further analysis to be performed on this string of modes only. An eigenvalue search is therefore conducted for this compressor to confirm this conjecture. To perform the calculations, the Moore-Greitzer assumptions are relaxed: gaps are introduced, a swirl-sensitive characteristic is introduced, and unsteady loss effects are considered. Results are shown in Figure 4-6 for harmonics n=1 to n=6, for the flow coefficient corresponding to neutral stability.

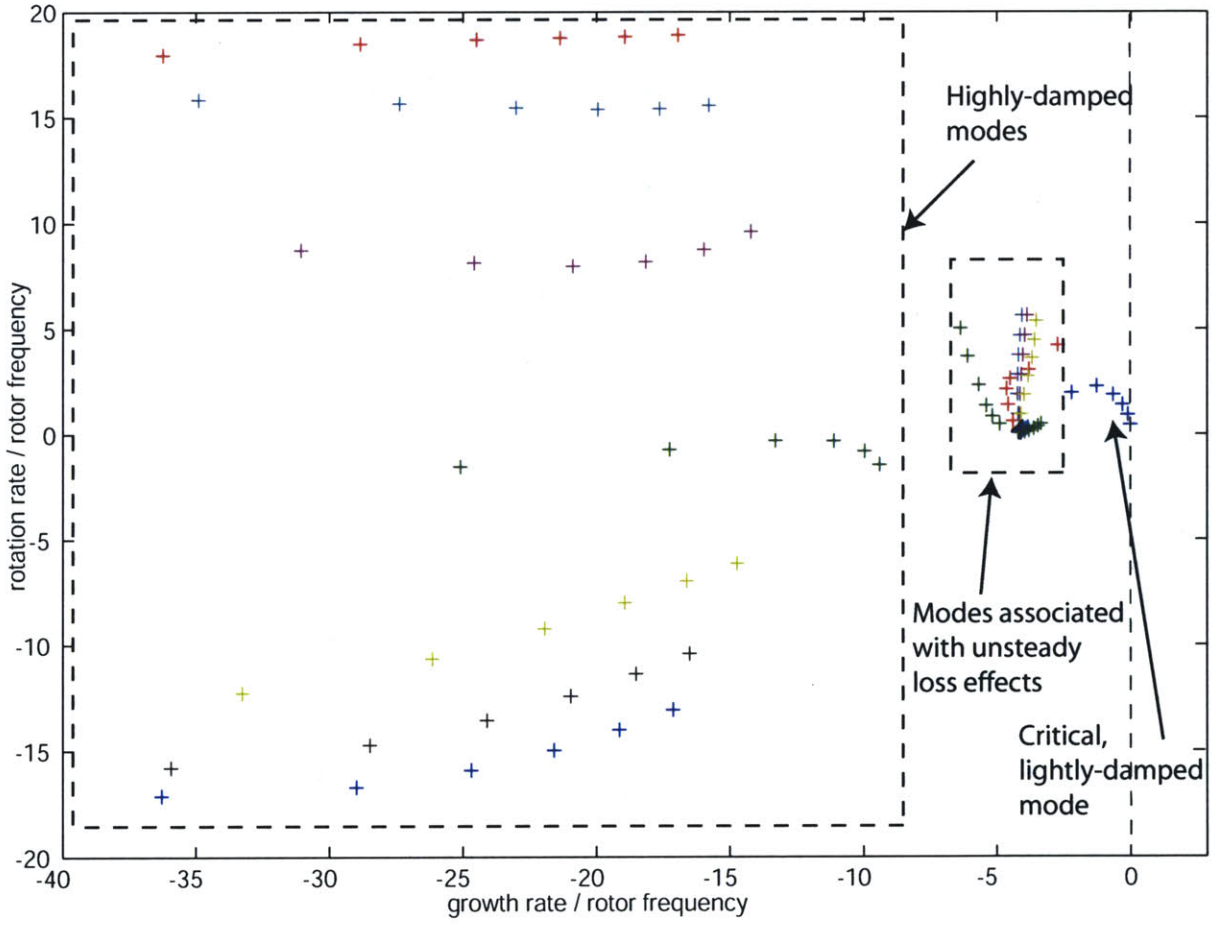

Figure 4-6: Eigenvalue Map of the 4-Stage Standard Compressor

As expected, only one string of modes is lightly-damped. This string is therefore the most critical for compressor stability. This analysis therefore focuses on this string of modes. Second, the overall structure of the system eigenvalues is similar to the one obtained for the CREATE compressor in Section 3.3.3. On a harmonic basis, the system modes are grouped as follows for the 4-stage standard compressor (which has eight blade-rows): seven very highly-damped modes, eight modes induced by unsteady loss time-lags, and one critical lightly-damped mode. There are consequently sixteen modes per harmonic, i.e. two per blade-row (including one induced by the unsteady loss effects). For further details on the analysis of the predominant effect of one blade-row on a mode, see Appendix D.

4.3.3 Detailed Analysis of the Lightly-Damped Mode

The hypothesis has been made earlier in this chapter that the lightly-damped mode (for all its harmonics) truly is, a "system mode" in the sense that it is influenced by all the components of the compressor system. This does not imply, however, that all blade-rows and the coupling between them influence this mode identically. The effect of the dynamics of each individual blade-row must therefore be considered separately.

The effects of three parameters on compressor dynamic stability are studied here:

- The effect of blade-row inertia defined as $\lambda = \frac{c_x}{R \cdot cos^2\gamma}$, governed by the blade chord and stagger angle;
- The effect of total pressure loss sensitivity to inlet flow angle blade-row;
- The effect of the gap length between blade-rows.

Effect of Changing Blade-Row Inertia

To assess how the critical mode is affected by changes in blade-row inertia, the inertia of each blade-row is doubled independently (e.g. the blade chord is doubled or the stagger angle is increased accordingly). The resulting eigenvalues are then computed. It can be observed that all harmonic modes are similarly affected by changes in the blade-row inertias. Harmonic #1, the least stable mode, is selected to illustrate this trend (cf. Figure 4-7).

The first observation is that doubling the inertia of any blade-row stabilizes this mode. The second observation is that an ordered pattern is evident here: increasing the blade-row inertia of any of the rotors is more beneficial than increasing the blade-row inertia of any of the stators. In addition, the most stabilizing effects come, among the rotors, from the *upstream rotors* (i.e. rotors closer to the compressor inlet), and among the stators, from the *downstream stators* (i.e. stators closer to the compressor exit). This pattern is also observed for other harmonics. From these

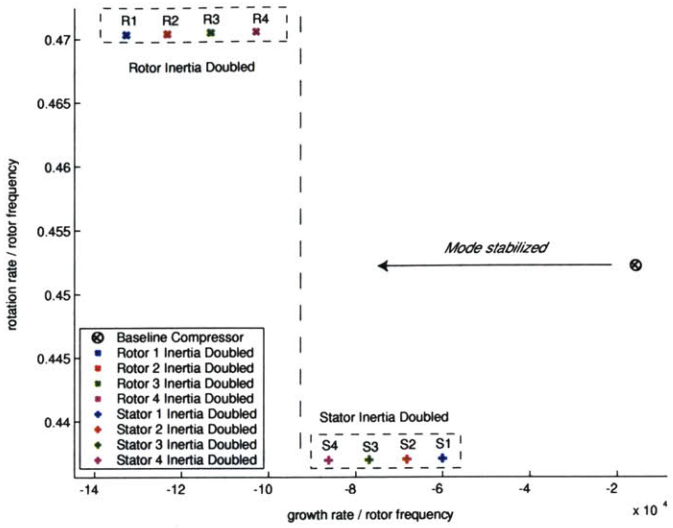

Figure 4-7: Inertia Sensitivity on the Critical Mode: Harmonic #1

observations, it is clear that changing the inertia of some specific blade-rows is more beneficial for compressor stability than changing the inertia of other blade-rows. Selective changes are made to obtain increased stability by a more adequate blade-row inertia redistribution.

The assumption is made that, to avoid an undesirable increase in compressor weight, the sum of all blade-row inertias should remain constant, and equal to the value for the baseline compressor. The inertia is increased by 50% for all the rotors, and decreased in all the stators by 50% to keep the sum of blade-row inertias constant. The change in stability gain following this blade-row inertia redistribution is only 0.01%, which is negligible and not worth a design change. The effects of blade stagger angle and chord length on dynamic stability are thus negligible. The focus now shifts to another compressor parameter that potentially drives the dynamics: the sensitivity of total pressure loss to blade-row inlet flow angle.

Effect of Modifying the Sensitivity of Total Pressure Loss to Blade-Row Inlet Flow Angle

Unlike blade-row inertia, which can be expressed analytically as a function of blade chord and stagger, the total pressure loss cannot be written as an analytical function of the aerodynamic and geometric parameters of the compressor. The losses thus cannot be assigned a value by a design choice. They are therefore "implicit" design variables, both aerodynamically driven (blade loading, etc.) and geometrically driven (blade profile, etc.). At this stage of the joint project, no tool is available to characterize the blade-row performance as a function of these aerodynamic and

geometric parameters. The need for this tool for future work has already been discussed in Chapter 3.

To determine the effect of blade-row performance on compressor dynamic stability, the following calculations are conducted. The flow coefficient is set such that the baseline compressor is neutrally stable. Then, for this given flow coefficient, the sensitivity of the total pressure loss to the blade-row inlet flow angle (i.e., the slope of the curve presented in Figure 4-8) is decreased by 10% for each blade-row independently.

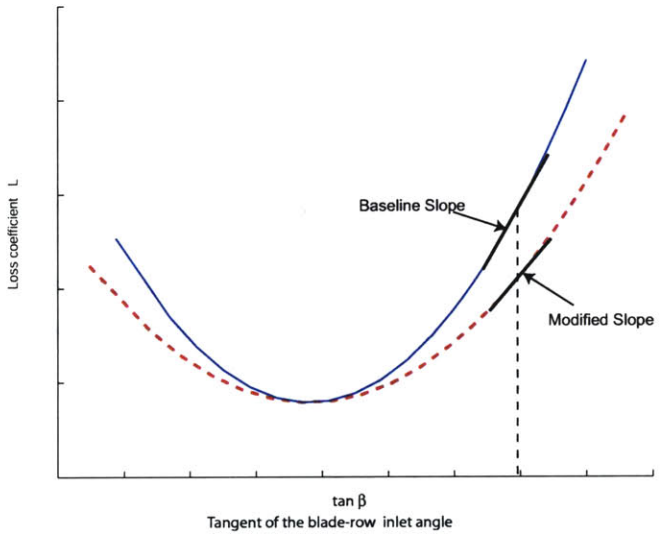

Figure 4-8: Modifying the Sensitivity of Total Pressure Loss to Blade-Row Inlet Flow Angle

The effect on the first harmonic of the critical mode is depicted in Figure 4-9. The first observation is that all rotors and stators behave in a similar way, and have almost the same stabilizing effect. It is therefore difficult to assess an optimal design. The choice is thus made to modify all blade-row performance curves identically.

In terms of stabilizing effects, a 10% decrease in the sensitivity of total pressure loss to blade-row inlet flow angle for any blade-row produces a 0.7% improvement in stability gain, which is only slightly better than the results obtained when changing the blade-row inertias. However, if a 10% reduction in the sensitivity of total pressure loss to blade-row inlet flow angle is simultaneously applied to all blade-rows, the improvement in terms of stability gain becomes 6.54%. Similarly, if the reduction is 20%, the improvement in stability gain is 14.27%, and if the reduction is 30%, the improvement in stability gain is 24.26%. These results indicate a non-linear trend. Significant improvement in stability gain can therefore be obtained only if the sensitivity of total pressure loss to blade-row inlet flow angle is decreased by more than 20%. However, as previously explained,

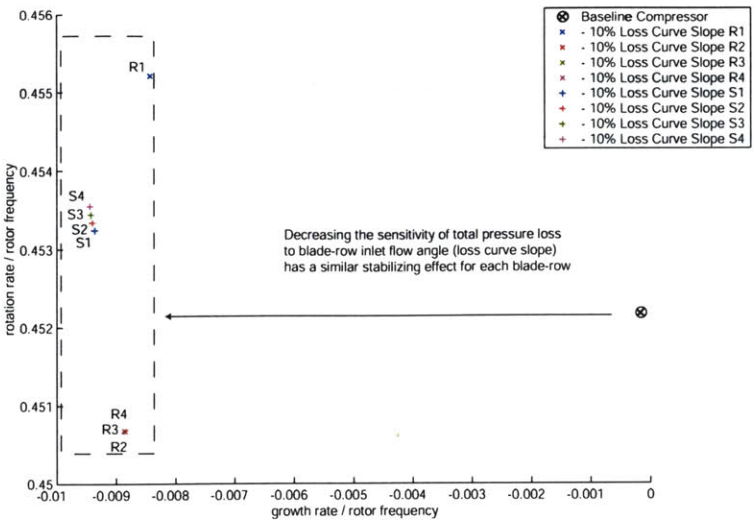

Figure 4-9: Loss Slopes Sensitivity on the Critical Mode: Harmonic 1

it cannot be determined at this point whether a 20% reduction is achievable or not. Establishing whether an improvement of such magnitude is feasible, as well as the design changes that might produce it will be a major focus of future work.

Axial Coupling: The Effect of the Gap Lengths

For a single-stage compressor, Spakovszky [16] has shown that changing the length of the duct between the rotor and the stator greatly affects the stability of the system.

Similarly to what was done earlier for the blade-row inertia, each gap length is doubled independently and the resulting system eigenvalues are computed. The nomenclature used for the gaps is shown in Figure 4-10. The gaps labeled with numbers are intra-stage gaps, i.e. between rotors

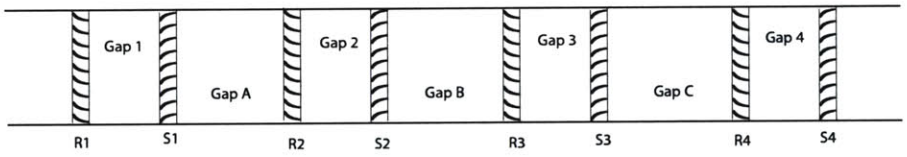

Figure 4-10: Gaps Nomenclature

and stators, whereas the gaps labeled with letters refer to inter-stage gaps, i.e. between stages. The results for the critical string of modes for harmonics n=1 to n=6 suggest the following: intra-stage gaps (axial gap between rotor and stator) have a stabilizing effect when their length is increased; and inter-stage gaps (axial gap between stator and rotor) have a destabilizing effect when their length

is increased. This is observed for all harmonics and only harmonic #1 is shown in Figure 4-11.

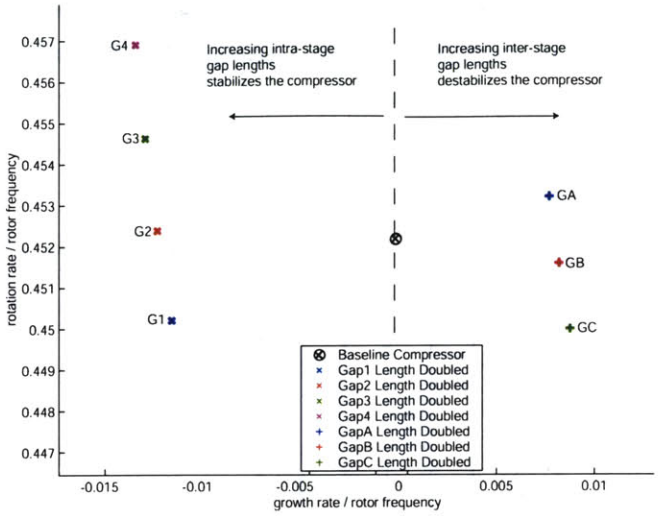

Figure 4-11: Gap Length Sensitivity on the Critical Mode: Harmonic 1

Based on the above results, gaps can grouped into two different categories: the inter-stage gaps and the intra-stage gaps. However, within these two categories, each gap seems to have a similar influence on the compressor stability when its length is doubled. Based on the results presented in Figure 4-11, it is conjectured that the best design for stability is obtained with longer intra-stage gaps and shorter inter-stage gaps. To support this conjecture, several calculations are performed, under the constraint of a constant total length of the compression system for weight considerations (similarly to what was done earlier for the study of the blade-row inertia effect). Results are shown in Table 4.2. The gap lengths are non-dimensionalized by the nominal gap length (identical for all stages).

Intra-Stage Gap	Inter-Stage Gap	Stability Gain
1.375	0.50	2.3%
1.500	0.33	3.3%
1.675	0.10	4.6%

Table 4.2: Gap Length Sensitivity

It therefore appears that the best practice, given a constant total compressor length, is to increase the length of intra-stage gaps (i.e., gaps 1, 2, 3, and 4), and to decrease the length of inter-stage gaps (i.e., gaps A, B, and C) as much as possible within the design constraints.

The difference in the dynamic behavior of the system between the effects of intra blade-row gaps and the effects of inter blade-row gaps raises the question of what the mechanism is behind this

phenomenon. A first step towards shedding more light on this effect is the visualization of the energy redistribution for the different cases. The definition of the energy distribution can be found in Spakovszky [16]. Gap 2 (intra blade-row gap) and Gap B (inter blade-row gap) are doubled independently. The resulting energy distributions for harmonic #1 are presented in Figure 4-12 and compared to the energy distribution for the baseline compressor.

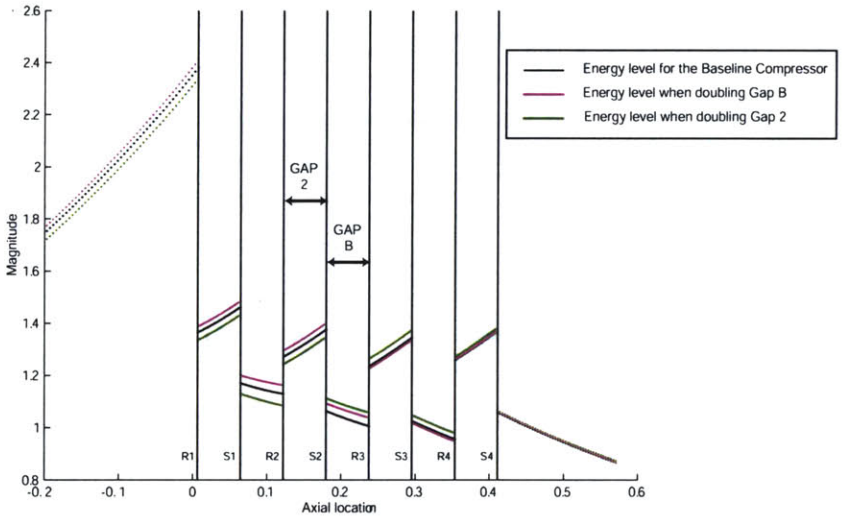

Figure 4-12: Energy Distribution for Two Gap-Length Changes

From these curves, some observations can be made. First, when Gap 2 length is doubled, the level of energy compared to the baseline decreases before Gap 2 and increases after Gap 2. On the other hand, when Gap B is doubled, the level of energy compared to the baseline increases before Gap B and decreases after Gap B. For the region of the compressor where the absolute level of energy are the highest (i.e. near the inlet of the compressor), it is noteworthy that the compressor with longest Gap B has the highest levels of energy in this area, and is also less stable than the baseline compressor.

To better understand the mechanisms behind this phenomenon, further analysis is required, which is not within the scope of this thesis.

The analysis conducted in this section has shown that several parameters can contribute to improve the compressor dynamic stability, but not all in the same magnitude. These results are summarized in Section 4.4 and recommendations for design practices are made.

4.3.4 Error Analysis: Assessing the Level of Confidence in the Results

Before further applying the above results on the actual design, the level of confidence in these results needs to be assessed and an error analysis is conducted.

The assumption is made that variability on geometric parameters can be neglected. On the other hand, there can be uncertainty about the aerodynamic parameters, i.e., the flow angle, as well as the stagnation pressure that assesses the blade-row performance. The following assumptions are made for the level of uncertainties: the uncertainty of the flow angle is assumed to be ± 0.2 degrees and the uncertainty of the total pressure used to compute the blade-row performance is assumed to be $\pm 0.1\%$. If compared to actual data, these are reasonable values.

From the definition of blade-row stagnation pressure loss L (cf. Equation B-1), the uncertainty for L can easily be determined:

$$uncertainty(L) \;=\; \pm \frac{\Delta P_t}{\rho \cdot U^2} \tag{4.3}$$

where ΔP_t is the uncertainty of the stagnation pressure.
From Frechette [11], the uncertainty on total pressure loss sensitivity to blade-row inlet flow angle can be computed:

$$uncertainty\left(\frac{\partial L}{\partial tan(\alpha)}\right) \;=\; \pm \frac{uncertainty(L)}{\alpha_1^+ \;-\; \alpha_1^-} \tag{4.4}$$

where $\alpha_1^+ \;-\; \alpha_1^-$ is the range of inlet flow angle. These uncertainties are then included in the model as biases and their impact on the system eigenvalues is examined. A worst case is considered with the uncertainties applied to all blade-rows simultaneously. Results are given in Table 4.3.

Quantity	Uncertainty	Derived Uncertainty on Stability Gain
$\frac{\partial L}{\partial tan(\alpha)}$	0.007	$\pm$ 4.0 %
α	0.2 deg.	$\pm$ 0.4 %

Table 4.3: Error Analysis

The uncertainty on the flow angle α has a negligible impact on stability gain. However, the uncertainty of the loss bucket slopes (i.e. of the total pressure loss sensitivity to blade-row inlet flow angle) overcomes the potential improvement from an inertia redistribution. The order of magnitude of this uncertainty is similar to the gain obtained from the gap length redistribution. However, as mentioned earlier, this uncertainty is computed for the worst case, and therefore, in most cases, the improvement provided by gap length redistribution is still noticeable. The uncertainty on the loss bucket slopes is determined to be $\pm$ 7.3%. The effect of the sensitivity of total pressure loss to

blade-row inlet flow angle is therefore higher than the error as long as it is increased or decreased by more than 7.3%.

4.4 Conclusions and Design Implications

4.4.1 Conclusions

The analysis conducted in this chapter has shown that in a multi-stage compressor environment, only one mode of the flow field is critical to the compressor stability as expected and captured by the Moore-Greitzer model [14]. This mode is driven by all the blade-rows of the compressor, and all blade-rows within each type (either rotor or stator) have a similar effect on the compressor stability in a repeating-stage environment.

The results summarized in Table 4.4 allow several assessments to be made.

Effect Studied	Stability Gain
None: Baseline Compressor	0.0%
Blade-Row Inertia Redistribution	0.03%
Gap-Length Redistribution	4.6%
10% Reduction in Total Pressure Loss Sensitivity to Inlet Flow Angle	6.54%
20% Reduction in Total Pressure Loss Sensitivity to Inlet Flow Angle	14.27%
30% Reduction in Total Pressure Loss Sensitivity to Inlet Flow Angle	24.26%

Table 4.4: Design Guidelines

First, the blade-row inertia is not a main driver of the compressor stability. Thus, blade chord and stagger angle are not key design parameters to be considered in a repeating-stage compressor designed for stability.

Second, in a repeating stage environment with identical rotors and stators, the length of the gaps between each blade-row plays an important role in the system dynamic stability. Even though all blade-rows have similar geometry, the gaps can be subdivided into two categories: the intra stage gaps and the inter-stage gaps. When increased, the intra-stage gaps, i.e. between a rotor and a stator, show to have a stabilizing effect on the compressor dynamic stability. On the other hand, the inter-stage gaps show to have a destabilizing effect on the compressor dynamic stability when their length is increased. These interesting results can therefore be used to redistribute the gap-lengths along the compressor to increase its dynamic stability. However, due to constraints summarized in Section 4.4.2, the potential improvement associated with this design change is limited.

Third, the main driver for the compressor stability is suggested to be the blade-row performance,

and specifically the sensitivity of the total pressure loss to the blade-row inlet flow angle. This "implicit" design variable is the most promising parameter to be used in a design methodology for enhanced stability.

A discussion on the implementation of these results and their quantitative benefits is conducted in the following section.

The conclusions stated above have been derived for the standard repeating-stage compressor and thus apply to this compressor only. A discussion on how these results could be extended to a more complex compressor (i.e. with variable duct area, different stages, uneven stage matching etc.) is provided in Chapter 5.

4.4.2 Design Guidelines

Based on the previous analysis, some design recommendations are made to improve the dynamic stability of a compressor.

Under the constraint of total compressor length, applying the following recommendations in terms of gap length can lead to a 4.6% improvement in stability gain:

- Decrease the inter-stage gap lengths as much as allowed by the mechanical tolerances;
- Increase the intra-stage gap lengths as much as allowed by weight considerations.

This improvement is noteworthy but has a moderate impact on the compressor stability. Consequently, to achieve higher dynamic stability by redistributing the gap length, a trade-off on the compressor weight must be made, by relaxing the assumption of constant compressor length.

In terms of stability gain improvement, reducing the sensitivity of the total pressure loss to blade-row inlet flow angle suggests to have the most significant impact. If a 30% increase is considered on the slope of the loss bucket at the flow coefficient for neutral stability, a gain of nearly 25% in stability gain can be achieved. However, no design recommendation can be made at this point on how to achieve this reduction in total pressure loss sensitivity to blade-row inlet flow angle. Neither can the magnitude of such an improvement be assessed.

Being able to characterize the blade-row performance from its geometry, and thus to evaluate the potential improvements in the slope of the loss buckets as a function of the compressor parameters is therefore a key to the success of the joint project in the future. With a tool for blade-row performance characterization, a complete optimization process could be set up and an optimization tool could automatically search for the best combination of the compressor design parameters for

increased stability.

Chapter 5

Conclusions and Future Work

5.1 Summary and Conclusions

The detailed study of compressor stability at several depths of analysis in this thesis allows three main objectives to be addressed. They are presented in the following sections.

5.1.1 Impact of Surge on Airline Operations

The study conducted in Chapter 2 suggests that an in-flight surge event has immediate consequences that affect all the functions of the airline:

- The flying operations are affected as the airplane has to be diverted and grounded and the crew reallocated;
- The maintenance department is highly involved with the engine inspection, its replacement and its repair;
- The ground operations have to reallocate the passengers on other flights;
- The scheduling and planning department has to reallocate the flight crew and aircraft in the airline schedule, after the original schedule has been disrupted.

Due to these company-wide impacts, an in-flight surge is a very unwanted event and can cost up to $3.5 million to the airline.
Overall, running a fleet of reduced-stability engines, with the recurrent costs associated with inspection, tracking and fleet management can cost a major airline up to $10 million a year.
Therefore, the revenue generated during one month per year by the fleet of aircraft carrying these engines is directly affected to the payment of the additional costs caused by these engines. These

expenses thus represent 8% of the total revenue potentially generated by the fleet powered by these engines.

Engine stability is consequently a major issue from the operator point of view and should lead the engine manufacturer to integrate it as a prime design objective in their design process.

5.1.2 Eigenvalue Structure in Multi-Stage Environment

Analysis of a standard repeating-stage compressor has demonstrated the following eigenvalue distribution for an n-stage standard compressor:

- N modes associated with unsteady loss effects : (n-2)/2 mainly influenced by the inner rotors, (n-2)/2 mainly influenced by the inner stators, and two extra modes, supposedly influenced by the outer blade-rows of the compressor;
- (N-2)/2 highly-damped modes mainly influenced by the inner rotors, with relatively high positive rotation rate ($\omega_n \geq 5$);
- (N-2)/2 highly-damped modes mainly influenced by the inner stators, with relatively high negative rotation rate ($\omega_n \leq -5$);
- 1 highly-damped "system mode," with relatively small rotation rate ($|\omega_n| < 5$), possibly associated with the last stator and the exit duct;
- 1 lightly-damped "system mode," critical to the compression system stability.

These above results, together with the results obtained from the analysis of the CREATE compressor indicate that, as predicted by the Moore-Greitzer model, only one string of modes is critical to the dynamic stability for multi-stage compressors. Further analysis can thus focus on the effects of the compressor design parameters on this single string of critical "system modes."

5.1.3 Design Guidelines for Increased Stability

The sensitivity analysis conducted on several design parameters has shown an influence on the critical mode as follows:

- Modifying blade-row inertia provides negligible improvement to the compressor stability ;
- Redistributing gap-lengths along the compressor (by increasing the intra-stage gaps and decreasing the inter-stage gaps) can provide noticeable improvement of 4.6% stability gain but inherently carries restrictions due to performance requirements that bound this improvement;

- Reducing the total pressure loss sensitivity to blade-row inlet flow angle can provide a significant stabilizing effect of more than 15% in stable operating range stability gain, provided that a sufficient reduction in loss-slope is achieved (20% and higher).

The most promising design modification is therefore to improve the total pressure loss sensitivity to blade-row inlet flow angle. This is therefore one of the main recommendations for future work.

5.2 Recommendations for Future Work

Many issues encountered during this work establish the need for new tools and for further analyses to be performed in the next steps of the joint project.

5.2.1 Tool Development

As assessed in Chapter 3, there is s strong need for a *mean line deck tool* for the CREATE compressor in order to provide:

- The steady mean-flow parameters to the dynamic model;
- The overall pressure ratio of the machine;
- The blade-row performance as a function of both inlet flow angle and Mach number;
- The characterization of the blade-row performance (cf previous bullet) for several candidate designs;
- Exit flow angle deviation effects as a function of inlet flow angle.

5.2.2 Eigenvalue Structure and Understanding of the Underlying Dynamics

To better understand the behavior of the dynamic modes, a more insightful measure of energy has to be determined. It would allow a better characterization of each mode, as well as an improved knowledge of its behavior along the compressor, and thus of the underlying physics driving each mode.

From this analysis, a new measure for dynamic stability has to be assessed in order to appropriately estimate the dynamic stability of the compressor. This measure will balance performance and efficiency in the optimization with trade-off conducted later on.

5.2.3 Evolution Towards Compressors with More Complex Design

Based on the insight developed in the present thesis on the effect of blade-row interaction on dynamic stability in multi-stage environment, for a reference repeating-stage compressor, new development should incorporate uneven stage-matching and blade-rows with different geometries to study a more representative model of actual compressors. In that context, the results from the present study should be used for benchmarking, to identify the changes generated by the increased complexity. For a compressor with different stage-loading, the effect of design parameters may vary from one blade-row to another. A multi-variable optimization tool will therefore be required to establish design guidelines.

5.2.4 Design Guidelines

If the predictive capability provided by a *mean-line deck* is achieved, a full optimization process, based on the framework set-up in Figure 3-1 can be performed. Insights from the sensitivity analysis conducted here can be used to adequately drive the optimization process. Multi objective optimization based on the new measure of stability, performance, and efficiency will then be performed to determine the best trade-off sustainable for a compressor designed for stability.

A fruitful cooperation, intensifying as the project matures, will hopefully enable these further developments.

Appendix A

Structure of the Mean-Flow Calculation

In the following calculations, due to compressibility, all flow parameters are functions of Mach number which is *a priori* unknown. Consequently, an iterative process is set up. The axial velocity is assumed to have relatively small variation and is selected as the variable to be iterated on.

A-1 Flow Field Quantities at the Inlet of a Blade-Row

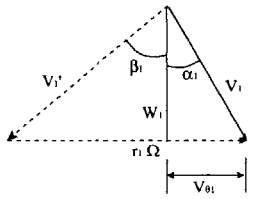

Figure A-1: Velocity Triangle at Inlet

The thermodynamic parameters known at the inlet are the total pressure and total temperature. To determine the velocity triangle (cf. A-1) at the compressor inlet, the axial velocity component must be computed . The absolute flow angle at the exit of a blade-row is assumed to match the blade metal angle (no flow angle deviation). Given the wheel speed, the axial velocity is computed iteratively. Figure A-2 depicts this process .

The equations used in this procedure are briefly outlined below. The equation of state can be written for a perfect gas using the stagnation quantities as :

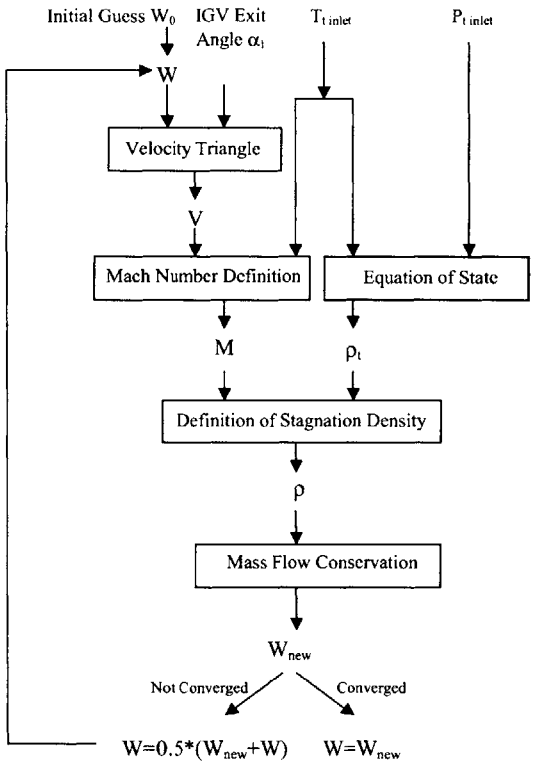

Figure A-2: Structure of the Inlet Flow Parameters Calculation

$$\frac{p_t}{\rho_t} = R \cdot T_t \tag{A-1}$$

By definition of the stagnation temperature, the static temperature can be written as

$$T = \frac{T_t}{1 + \frac{\gamma-1}{2} \cdot M^2} \quad \text{where} \quad M = \frac{V}{\sqrt{\gamma \cdot R \cdot T}} \quad \text{is the absolute Mach number.} \tag{A-2}$$

Combining the two equations of A-2 , an implicit equation for the Mach number is obtained. The Mach number can be written explicitly (cf A-3), assuming that, in the following form, it is always positive.

$$M = \sqrt{\frac{M_t^2}{1 - \frac{\gamma-1}{2} \cdot M_t^2}} \quad \text{where} \quad M_t = \frac{V}{\sqrt{\gamma \cdot R \cdot T_t}} \tag{A-3}$$

Together with the definition of stagnation density (cf A-4)

$$\rho_t = \rho \cdot \left(1 + \frac{\gamma - 1}{2} \cdot M^2\right)^{\frac{1}{\gamma-1}} \tag{A-4}$$

and the mass flow conservation (cf A-5),

$$\dot{m} = \rho \cdot S \cdot W \tag{A-5}$$

these equations determine the axial velocity W as shown in Figure A-2.

A-2 Flow Field Quantities Between Blade-Rows

The flow is assumed inviscid in the inter-blade-row gaps and inlet duct and consequently, the conservation of angular momentum holds:

$$r_1 \cdot V_{\theta 1} = r_2 \cdot V_{\theta 2} \tag{A-6}$$

Once again, an iterative procedure is used to compute the velocity triangles as depicted in Figure A-4 using:

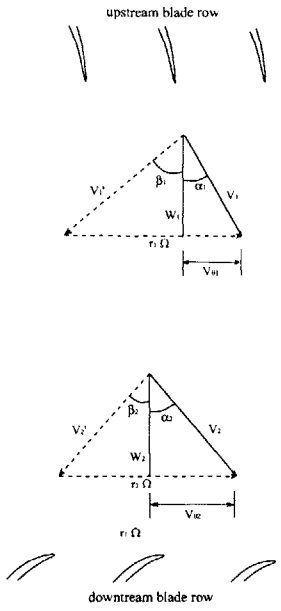

Figure A-3: Evolution of the Velocity Across the Inter-Blade-Row Gap

the definition of absolute velocity

$$V_2 = \sqrt{V_{\theta 2}^2 + W_2^2}, \tag{A-7}$$

the mass flow conservation (assuming no air bleed in between blade-rows)

$$\rho_2 \cdot S_2 \cdot W_2 = \rho_1 \cdot S_1 \cdot W_1, \tag{A-8}$$

the definition of the stagnation density (equation A-4) and Mach number equation. (equation A-3)

A-3 Mean-Flow Across a Rotor Blade-Row

The calculation procedure for the flow across a rotor blade is summarized in Figure A-6. The equations used are similar to those previously discussed. However, three more relations are used to close the problem: the isentropic relation ,

$$\frac{P_{t'outlet\ is}}{P_{t'inlet}} = \left(\frac{T_{t'outlet}}{T_{t'inlet}}\right)^{\frac{\gamma}{\gamma-1}} \tag{A-9}$$

the definition of stagnation pressure loss and the conservation of rothalpy. At this stage of the project, stagnation pressure loss curves as a function of the inlet flow angle were available for each

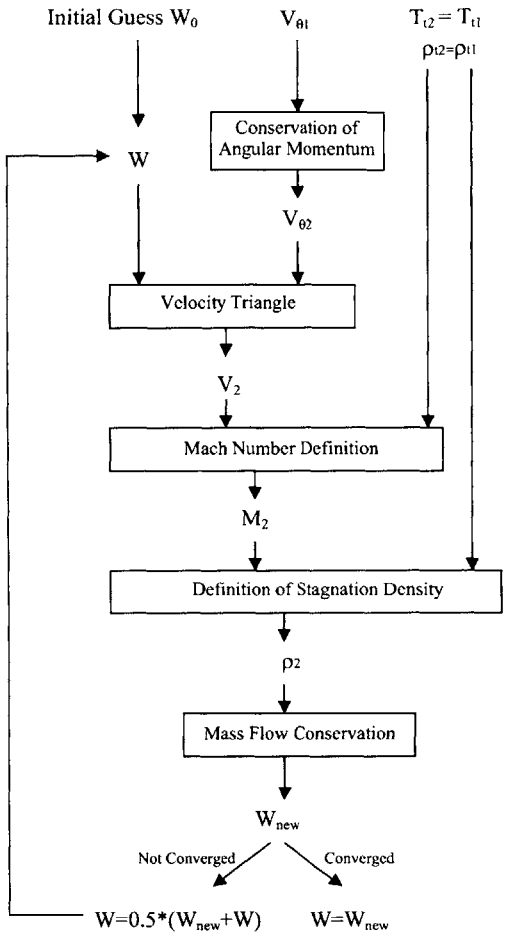

Figure A-4: Structure of the Inter-Blade-Row Gap Mean-Flow Calculation

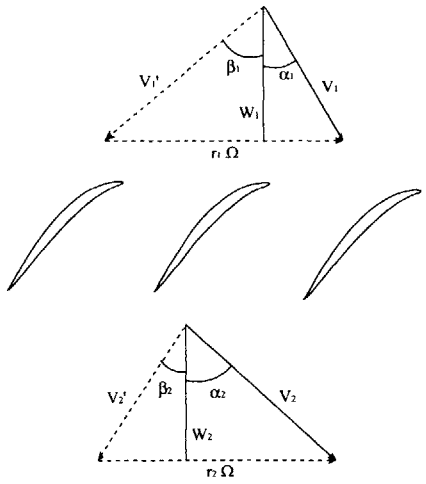

Figure A-5: Velocity Triangles for the Rotor

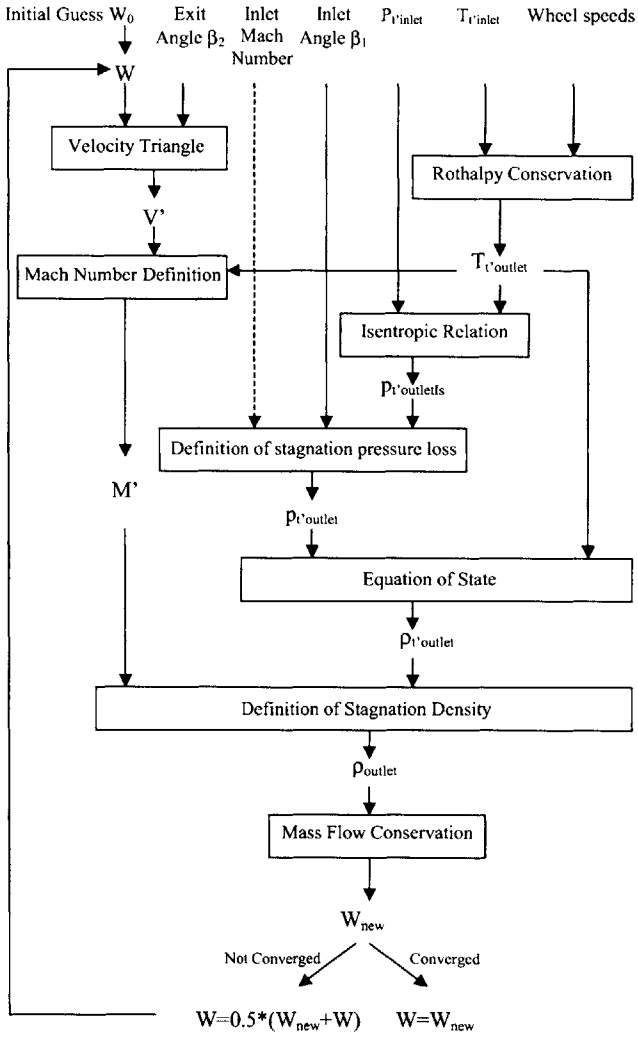

Figure A-6: Structure of the Rotor Mean-Flow Calculation

blade-row. However, the dependency of stagnation pressure loss on Mach number was not included in the data set. This Mach dependency will be implemented in future work, as suggested by the dashed line in figure A-6. Once the inlet flow angle is known, the corresponding loss coefficient ω can be found by interpolation. By definition, ω is :

$$\omega = \frac{P_{t'outlet\ is} - P_{t'outlet}}{P_{t'inlet} - P_{s\ inlet}} \tag{A-10}$$

using this definition, the total exit pressure can be written as

$$P_{t'outlet} = P_{t'outlet\ is} - \omega \cdot (P_{t'inlet} - P_{s\ inlet}) \tag{A-11}$$

From the conservation of rothalpy across the rotor blade-row, one can write

$$T_1 + \frac{V_{1'}^2}{2 \cdot c_p} - \frac{U_1^2}{2 \cdot c_p} = T_2 + \frac{V_{2'}^2}{2 \cdot c_p} - \frac{U_2^2}{2 \cdot c_p} \qquad where \qquad U = r \cdot \Omega \tag{A-12}$$

Assuming constant specific heats, this can simply be written as:

$$T_{t1'} - \frac{U_1^2}{2 \cdot c_p} = T_{t2'} - \frac{U_2^2}{2 \cdot c_p} \tag{A-13}$$

A-4 Mean-Flow Across a Stator Blade-Row

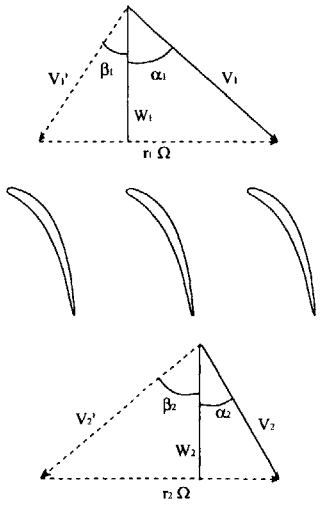

Figure A-7: Velocity Triangles for the Stator

The stator case (cf. Figure A-7) is similar to the rotor case, except that calculations are conducted in the absolute frame. Small simplifications are to be made in the structure, shown in Figure A-8.

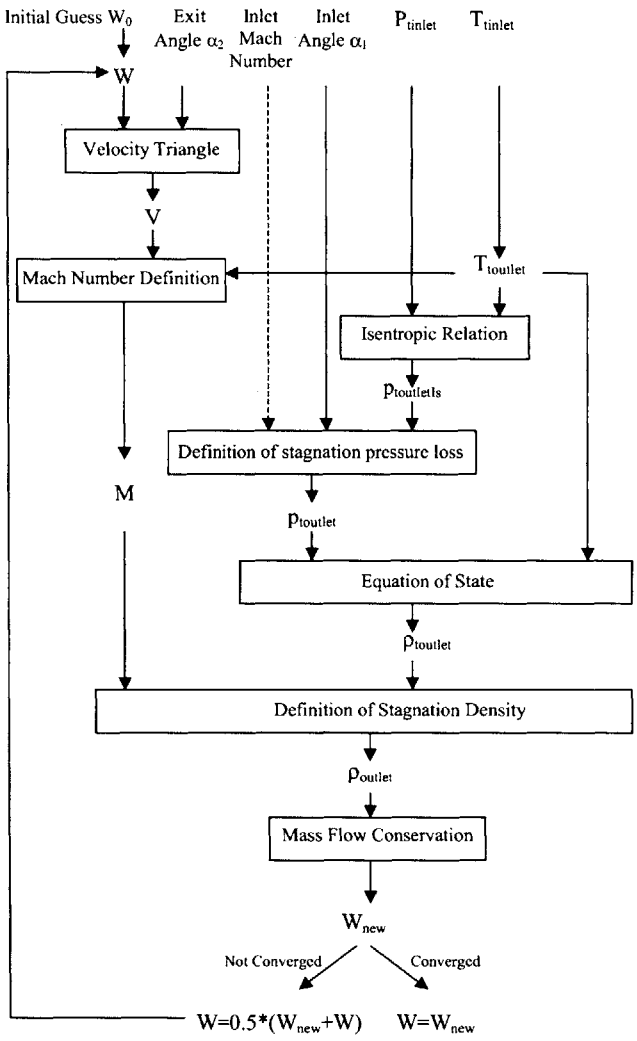

Figure A-8: Structure of the Stator Mean-Flow Calculation

So, in the stator case, the isentropic relation is expressed in the absolute frame.

$$\frac{P_{t\ outlet}}{P_{t\ inlet}} = \left(\frac{T_{t\ outlet}}{T_{t\ inlet}}\right)^{\frac{\gamma}{\gamma-1}}, \tag{A-14}$$

and the loss coefficient is defined by :

$$\omega = \frac{P_{t\ inlet} - P_{t\ outlet}}{P_{t\ inlet} - P_{s\ inlet}} \tag{A-15}$$

Using this definition, the stagnation exit pressure can be written as:

$$P_{t\ outlet} = P_{t\ inlet} - \omega \cdot (P_{t\ inlet} - P_{s\ inlet}) \tag{A-16}$$

In the stator case, the rothalpy conservation simply becomes the conservation of the stagnation enthalpy:

$$T_{inlet} + \frac{V_{inlet}^2}{2 \cdot c_p} = T_{outlet} + \frac{V_{outlet}^2}{2 \cdot c_p} \tag{A-17}$$

which simply yields:

$$T_{t\ inlet} = T_{t\ outlet}. \tag{A-18}$$

Appendix B

Data Processing of Blade-Row Stagnation Pressure Loss Characteristics

B-1 General Loss Processing

The data provided by Snecma Moteurs contains the loss coefficients ω of each blade-row for given values of the blade-row inlet flow angle. In general, these losses depend on both the inlet flow angle and the Mach number. In this study, given the data available, the Mach number sensitivity of the losses is not modeled. Blade-row losses can be non-dimensionalized in two forms : ω (cf Equation A-10) and L (defined in Equation B-1 in the case of a rotor):

$$L = \frac{P_{t'outlet\ is} - P_{t'outlet}}{\rho \cdot U^2} \tag{B-1}$$

Combining B-1 and A-10 yields :

$$L = \omega \cdot \frac{P_{t'inlet} - P_{s\ inlet}}{\rho \cdot U^2} \tag{B-2}$$

The derivative of $L = f(tan\beta)$ with respect to $tan\beta$, the sensitivity of total pressure loss to the tangent of the inlet flow angle, is an important quantity for the dynamic behavior of the compressor system. The following procedure (cf Figure B-1) is used to compute this quantity from the data provided by Snecma Moteurs.

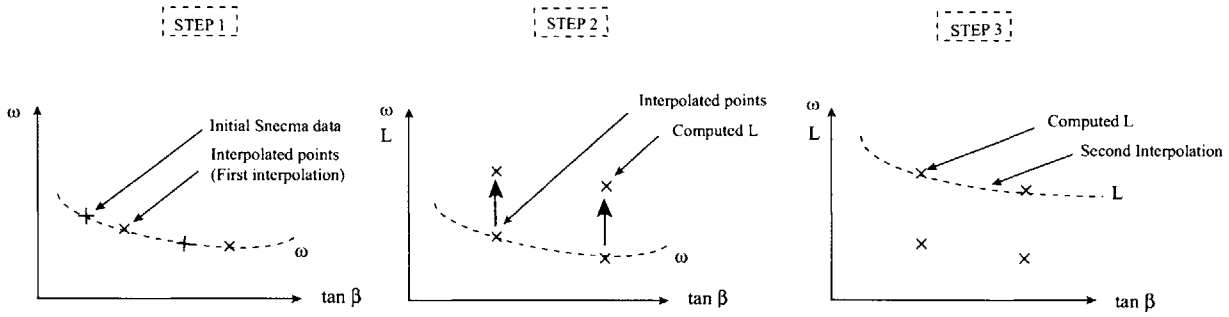

Figure B-1: Sequence of Operations to Compute the Sensitivity of Total Pressure Loss to Blade-Row Inlet Flow Angle

1. Generate a set of $L = f(tan\beta)$ values [Offline Calculation]

   - Pick a set of operating points determined by the compressor mass flow $\dot{m}$;
   - Compute the inlet flow angle associated with each operating point for each blade-row ;
   - Compute the corresponding loss coefficient ω by interpolation [STEP 1];
   - Transform ω into the blade-row loss L using B-2 for those operating points. [STEP 2]

2. Determine the derivative $\frac{\partial L}{\partial tan(\beta)}$ [Online Calculation]
   Once the set of data points L has been generated using the mean-flow calculation in the offline procedure, it is stored in matrices and does not need to be further recomputed . Next, it is possible to fit a polynomial to the computed data set $L = f(tan\beta)$ [STEP 3]. The derivative of this polynomial is readily obtained and thus, for any mass flow that is picked (in the Online Calculation), the derivative of $L(tan\beta)$ can be determined. The implementation of this procedure is described in Figure B-2.

Among the steps mentioned above, the central step is the interpolation, in both the online and offline calculations. Thus, special attention must be paid to the interpolation process.

B-2 Interpolation Process

The best fits were obtained by:

- Creating a large set of data points (as in the previous case);
- Fitting low order polynomial through those points.

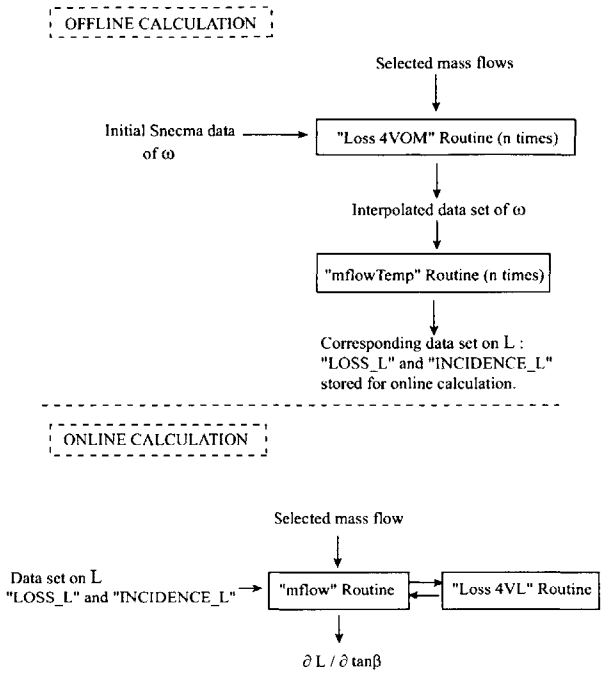

Figure B-2: Determination of the Appropriate Description of Losses that are Input to the Dynamic Model

In addition, since the focus is on the pre-stall region of the loss bucket (corresponding to high inlet flow angles), performing the interpolation on a reduced number of points in this region, rather than on the entire data set increases the fidelity of the fit. This method provides acceptable fits representative of the shape of the loss bucket and offers room for adjustments to each of the individual loss buckets. The tuning parameters used to best fit the loss buckets are:

- The range of data were the interpolation is performed;
- The order of the polynomial used;
- The type of interpolation used in Matlab's "interp1" function (either "square" or "cubic").

These settings vary from one blade-row to another. The best settings are selected based on the least square results. The non-dimensionalized results obtained in the case of the "L" Losses are presented in Figure B-3. The settings are summarized in Table B.1.

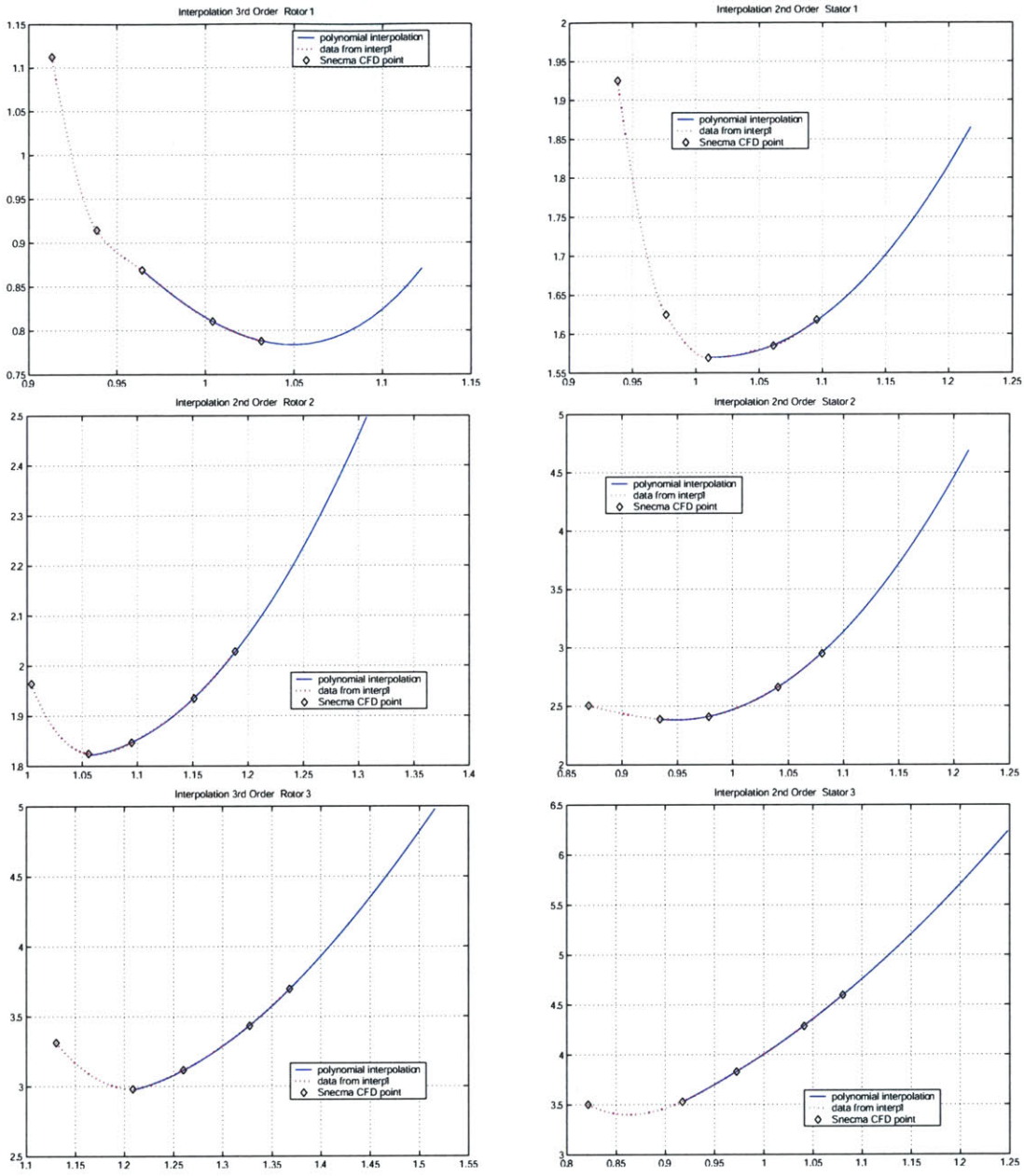

Figure B-3: Interpolated Loss Curves for L

Blade-row	Range of data in points	Order of polynomial fit	Interpolation type
R1	3	3	cubic
S1	3	2	cubic
R2	4	2	square
S2	4	2	square
R3	4	3	cubic
S3	4	2	square

Table B.1: Interpolation Settings for the L Losses

Appendix C

Penalty Method for Eigenvalue Search Routines

As stated in Chapter 3, the objective of the penalty methods in the present study is to fill the sink as soon as the zero associated with it has been found.

A candidate penalty function to perform this task is the Gaussian function, that, in addition of meeting the requirements for compactness and "peaky" shape also has the advantage of having a compact analytical expression. Its general expression is given by:

$$penalty(\sigma,\omega) \;=\; height \cdot e^{-\left(\left(\frac{\sigma-\sigma_0}{\sigma_{scal}}\right)^2+\left(\frac{\omega-\omega_0}{\omega_{scal}}\right)^2\right)} \tag{C-1}$$

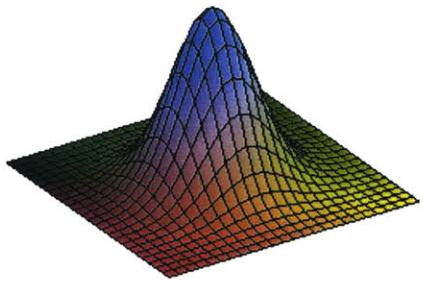

Figure C-1: Shape of the Penalty Function

The different parameters of this correction function to be adjusted are:

- The amplitude 'height';
- The σ scaling factor 'σ_{scal}';
- The ω scaling factor 'ω_{scal}'.

The center of the penalty function $[\sigma_0, \omega_0]$ will be located where the eigenvalue is. To fit a penalty function to the sink, the following steps are performed:
Note: the cases of the σ direction and the ω direction will be treated independently so that the problem can be studied as a one-dimensional function problem.

1. Evenly spaced points are selected on both sides of the sink, within a given range. The determinant is computed at these points.
2. On each side, the point where the determinant has the maximum value is selected.
3. On each side, the point where the determinant has a given fraction ($0 \leq semi_{max} \leq 1$) of the maximum value is selected.
4. The values of σ associated with these points are collected. $abs(\sigma - \sigma_0)$ is called R_1 on the left, R_2 on the right.
5. $R = max(R_1, R_2)$ is selected and the associated side becomes the predominant one. The maximum value of the determinant on this side becomes det_{max}.

These steps are illustrated in Figure C-3.

Once the sink is characterized by the parameters R and det_{max}, the penalty function has to be fitted to it as shown in Figure C-3:B , i.e. to satisfy the following constraints:

$$semi_{max} \cdot det_{max} = semi_{max\ gaussian} \cdot height \tag{C-2}$$

$$semi_{max} \cdot det_{max} = height \cdot e^{-\left(\left(\frac{R}{\sigma_{scal}}\right)^2\right)} \tag{C-3}$$

Note: Since the problem was restricted to a one-variable function problem, the plane studied is the plane $\omega = \omega_0$.
From the above two equations, it is possible to express the two unknowns "height" and σ_{scal} as functions of the known variables R and det_{max} and of the setting parameters $semi_{max}$ and $semi_{max\ gaussian}$.

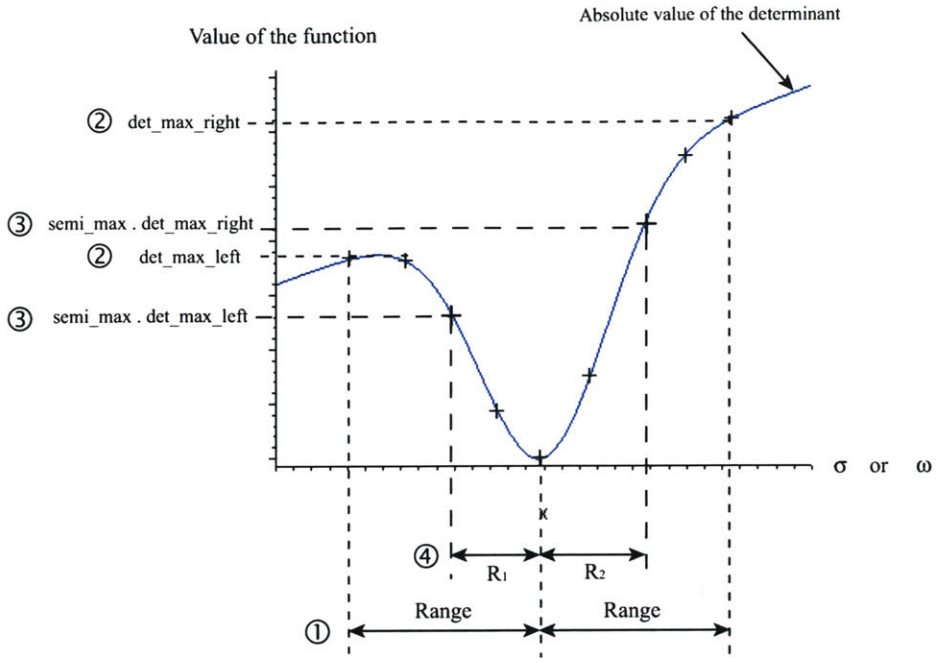

Figure C-2: A: Fitting of a Penalty Function

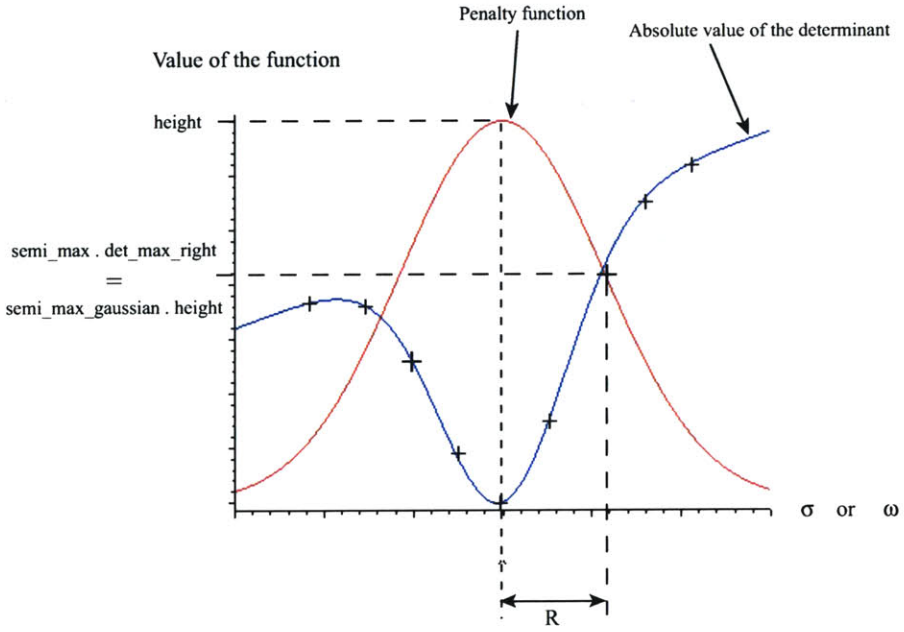

Figure C-3: B: Fitting of a Penalty Function (continued)

This yields:

$$height = \frac{semi_{max}}{semi_{max\ gaussian}} \cdot det_{max} \tag{C-4}$$

$$\sigma_{scal} = \frac{R_\sigma}{sqrt(-log(semi_{max\ gaussian}))} \tag{C-5}$$

The same results are valid in the ω direction.

$$\omega_{scal} = \frac{R_\omega}{sqrt(-log(semi_{max\ gaussian}))} \tag{C-6}$$

Note: An arbitrary choice is made that the "height" is set by the computation of the σ direction.

Once the scaling parameters of the penalty function have been determined, the tuning parameters $semi_{max}$ and $semi_{max\ gaussian}$ have to be adjusted to best fill the sink.

First, Figure C-4 shows that when $semi_{max}$ increases, this tends to reduce the presence of local minima on both sides on the peak. However, it also tends to enlarge the width of the peak , thus generating risks of obstruction of the neighbor sinks. From the situations described in Figure C-4, it appears that the best value of the height (cf. Equation C-4) is between 0.6 and 0.7. From this, the value of 2/3 is chosen.

Second, Figure C-5 illustrates the fact that when $semi_{max\ gaussian}$ increases, two negative effects arise : a local minimum appears on the middle of the peak and the width of the peak generates risk of obstruction on the neighbor sinks. Therefore, a low value of $semi_{max\ gaussian}$ is required, 0.2 is chosen.

After the value of $semi_{max}$ and $semi_{max\ gaussian}$ are chosen, the robustness of these settings is tested on other roots and a visualization of the results is also made in the ω direction. These settings are proved to be satisfy the requirements stated in Section 3.3.2.

To illustrate this phenomenon, the determinant is plotted in 3D before and after the penalty methods are added (The case presented on Figure C-6 illustrates the absolute value of the determinant function for the second stage of the CREATE compressor, for harmonic # 3).

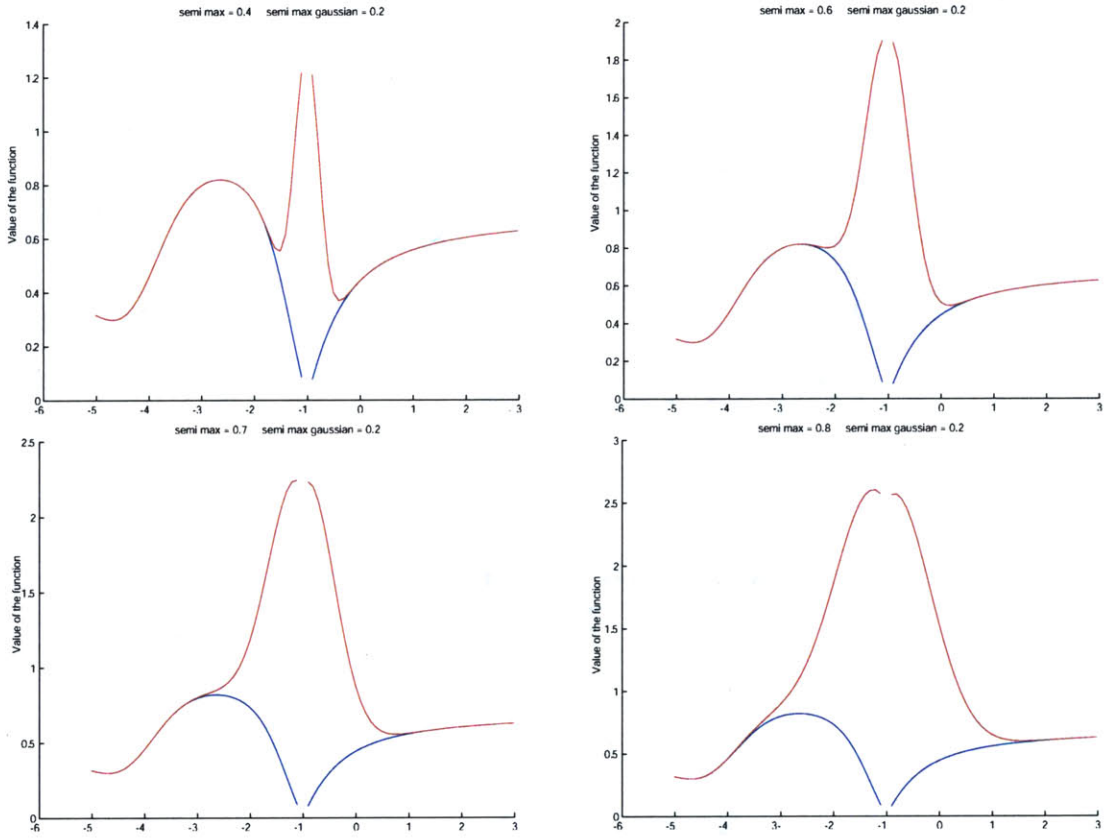

Figure C-4: Impact of Semi Max on the Penalty Function

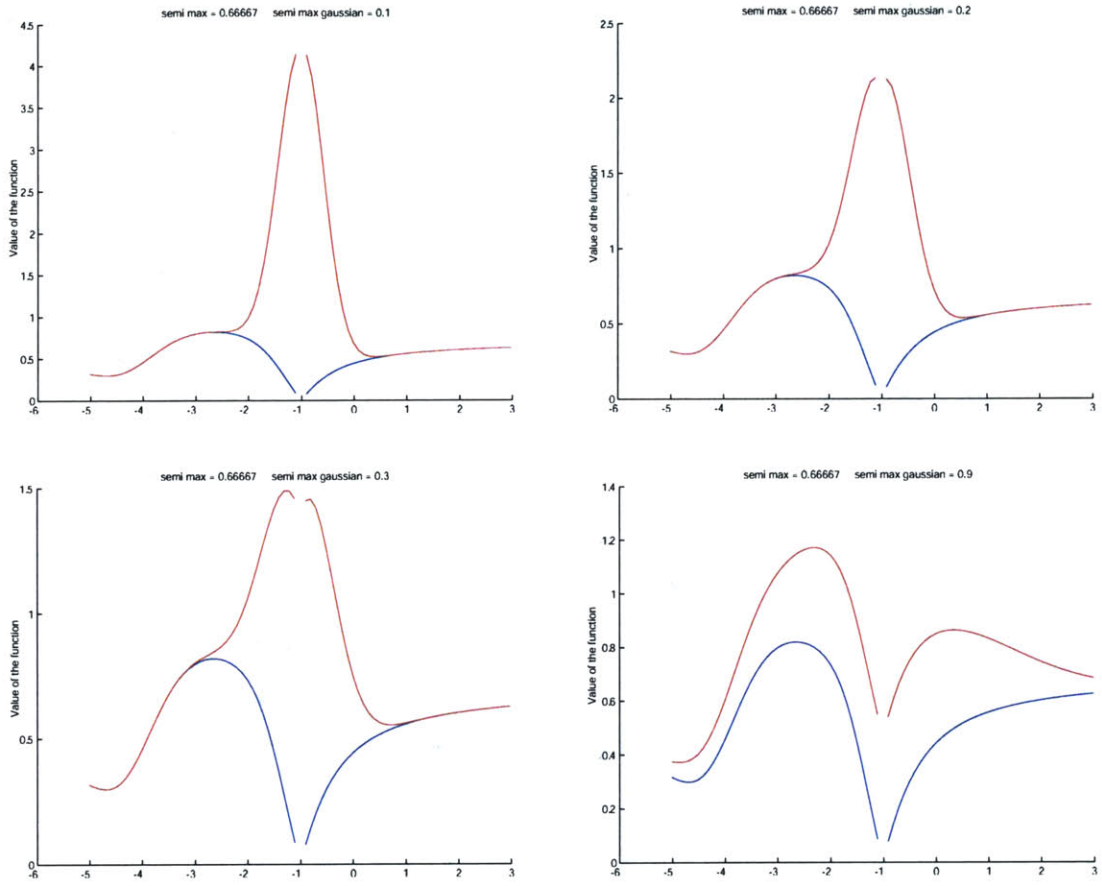

Figure C-5: Impact of Semi Max Gaussian on the Penalty Function

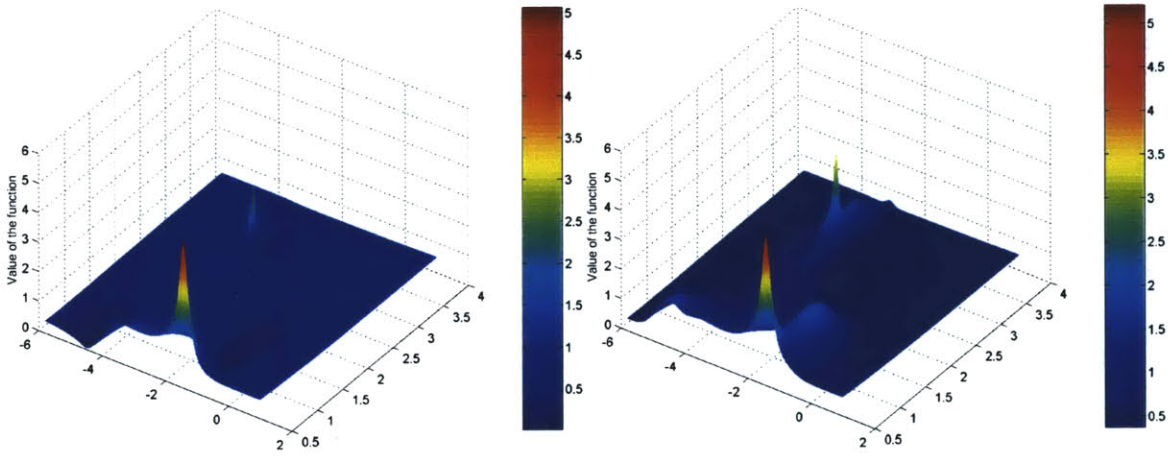

Figure C-6: Penalty Function Corrections

Appendix D

Analysis of the Nature of Non-Critical Compressor Modes

In this section, a study of the dynamics of the non-critical modes is conducted, to determine the dynamics associated with each mode, and therefore the impact of the design on the system modes. The non-critical modes can be divided into two groups (cf. 4-6):

- The modes associated with unsteady loss effects;
- The highly-damped modes.

These groups are studied in Sections D-1 and D-2, respectively.

D-1 Analysis of Modes Associated with Unsteady Loss Effects

A first glance at the modes associated with unsteady loss effects (cf. Figure D-1) helps in identifying three different subgroups of modes:

- Two strings of modes (X and Y) with relatively low rotation rate ($\omega \ll 1$) ;
- Two strings of modes (U and V) with relatively higher rotation rate ($\omega \gtrapprox 1$) ;
- Two independent modes (S and T).

Explaining the origin of these groups is not obvious, all the more because the three subgroups have the same number of strings of modes (i.e. two). In order to better understand the distribution

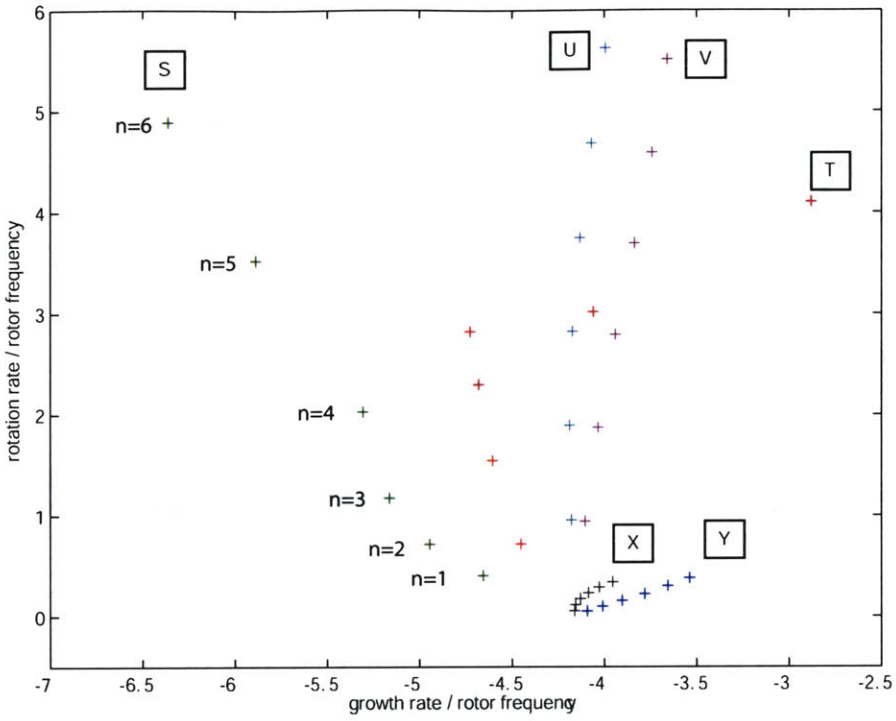

Figure D-1: Modes Associated With Unsteady Loss Effects of the 3-Stage Symmetric Compressor

of the modes between these subgroups, another stage (i.e. a rotor and a stator), identical to the existing stages, is added to the compressor.

The modes associated with unsteady loss effects for the 4-stage standard compressor (described in Chapter 4) are shown in Figure D-2. These results suggest the following grouping of modes:

- Three strings of modes (X', Y', and Z') with relatively low rotation rate ($\omega \ll 1$) ;
- Three strings of modes (U', V', and W') with relatively higher rotation rate ($\omega \gtrapprox 1$);
- Two independent modes (S' and T').

Comparing Figures D-1 and D-2 suggests that if an additional stage is added to the machine, two new modes associated with unsteady loss effects appear, and that they are distributed between the first two subgroups. On the other hand, the independent modes for the 4-stage standard compressor S' and T' look very close to the independent modes for the 3-stage standard compressor S and T. The dynamics of these independent modes must therefore correspond to the dynamics of some design characteristic that is present in all compressors, independently of the number of stages. It can be conjectured that these independent modes relate to the inlet of the compressor (i.e. the infinite inlet duct and the first rotor) and to the exit of the compressor (i.e. the infinite exit duct and the last

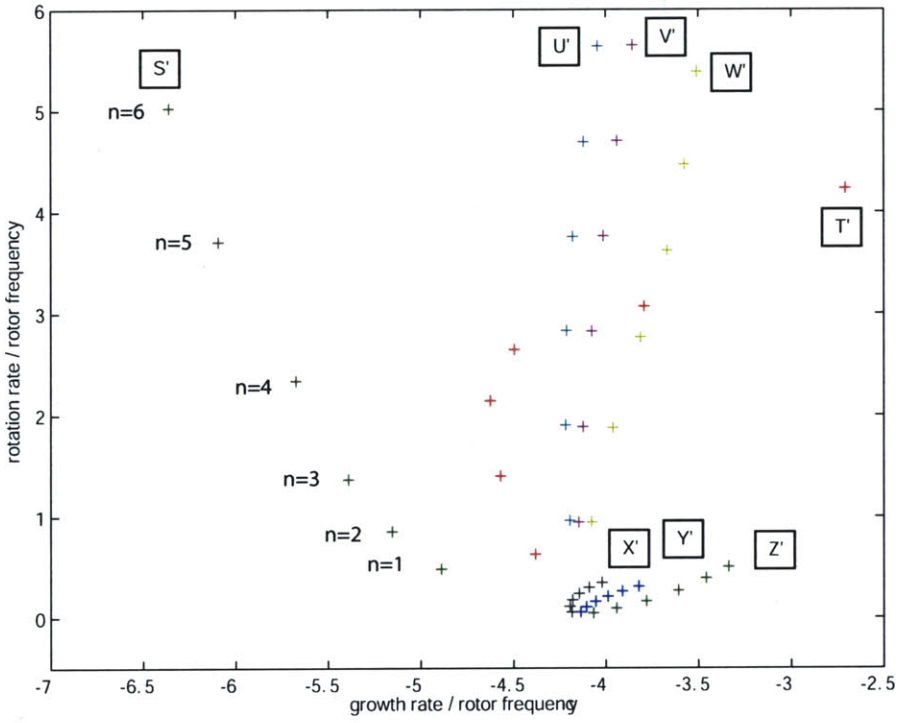

Figure D-2: Modes Associated With Unsteady Loss Effects of the 4-Stage Symmetric Compressor

stator).

A detailed analysis of the three subgroups of modes is therefore needed to understand which component of the compressor system may influence the dynamics of each group. Since the modes presently studied are associated with unsteady loss effects, the effect of the unsteady loss time-lags on these modes is analyzed. For each blade-row, the time-lag, defined as

$$\tau = \tau_u \frac{c_x}{R \cdot \cos\gamma} \tag{D-1}$$

is increased by 15% independently, and the system modes are computed. (Note: τ_u is a proportionality constant, and is modified to change the value of the time-lag τ.)
From this sensitivity analysis, three trends are noticeable:

- The modes of the first subgroup (modes U', V', W') are sensitive to the rotors' unsteady loss time-lags only;
- The modes of the second subgroup (modes X', Y', Z') are sensitive to the stators' unsteady loss time-lags only;
- The modes of the third subgroup (modes S', T') are sensitive to both rotors' and stators' unsteady loss time-lags.

Figure D-3 illustrates this effect on modes X', Y', and Z'.
However, within each of this subgroup, there is no dominant effect of one blade-row time-lag to one specific mode.

Consequently, it can be concluded that the dynamics of the modes of the first subgroup (modes U', V', W') are dominated by perturbations in the rotor blade-rows, whereas the dynamics of the modes of the second subgroup (modes X', Y', Z') are dominated by perturbations in the stator blade-rows.

The independent modes are studied next.

First, the fact that these two modes belong to the same subgroup has to be justified. The perturbation energy distribution along the compressor (defined in [16]) is computed for modes S' and T'. The results are presented on Figure D-4.

The perturbation energy distribution of modes S' and T' show a similar behavior along the compressor. This similarity cannot be found for the other types of modes associated with unsteady loss effects. This suggests that modes S' and T' are of a common type and can be grouped under the third subgroup. However, the perturbation energy does not provide evidence that the dynamics of modes S' and T' might be influenced by the compressor inlet dynamics or by the compressor exit

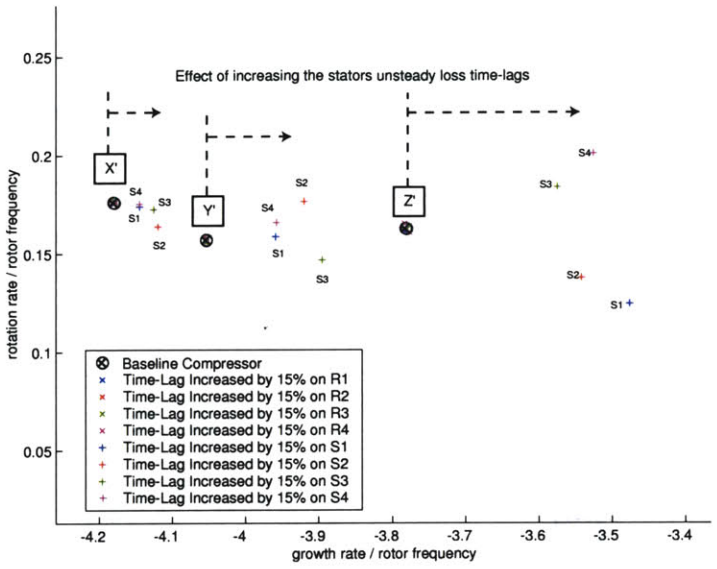

Figure D-3: Unsteady Loss Time-Lag Sensitivity on Mode X', Y', Z' - Harmonic 3

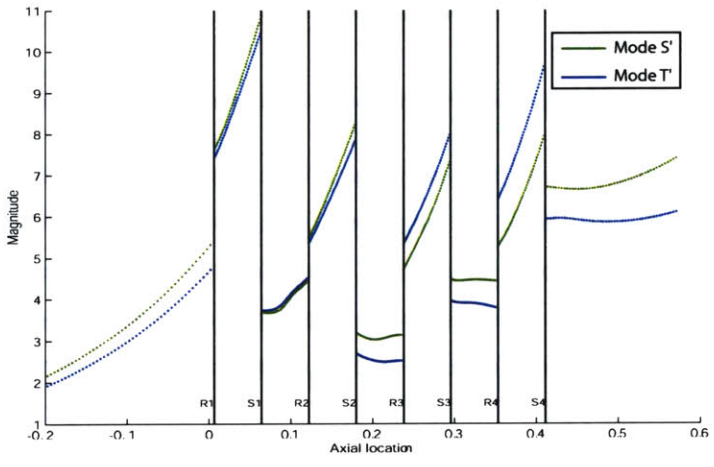

Figure D-4: Perturbation Energy Distribution for modes S' and T' - Harmonic #1

dynamics. Thus, no additional statement can be made regarding the dynamics of these two modes.

D-2 Analysis of Highly-Damped Modes

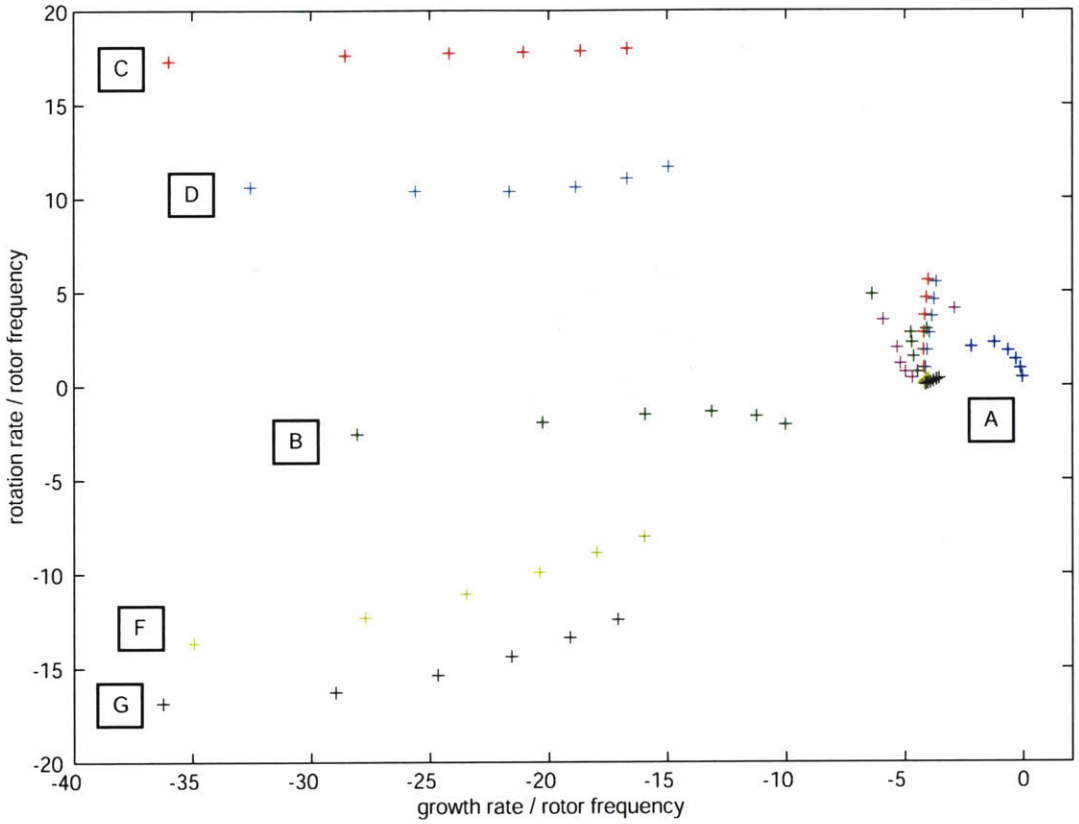

Figure D-5: Eigenvalue Map for the 3-Stage Standard Compressor

Unlike the modes associated with unsteady loss effects, that can be clearly identified since they disappear when unsteady-loss effects are neglected (cf. Figure 3-10), it is unclear whether the remaining modes (A to F on Figure D-5) belong to a single group. The first observation is that mode A is the least stable mode, critical for the overall compressor system stability. All the other modes (B to F) are highly-damped. For the 3-stage standard compressor, modes can be subdivided into four subgroups:

- Two strings of modes (C and D) with relatively high positive rotation rate ($\omega_n \geq 5$) ;
- Two strings of modes (F and G) with relatively high negative rotation rate ($\omega_n \leq -5$);
- One independent mode (B) with relatively low rotation rate; ($|\omega_n| < 5$)

- The least stable mode (A).

In order to better understand the distribution of the modes among these subgroups, another stage (i.e. a rotor and a stator), identical to the existing stages, is added to the 3-stage compressor.

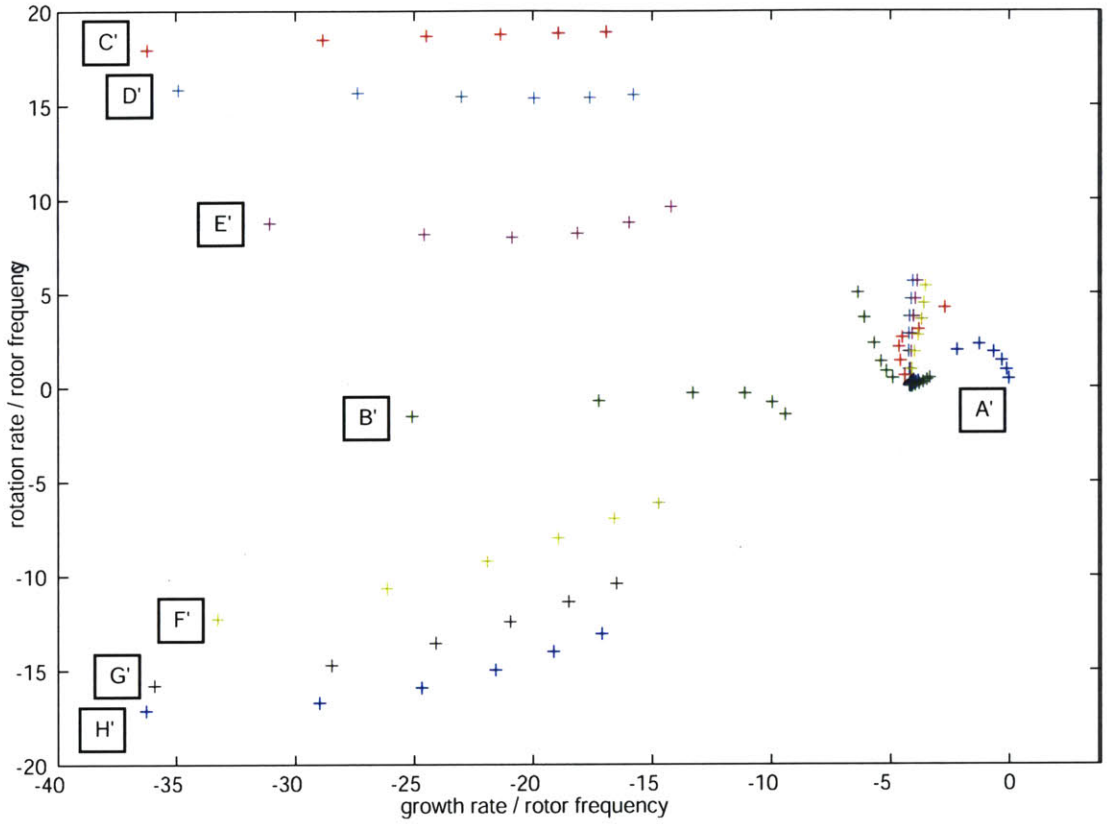

Figure D-6: Eigenvalue Map for the 4-Stage Standard Compressor

The eigenvalues for the 4-stage standard compressor are shown in Figure D-6. The results suggest that the modes can be grouped into the following subgroups:

- Three strings of modes (C', D', E') with high positive rotation rate ($\omega_n \geq 5$) ;
- Three strings of modes (F', G', H') with high negative rotation rate ($\omega_n \leq -5$) ;
- One independent mode (B') with low rotation rate ($|\omega_n| < 5$);
- The least stable mode (A').

Comparing Figures D-5 and D-6 suggests that if an additional stage is added to the machine, two new highly-damped modes appear, and that they are distributed between the first two subgroups.

On the other hand, modes A' and B' for the 4-stage standard compressor seem to behave similarly to the independent modes for the 3-stage standard compressor A and B. This suggests that these two may correspond to the dynamics of some components that are present in all compressors, independently of the number of stages. In addition, it is not trivial to determine which mode, within each subgroup (C', D'and E' or F', G'and H') appeared when the new stage was added. Consequently, a study of each individual mode must be conducted to understand the dynamics associated with each subgroup and with each mode within these subgroups.

Next, the blade-row inertia, defined as $\lambda = \frac{c_x}{R \cdot cos^2\gamma}$, is doubled independently for each blade-row and the system eigenvalues are computed. The results show evidence that some modes are particularly sensitive to changes in the blade-row inertia of one specific blade-row. This suggests that the dynamics of a particular mode might correspond to the dynamics related to a specific blade-row. An example of this behavior is given on Figure D-7, for mode C'.

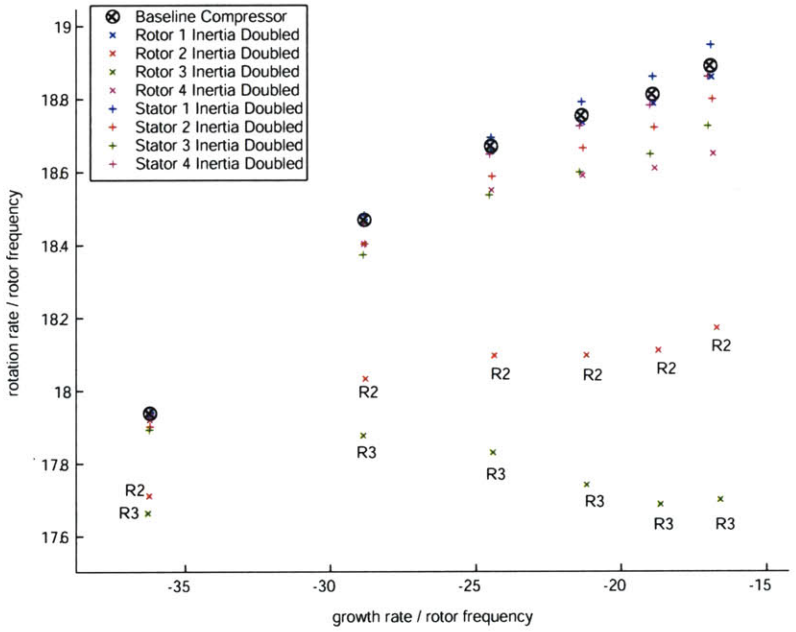

Figure D-7: Blade-Row Inertia Sensitivity on Mode C'

From the above results, the dynamics of modes C' to H' can be associated with the dynamics of a specific blade-row. The conjectures for these "associations" are summarized in Table D.1.

In order to confirm these conjectures, an energy analysis is conducted for each of these modes, for all the harmonics (cf. definition [16]). The results show similar trends for all harmonics. Only the results for harmonic #1 are presented here in Figure D-13. Figure D-13 depicts the distribution over the length of the compressor of the perturbation energy, for the modes C' through H' (Note:

Mode	Mostly influenced by blade-row
C'	R3
D'	R2
E'	R4
F'	S1
G'	S3
H'	S2

Table D.1: Hypothesis of Correspondence between the Modes Dynamics and the Blade-Rows Dynamics

the solid vertical lines indicate the location of blade-rows).

The energy analysis tends to confirm the conjecture made in Table D.1. For most of the modes, the perturbation energy peaks upstream of its "associated" blade-row. This suggests that the dynamics of the mode might correspond to the dynamics related to one specific blade-row.

After the modes of the first two subgroups are analyzed, modes A' and B' are studied. Similarly to the statement made in Section D-1, the occurrence of these two modes at similar locations for one (cf. Figure 3-8), three (cf. Figure D-5) or four stages (cf. Figure D-6) suggests that the two modes might correspond to the dynamics of components of the compressor system that are common to all of these compressors. These two modes could consequently be thought to relate to the association of the infinite upstream duct and the first rotor (R1), and of the infinite downstream duct and the last stator (S4). The energy analysis conducted for the two modes tend to support this conjecture. Figure D-15 shows that for mode B', the energy has a maximum before S4 and tends to increase in the exit duct much more rapidly than any of the other modes, thus suggesting that the dynamics of mode B could correspond to the dynamics of the infinite exit duct and to S4. On the other hand, the energy of mode A' displays a totally different pattern compared to the other modes, which might be related to its slightly negative growth rate. The perturbation energy distribution energy has a maximum before R1. One might therefore conjecture that the dynamics of A' corresponds to the dynamics of R1 and the inlet duct.

From this study, each mode can be associated to a blade-row, which is shown in Figure D-16.

If compared to the eigenvalue map (cf. Figure D-6), this sketch highlights two significant trends. First, the two "distinct modes" A' and B' are associated to the outer blade-rows of the compressor, the first subgroup modes (C', D', and E') are associated to the inner rotors, and the second subgroup modes (F', G', and H') to the inner stators.

Second, the closer one blade-row is to the center of the compressor , the higher the rotation rate of its associated mode (in absolute value). This is applicable for both rotors and stators. Likewise, the closer to the edge of the compressor (i.e. E' and F'), the lower the rotation rate. In addition, it is noteworthy that the modes associated with the blade-rows closer to the edge of the compressor

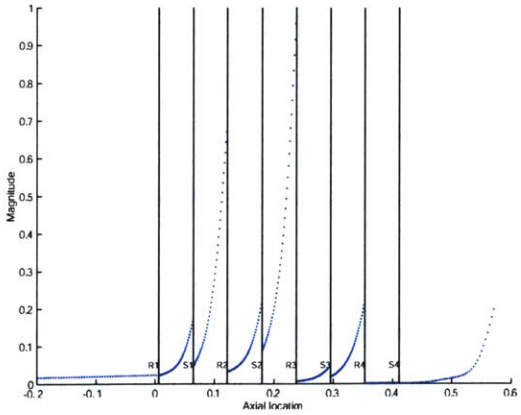

Figure D-8: Energy Distribution for Mode C'

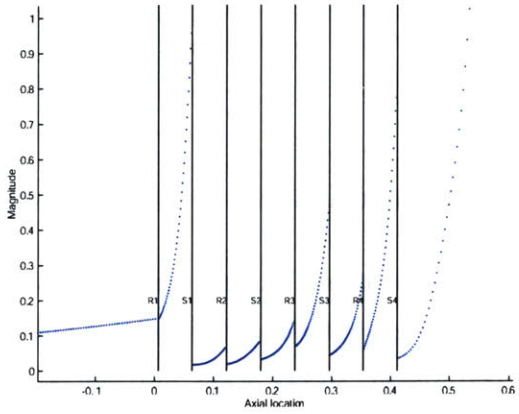

Figure D-9: Energy Distribution for Mode F'

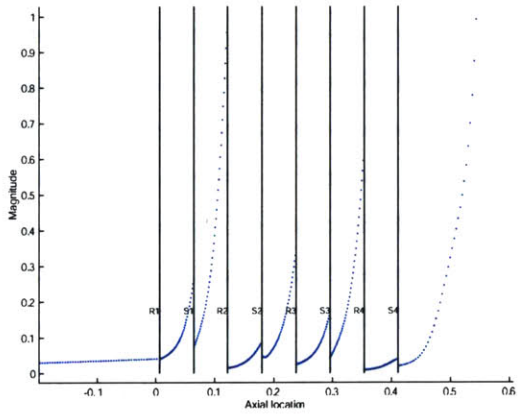

Figure D-10: Energy Distribution for Mode D'

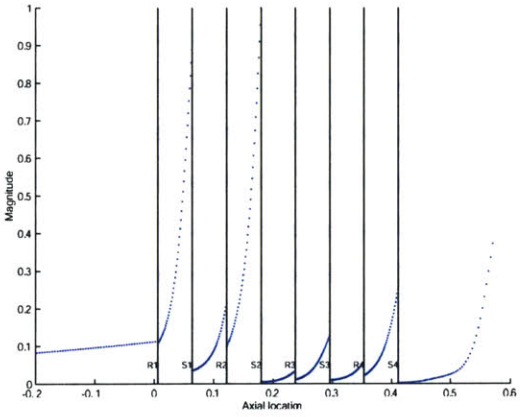

Figure D-11: Energy Distribution for Mode G'

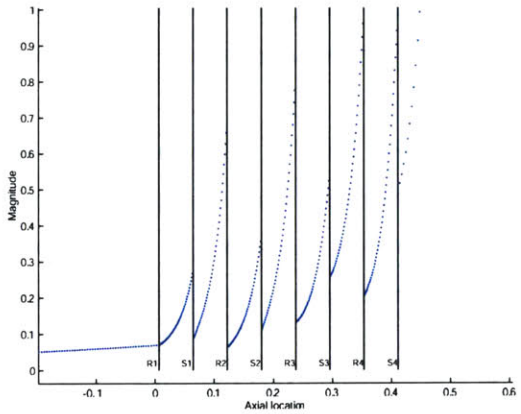

Figure D-12: Energy Distribution for Mode E'

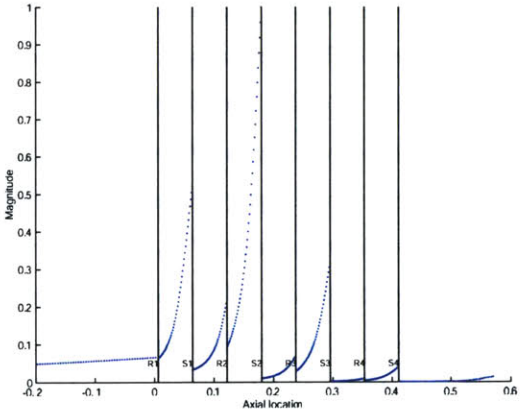

Figure D-13: Energy Distribution for Mode H'

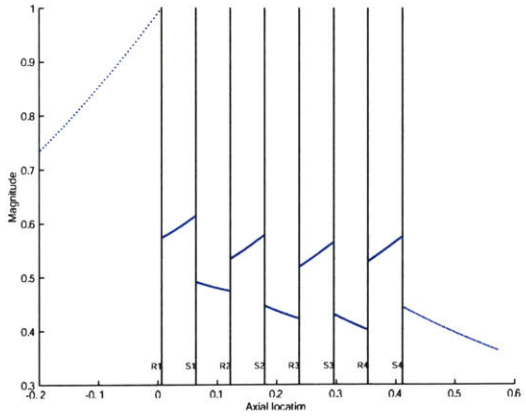

Figure D-14: Energy for Mode A'

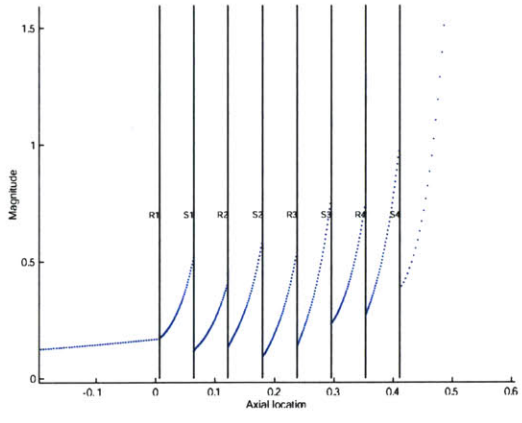

Figure D-15: Energy for Mode B'

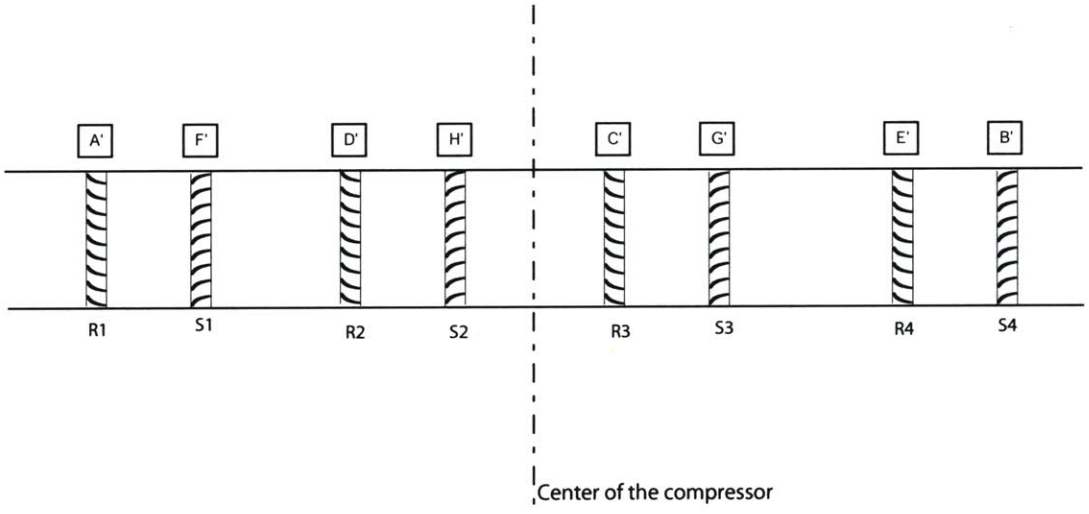

Figure D-16: Hypothesis of Correspondence between the Modes Dynamics and the Blade-Rows Dynamics for the 4-Stage Standard Compressor

(E' and F') have much higher sensitivity to blade-row inertia than the modes corresponding to the center blade-rows.

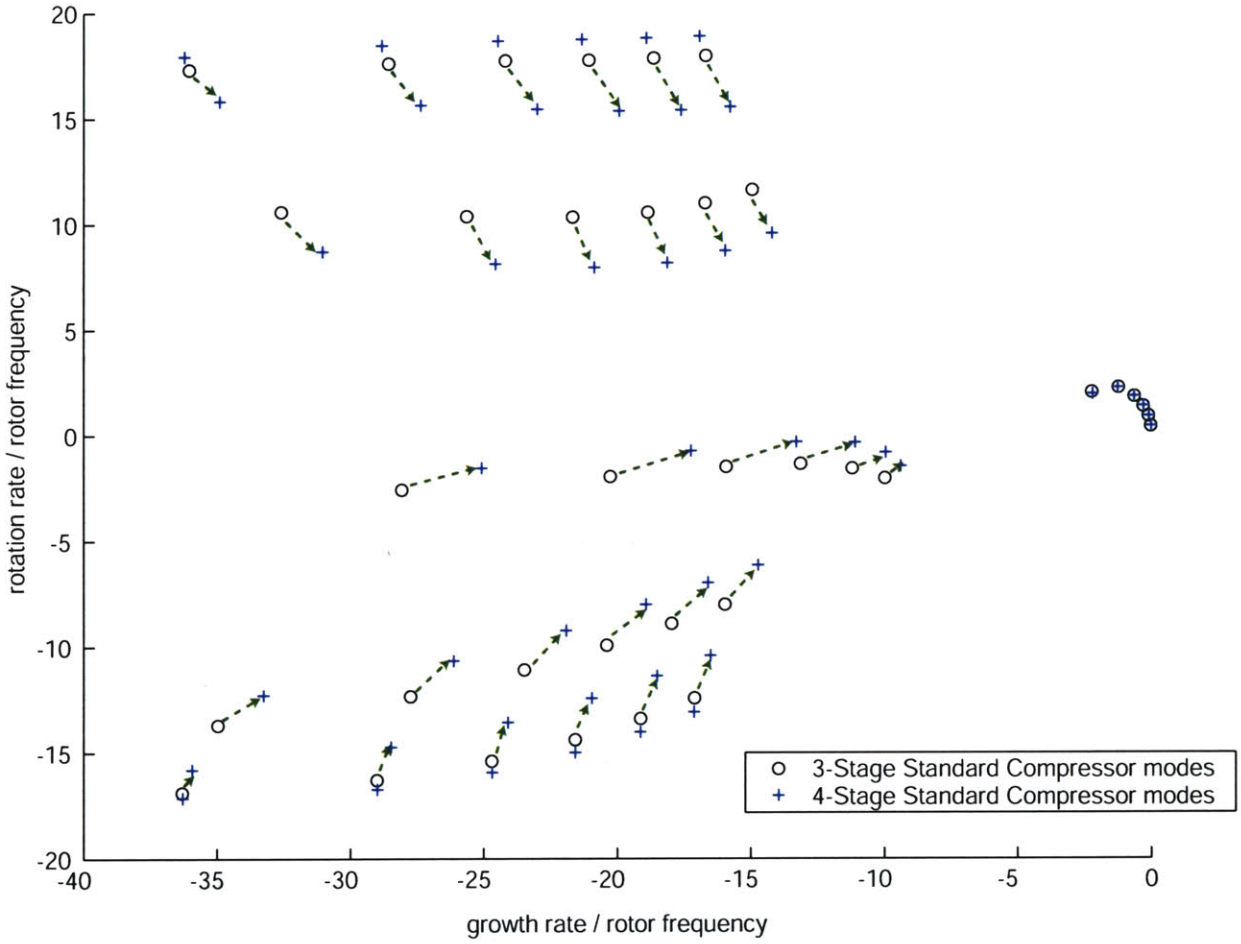

Figure D-17: Highly Damped Modes for a 3-Stage Standard Compressor and a 4-Stage Standard Compressor

From Figure D-17, it appears that, from a dynamic point of view, "expanding a compressor" can be thought of as inserting a stage into the center of the compressor, as shown in Figure D-18. Therefore, two new system modes appear, with dynamics most dominant on the center blade-rows with relatively high $|\omega|$.

This analysis has emphasized the potential correspondence that can be made between the modes dynamics and the blade-rows dynamics. However, as illustrated by modes A' and B', the compressor dynamics consist of strongly coupled system modes.

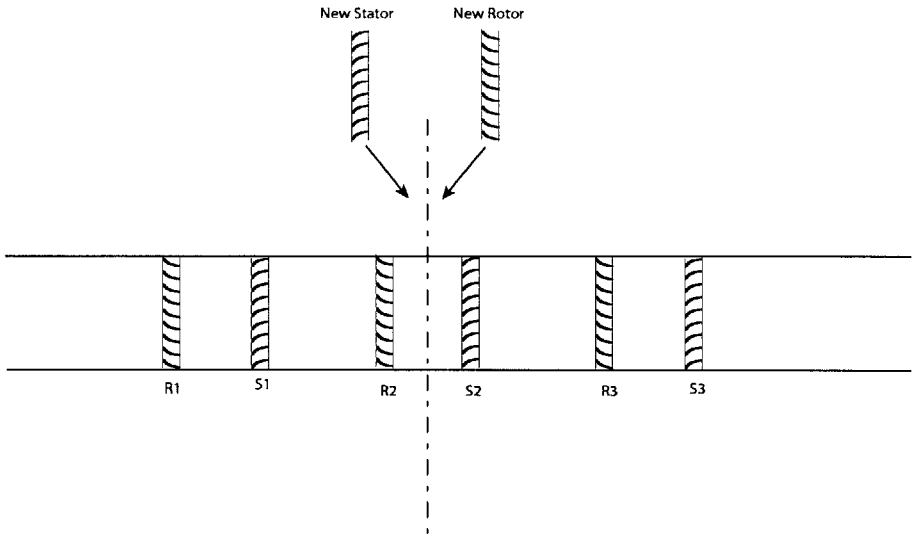

Figure D-18: System Dynamics View of "Expanding" a Compressor

Bibliography

[1] ALLAVIATIONFLIGHTLINEONLINE. "AAFO News : 4/22/1999". *http://www.aafo.com* (4/22/1999).

[2] AVIATIONDAILY. "Aircraft Utilization - Jet Aircraft (181-290 seats)". *Aviation Daily* (Tuesday, June 11, 2002), p. 7.

[3] BONNAURE, L. "Modelling High Speed Multistage Compressor Stability". Master's thesis, Department of Aeronautics and Astronautics, MIT, 1991.

[4] CAMP, T., AND DAY, I. "A Study of Spike and Modal Stall Phenomena in a Low-Speed Axial Compressor". In *ASME Turbo Expo, Orlando, FL, Paper 97-GT-526* (June 1997).

[5] CUMPSTY, N. *Compressor Aerodynamics.* Addison-Wesley Publishing Company, 1989.

[6] FAA. "Emergency Airworthiness Directive 2001-08-52". *US DoT Publications* (2001).

[7] FAA. "Airplane Turbofan Engine Operation and Malfunctions Basic Familiarization for Flight Crews". *Aircraft Certification Service Products and Services Home Page* (2002).

[8] FAA. "PART 33–AIRWORTHINESS STANDARDS: AIRCRAFT ENGINES ". *Code of Federal Regulations* (2002).

[9] FAA. "Airworthiness Directive 2001-15-12, Amendment 39-12346 ". *Federal Register, Vol. Volume 67, Number 207* (October 25, 2002), pp. 65484–65493.

[10] FEULNER, M., HENDRICKS, G., AND PADUANO, J. "Modeling for Control of Rotating Stall in High Speed Multi-Stage Axial Compressors". *ASME J. of Turbomachinary, Vol. 118* (Jan. 1996), pp. 1–10.

[11] FRÉCHETTE, L. G. "Implications of Stability Modeling for High-Speed Axial Compressor Design". Master's thesis, Department of Aeronautics and Astronautics, MIT, Feb. 1997.

[12] GREITZER, E. "The Stability of Pumping Systems — the 1980 Freeman Scholar Lecture". *ASME J. of Fluids Engineering, Vol. 103* (1981), pp. 193–243.

[13] LONGLEY, J. "A Review of Nonsteady Flow Models for Compressor Stability". *ASME J. of Turbomachinary* (Apr. 1994), pp. 202–215.

[14] MOORE, F., AND GREITZER, E. "A Theory of Post-Stall Transients in Axial Compressors: Part I – Development of the Equations". *ASME J. of Engineering for Gas Turbines and Power, Vol. 108* (1986), pp. 68–76.

[15] PADUANO, J., EPSTEIN, A., VALAVANI, L., LONGLEY, J., GREITZER, E., AND GUENETTE, G. "Active Control of Rotating Stall in a Low-Speed Axial Compressor". *ASME J. of Turbomachinary, Vol. 115* (Jan. 1993), pp. 48–56.

[16] SPAKOVSZKY, Z. *Applications of Axial and Radial Compressor Dynamic System Modeling.* PhD thesis, Department of Aeronautics and Astronautics, MIT, 2000.

[17] SPAKOVSZKY, Z., GERTZ, J., SHARMA, O., PADUANO, J., EPSTEIN, A., AND GREITZER, E. "Influence of Compressor Deterioration on Engine Dynamic Behavior and Transient Stall-Margin". *ASME J. of Turbomachinary, Vol. 122* (July 2000), pp. 477–484.

[18] TRYFONIDIS, M., ETCHEVERS, O., PADUANO, J., EPSTEIN, A., AND HENDRICKS, G. "Pre-Stall Behavior of Several High-Speed Compressors". *ASME J. of Turbomachinary, Vol. 117* (Jan. 1995), pp. 62–80.

[19] WILLIAMS, D., AND SURBER, L. "Intake/Engine Compatibility". In *Practical Intake Aerodynamic Design*, J. Seddon and E. Goldsmith, Eds. Blackwell Scientific Publications, 1993, pp. 21–71.